

Technical Report Documentation Page

1. Report No. FHWA/TX-09/0-5482-2		2. Government Accession No.		3. Recipient's Catalog No.	
4. Title and Subtitle Development of the Thickness Design for Concrete Pavement Overlays over Existing Asphalt Pavement Structures				5. Report Date February 2008; Revised September 2008	
				6. Performing Organization Code	
7. Author(s) Chul Suh, Dongho Kim, Moon Won				8. Performing Organization Report No. 0-5482-2	
9. Performing Organization Name and Address Center for Transportation Research The University of Texas at Austin 3208 Red River, Suite 200 Austin, TX 78705-2650				10. Work Unit No. (TRAIS)	
				11. Contract or Grant No. 0-5482	
12. Sponsoring Agency Name and Address Texas Department of Transportation Research and Technology Implementation Office P.O. Box 5080 Austin, TX 78763-5080				13. Type of Report and Period Covered Technical Report, 09/2005-08/2007	
				14. Sponsoring Agency Code	
15. Supplementary Notes Project performed in cooperation with the Texas Department of Transportation and the Federal Highway Administration.					
16. Abstract Several thin whitetopping (TWT) projects in the U.S. were reviewed to identify variables with significant effects on TWT behavior and performance. The joint spacing has a significant effect on performance as it determines the wheel loading condition in the slabs. Joints placed under or near the wheel paths caused serious distresses in TWT due to corner loading condition. Full-scale whitetopping pavement was constructed and tested under static and constant cyclic loading for fatigue. The concept of equivalent fatigue life was applied to correct the effect of the different stress ratios. The S-N curve developed from this study was very close to Thompson and Barenburg's S-N curve after the application of the equivalent fatigue life concept. A factorial experiment was developed that included almost all the variables related to TWT designs. A total of 7,776 treatments were identified. Computer program ISLAB2000 was selected as an analysis tool, as it was used in the development of MEPDG. ISLAB2000 was run 7,776 times and the results were statistically analyzed. Using log-log regression, the analysis results were approximated with the generalized English unit design equation for the determination of the required whitetopping thickness with several conservative assumptions. Current TxDOT design method for TWT does not account for the condition of the existing hot mix asphalt pavement. Rather, the slab thickness is determined solely by the future truck traffic. In addition, current TxDOT design method for TWT requires truck traffic as input while TP&P provides traffic information in terms of ESALs. The proposed design equation is more realistic in that it accounts for all the design variables including layer characteristics. It also utilizes ESAL as traffic input. Therefore, the proposed design equation will provide TxDOT engineers with more accurate and convenient design tool for TWT.					
17. Key Words whitetopping, pavement performance, fatigue, design, pavement rehabilitation				18. Distribution Statement No restrictions. This document is available to the public through the National Technical Information Service, Springfield, Virginia 22161; www.ntis.gov.	
19. Security Classif. (of report) Unclassified	20. Security Classif. (of this page) Unclassified		21. No. of pages 122		22. Price





# **Development of the Thickness Design for Concrete Pavement Overlays over Existing Asphalt Pavement Structures**

Chul Suh  
Dongho Kim  
Moon Won

---

CTR Technical Report:	0-5482-2
Report Date:	February 2008; Revised September 2008
Project:	0-5482
Project Title:	Concrete Pavement Overlays Over Existing Asphalt Pavement Structures
Sponsoring Agency:	Texas Department of Transportation
Performing Agency:	Center for Transportation Research at The University of Texas at Austin

Project performed in cooperation with the Texas Department of Transportation and the Federal Highway Administration.

Center for Transportation Research  
The University of Texas at Austin  
3208 Red River  
Austin, TX 78705

[www.utexas.edu/research/ctr](http://www.utexas.edu/research/ctr)

Copyright (c) 2008  
Center for Transportation Research  
The University of Texas at Austin

All rights reserved  
Printed in the United States of America

## **Disclaimers**

**Author's Disclaimer:** The contents of this report reflect the views of the authors, who are responsible for the facts and the accuracy of the data presented herein. The contents do not necessarily reflect the official view or policies of the Federal Highway Administration or the Texas Department of Transportation (TxDOT). This report does not constitute a standard, specification, or regulation.

**Patent Disclaimer:** There was no invention or discovery conceived or first actually reduced to practice in the course of or under this contract, including any art, method, process, machine manufacture, design or composition of matter, or any new useful improvement thereof, or any variety of plant, which is or may be patentable under the patent laws of the United States of America or any foreign country.

## **Engineering Disclaimer**

NOT INTENDED FOR CONSTRUCTION, BIDDING, OR PERMIT PURPOSES.

Project Engineer: Moon Won  
Professional Engineer License State and Number: Texas No. 76918  
P. E. Designation: Research Supervisor

## **Acknowledgments**

The authors express sincere appreciation to the Project Director, Tomas Saenz, and Project Advisors, Paul Hoelscher and Joe Leidy, who have provided valuable advices and suggestions. Also, the support received from David Head, the Program Coordinator, and German Claros, RTI Research Engineer, has been invaluable. The researchers would like to acknowledge the expert assistance provided by Larry Thames Contracting and Ecocreto of Texas, Inc. for the construction of the testing slabs.

## **Products**

This report contains four products: 0-5482-P1, 0-5482-P2, and 0-5482-P3, which are included in Chapter 5. 0-5482-P4 is included in the Appendix.

# Table of Contents

<b>Chapter 1. Introduction.....</b>	<b>1</b>
1.1 Background.....	1
1.2 Objectives .....	2
1.3 Report Organization.....	2
<b>Chapter 2. In-Depth Literature Review on Whitetopping Performance.....</b>	<b>3</b>
2.1 Illinois .....	3
2.2 Minnesota.....	7
2.3 Colorado.....	16
2.4 Summary of Distress.....	21
<b>Chapter 3. In-Depth Literature Review on Design Procedures .....</b>	<b>23</b>
3.1 Colorado Design Procedure .....	23
3.1.1 Determination of Critical Load Location.....	23
3.1.2 Determination of Load-Induced Stress at Zero Temperature Gradient .....	24
3.1.3 Analysis of the Effect of Interface Bond on Load-Induced Asphalt Strain .....	25
3.1.4 Analysis of Temperature Effects on Load-Induced Stresses .....	25
3.1.5 Development of Revised Design Equations .....	26
3.1.6 Mechanistic Whitetopping Thickness Design Procedure .....	29
3.1.7 Sensitivity Analysis .....	31
3.2 ACPA Design Procedure .....	31
3.2.1 Support provided by the existing asphalt pavement .....	31
3.2.2 Flexural Strength Design Value for Concrete.....	33
3.2.3 Truck Traffic.....	33
3.2.4 Design Period.....	33
3.2.5 Determination of Pavement Thickness .....	33
3.3 New Jersey Design Procedure .....	35
3.3.1 Field Testing .....	35
3.3.2 Finite Element Analysis and Verification.....	35
3.3.3 Design Procedure .....	38
3.4 PCA Design Procedure .....	41
3.4.1 Development of the 3D FEM.....	41
3.4.2 Verification of the 3D FEM.....	41
3.4.3 Development of a Modified 2D FEM and Prediction Equations.....	41
3.4.4 Fatigue Model .....	42
<b>Chapter 4. Field Testing Program.....</b>	<b>45</b>
4.1 Overview.....	45
4.2 Full-Scale Whitetopping Pavement .....	45
4.2.1 Test Pavement.....	45
4.2.2 Mixture Proportion.....	46
4.2.3 Construction of Full-Scale Whitetopping Slab .....	46
4.2.4 Mechanical Properties of Whitetopping Concrete.....	46
4.3 Foundation Properties .....	50
4.3.1 Falling Weight Deflection test .....	50
4.3.2 Dynamic Cone Penetrometer (DCP) test .....	51

4.3.3 Modulus of Subgrade Reaction (k-value) Test—Plate Load Test .....	55
4.4 Super Accelerated Testing .....	62
4.4.1 Description of the Stationary Dynamic Deflectometer (SDD) .....	63
4.4.2 Super-Accelerated SDD Slab Testing Procedure .....	63
4.4.3 Super-Accelerated Full-Scale Concrete Slab Testing Results .....	66
<b>Chapter 5. Development of Mechanistic Design Procedures .....</b>	<b>71</b>
5.1 Design Logic .....	71
5.2 Stress Computation Using ISLAB2000 .....	72
5.2.1 Input and Output .....	72
5.2.2 Analysis of ISLAB2000 Output .....	82
5.3 Regression Analysis .....	85
5.4 Development of TWT Design Equations .....	87
5.4.1 Stress Prediction of Unbonded Interface Conditions .....	87
5.4.2 Calibration of Stress Prediction using Fatigue Behavior of Whitetopping .....	87
5.4.3 Development of Thickness Prediction Equations .....	88
5.5 Sensitivity Analysis .....	88
5.6 Comparison with Current TxDOT Design Thickness .....	93
5.7 TWT Design Procedures for TxDOT .....	100
<b>Chapter 6. Conclusions and Recommendations .....</b>	<b>103</b>
<b>References .....</b>	<b>105</b>
<b>Appendix: Modified Standards and Specifications for Thin Whitetopping and Full Depth PCC Pavement .....</b>	<b>107</b>



## List of Figures

Figure 2.1: Panel Movements in Project 1 .....	4
Figure 2.2: Panel Corner Break for Project 4 .....	5
Figure 2.3: Ride Quality History for Test Cell 93 .....	8
Figure 2.4: Ride Quality History for Test Cell 94 .....	8
Figure 2.5: Ride Quality History for Test Cell 95 .....	9
Figure 2.6: Corner cracked areas beginning to punch out in test cell 94.....	9
Figure 2.7: Corner cracks near outside wheelpath in test cell 93 .....	10
Figure 2.8: Patched corner crack areas near outside wheelpath of test cell 93 driving lane .....	11
Figure 2.9: Cracks from underlying asphalt layer reflected through UTW overlay in test cell 93.....	11
Figure 2.10: Load-related cracking and surface depression (punchout) near existing transverse crack of test cell 93 .....	12
Figure 2.11: Load-related cracking and large surface depression of test cell 93 driving lane.....	12
Figure 2.12: Extensive corner cracking of test cell 94, November 2003.....	13
Figure 2.13: Asphalt patching on nearly every panel in the driving lane of test cell 94, September 2004 .....	13
Figure 2.14: Passing lane of test cell 94, November 2003.....	14
Figure 2.15: Corner cracking on the outside edge of test cell 95, for driving lane, November 2003.....	15
Figure 2.16: Corner cracking on the outside edge of test cell 95, for passing lane, November 2003.....	15
Figure 2.17: Typical Pavement Condition .....	18
Figure 2.18: Distressed Area at Stop Sign Approach .....	18
Figure 2.19: Typical Pavement Condition .....	19
Figure 2.20: Slab Cracking Filled with Asphalt Sealant.....	19
Figure 2.21: Typical Pavement Condition .....	20
Figure 2.22: Cracked Slabs .....	20
Figure 3.1: Location of Load Resulting in Maximum Stress.....	23
Figure 3.2: Increase in Critical Load Stress Due to Partial Bonding Condition.....	24
Figure 3.3: Asphalt Surface Strain vs. Concrete Bottom Strain .....	25
Figure 3.4: Increase in Load Stress Due to Curling Loss of Support .....	26
Figure 3.5: Flow Chart for Colorado Design Procedure.....	30
Figure 3.6: K-value on top of asphalt pavement with granular base .....	32
Figure 3.7: K-value on top of asphalt pavement with cement-treated base.....	32
Figure 3.8: Finite Element Model.....	36
Figure 3.9: Detail of the finite element model.....	36
Figure 4.1: Cross-section of the whitetopping pavement system .....	45

Figure 4.2: Construction of the full-scale whitetopping slab.....	49
Figure 4.3: Saw cut (2-in. depth, 6-ft spacing) at the age of 12 hours.....	50
Figure 4.4: FWD testing .....	52
Figure 4.5: DCP testing.....	53
Figure 4.6: Comparison of DCP and FWD results .....	54
Figure 4.7: DCP results for k-value testing locations .....	54
Figure 4.8: Schematic diagram of plate load test.....	55
Figure 4.9: Plate load testing apparatus .....	56
Figure 4.10: Plate load test at testing site .....	57
Figure 4.11: Selected k-value test locations based on FWD results .....	58
Figure 4.12: Removal of asphalt surface .....	59
Figure 4.13: Load-settlement curves from k-value tests.....	60
Figure 4.14: ELSYM5 inputs.....	61
Figure 4.15: Comparison of k-values from field test and ELSYM5.....	61
Figure 4.16: Illustrations of SDD testing method .....	62
Figure 4.17: Additional saw cut.....	63
Figure 4.18: Super-accelerated SDD testing plan.....	64
Figure 4.19: Field testing arrangement .....	64
Figure 4.20: Arrangement of loading frame and LVDTs .....	65
Figure 4.21: Slab failure patterns.....	68
Figure 4.22: Variation of normalized dynamic displacement for full-scale slabs .....	69
Figure 4.23: Comparison of existing fatigue curves and full-scale slab fatigue data .....	70
Figure 5.1: Flow diagram of design logic .....	71
Figure 5.2: Flow diagram of mechanistic design procedure .....	72
Figure 5.3: Whitetopping model using ISLAB2000.....	73
Figure 5.4: Initial input screen of program .....	75
Figure 5.5: Geometry options .....	75
Figure 5.6: Input screens for each pavement layer .....	76
Figure 5.7: Subgrade options .....	77
Figure 5.8: Joint options .....	77
Figure 5.9: Temperature properties of each layer.....	78
Figure 5.10: Load options.....	78
Figure 5.11: Analysis options .....	79
Figure 5.12: Stress contour in x-direction.....	79
Figure 5.13: Stress contour in y-direction.....	80
Figure 5.14: Shear stress contour.....	80
Figure 5.15: Principal stress contour .....	81
Figure 5.16: Deflection contour.....	81

Figure 5.17: Effect of bond conditions on maximum stress .....	83
Figure 5.18: Effect of LTE on maximum stress: SAL, bonded interface .....	84
Figure 5.19: Effect of loading type on maximum stress .....	85
Figure 5.20: Regression output vs. ISLAB2000 output: bonded, SAL, 1% LTE.....	87
Figure 5.21: Whitetopping thickness sensitivity to asphalt thickness .....	89
Figure 5.22: Whitetopping thickness sensitivity to base thickness.....	90
Figure 5.23: Whitetopping thickness sensitivity to concrete elastic modulus .....	90
Figure 5.24: Whitetopping thickness sensitivity to asphalt modulus .....	91
Figure 5.25: Whitetopping thickness sensitivity to base modulus.....	91
Figure 5.26: Minimum whitetopping thickness sensitivity to asphalt thickness .....	92
Figure 5.27: Whitetopping thickness sensitivity to subgrade reaction modulus .....	93
Figure 5.28: Whitetopping thickness sensitivity to modulus of rupture of concrete .....	93
Figure 5.29: Whitetopping thickness with various AC thickness using design equation .....	98
Figure 5.30: Whitetopping thickness with various AC modulus using design equation .....	99



## List of Tables

Table 2.1: Information Pertaining to Illinois DOT (2002) Projects.....	3
Table 2.2: Project Construction Cost Information.....	6
Table 2.3: Ultra-thin Whitetopping test cell design features .....	7
Table 2.4: Type and quantities of distress for UTW test cells.....	10
Table 2.5: Test Slab Characteristics and Test Results .....	17
Table 3.1: Combinations of Parameters.....	28
Table 3.2: Subgrade Soil Types and Approximate k-value .....	33
Table 3.3: Slab Thickness, Light to Medium Truck Traffic .....	34
Table 3.4: Slab Thickness, Heavy Truck Traffic .....	34
Table 3.5: Parameters Investigated .....	37
Table 4.1: Mixture proportion for whitetopping.....	46
Table 4.2: Mechanical properties of whitetopping concrete.....	47
Table 4.3: Average back-calculated elastic modulus from FWD testing .....	51
Table 4.4: k-value test locations .....	58
Table 4.5: k-value test results with corresponding DCP values .....	59
Table 4.6: Summary of concrete fatigue curves from other researchers .....	66
Table 4.7: Super-accelerated full-scale whitetopping test results.....	67
Table 5.1: Summary of used input variables for ISLAB2000 .....	74
Table 5.2: Regression coefficients for Equation (5.2)—bonded, SAL, and 1% LTE .....	86
Table 5.3: Current TxDOT thin whitetopping thickness design.....	94
Table 5.4: AASHTO Equivalent axle load factors for rigid pavements ( $D = 9$ in, $p_t = 2.5$ ) .....	95
Table 5.5: Converted ESALs for current TxDOT design: EALF = 0.5.....	95
Table 5.6: Converted ESALs for current TxDOT design: EALF = 1.0.....	96
Table 5.7: Converted ESALs for current TxDOT design: EALF = 1.5.....	96
Table 5.8: Converted ESALs for current TxDOT design: EALF = 2.0.....	97



# Chapter 1. Introduction

## 1.1 Background

Whitetopping is a pavement system of Portland cement concrete (PCC) placed on hot mix asphalt concrete (HMAC) pavement. Whitetopping is used to address distresses in asphalt pavement such as rutting and shoving. Three types of whitetopping pavements are commonly used. These types are classified according to the PCC slab thickness as follows:

- Ultra-thin whitetopping (UTW): slab thickness between two to less than four inches
- Thin whitetopping (TWT): slab thickness of four to less than eight inches
- Conventional white topping: slab thickness of eight inches or more.

Whether whitetopping is a good candidate to rehabilitate deteriorated HMAC pavement depends on the supporting capability of the existing HMAC pavement. Without proper evaluations of the existing HMAC pavement, it is quite difficult to arrive at reasonable and effective rehabilitation strategies. In current rigid pavement design philosophy, the support condition is considered to have minor effects on long-term performance. It is because the stress level on the top of the subbase is kept quite low due to the high stiffness of the concrete slab and relatively large thickness of concrete slabs used in modern PCC pavements. Although the evaluations of PCC pavements in Texas do not necessarily corroborate this theory, it is indeed true that the stress level on top of the subbase due to the applications of wheel loading is quite low. However, the same philosophy cannot be applied to the whitetopping system. First, the slab thickness for whitetopping is smaller than that used in normal PCC pavement. Second, the joint system used in whitetopping does not fully utilize the benefits of the bending action of the slabs. The resulting effects are that the stress level on top of the HMAC pavement is greater than that on top of the subbase in traditional PCC pavement. Accordingly, the performance of the whitetopping system depends on two structural factors: the support condition provided by the existing HMAC pavement and the combination of proposed PCC slab thickness and joint layouts. The required thickness for a given traffic application highly depends on the support conditions of the existing HMAC pavement.

Many states agencies including the Texas Department of Transportation (TxDOT) have used whitetopping overlays and reported positive results. Traffic interruptions at intersections and along main arterials due to frequent repair or rehabilitation activities are often associated with delay and high user cost. Thus, it is desirable to build a durable and reliable pavement system that requires minimum repair and rehabilitation activities. If designed and constructed properly, whitetopping could meet these requirement and help mitigate the adverse effects associated with frequent and costly pavement repairs and rehabilitations.

TxDOT developed design standards and special specifications for thin whitetopping. Currently, however, the agency does not have guidelines or design procedures for the rehabilitation of HMAC pavement exhibiting rutting and shoving. Proper design procedures and guidelines for the use of whitetopping will improve the efficiency of TxDOT's operations in rehabilitation of deteriorated HMAC pavements.

## **1.2 Objectives**

The primary objective of this research undertaking is to develop guidelines and design procedures for whitetopping. It is anticipated that the products of this research project will enhance TxDOT engineers' ability to develop the most cost-effective rehabilitation strategies for distressed HMAC pavement. The following list briefly itemizes the main objectives of this research program:

- 1) Summarize the findings of the literature review on the performance of whitetopping test sections and design procedures
- 2) Evaluate the static and fatigue behavior of whitetopping to find a proper fatigue criteria of whitetopping
- 3) Develop a procedure to determine the required thickness of whitetopping, considering levels of design variables

## **1.3 Report Organization**

This report is organized into six chapters, including the current, introductory Chapter 1. Following is a brief description of Chapters 2 through 6.

Chapter 2 summarizes the literature review on whitetopping performance, while Chapter 3 presents the literature review on whitetopping design procedures from various state agencies. Chapter 4 provides the procedures and results of the full-scale accelerated load test for whitetopping pavement. Chapter 5 presents the development of the mechanistic design procedure for the whitetopping pavement. Finally, Chapter 6 provides an overall summary and conclusions of this study. The appendix contains the modified standards and specifications for thin whitetopping and full depth PCC pavement.



## Chapter 2. In-Depth Literature Review on Whitetopping Performance

### 2.1 Illinois

The Illinois DOT (2002) constructed seven experimental whitetopping projects between 1998 and 2001. The performance of these projects was monitored through visual distress surveys and data collected on cracking, areas of debonding, and panel movements. Table 2.1 gives a description for each sub-project.

**Table 2.1: Information Pertaining to Illinois DOT (2002) Projects**

Project No.	Location	Route No.	Length	Construction Date	Overlay Thickness	Overlaid Surface
1	Decatur	U.S. 36	Intersection	April 1998	3.5 in.	1/3 PCC 2/3 Bit. Conc.
2	Decatur	U.S. 36	Intersection	April–May 1998	3.5 in. EB 2.5 in. WB	PCC
3	Carbondale	U.S. 51	Intersection	June–July 1998	3.5 in.	1/2 PCC 1/2 Bit. Conc.
4	Tuscola	U.S. 36	0.8 miles	May 1999	4–7.5 in.	Bit. Conc.
5	Clay County	CH3	7.85 miles	August 1998	5 in. and 6 in.	Bit. Conc.
6	Piatt County	CH4	4.94 miles	Sep.–Oct. 2000	5 in.	Bit. Conc.
7	Cumberland County	CH2	3.54 miles	September 2001	5.75 in.	Bit. Conc.

Project 1 was constructed in April 1998 with an average panel dimension of 3.6-ft by 4.3-ft. Three annual surveys were completed on this project. The number of panels was 181, 4 of which experienced cracks in the first year. Fourteen panels were cracked in the second year and 21 panels showed cracks in the third year after construction. The most common cracking pattern was a transverse, mid-panel crack with a few corner breaks and random cracks. The panels within the driving lane appear to be shifting toward the intersection in relation to the outside row of panels. The movement was approximately 2 in. Figure 2.1 shows the panel movement. The panel movement indicates poor or no aggregate interlock.

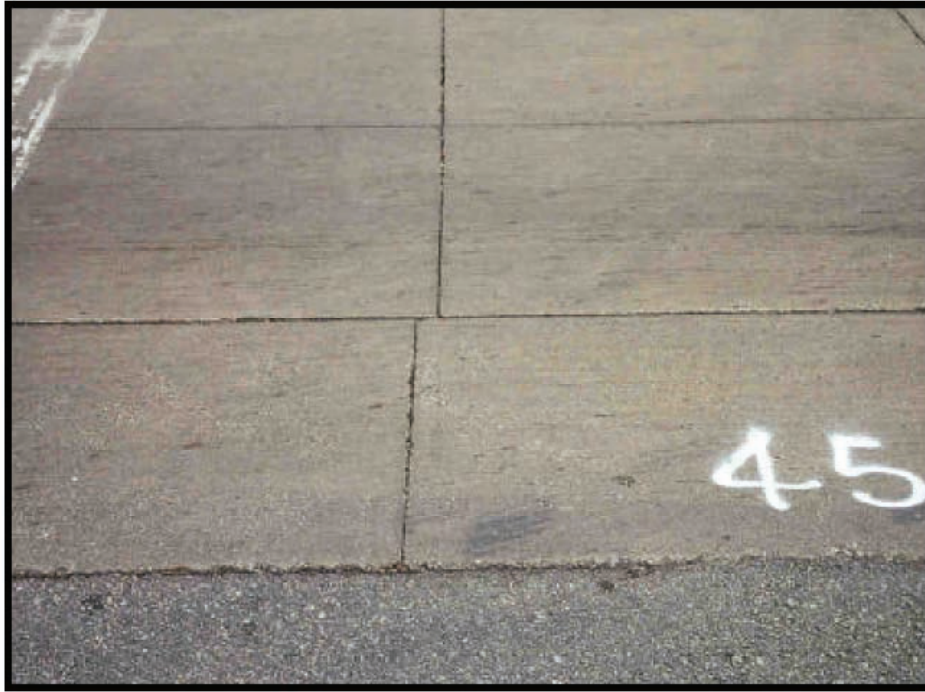


*Figure 2.1: Panel Movements in Project 1*

Project 2 included a thin bonded concrete overlay over concrete, not whitetopping. Project 3 was constructed during June and July 1998. The average panel dimension was 3.2-ft by 3.3-ft. Polypropylene fibers were incorporated at the rate of 3 pounds per cubic yard into the concrete mixture to reduce early plastic shrinkage cracks. Three annual surveys were completed on this project. This project included 906 panels. The number of cracked panels was 4 (0.4%) for the first year, 7 (0.8%) for the second year, and 9 (1.0%) for the third year after construction.

Project 4 included conventional whitetopping sections. It was completed in May 1999. The project consists of conventional whitetopping with an overlay thickness ranging from 4 to 7 in. Typical panel dimensions for this project were 5.0-ft by 5.5-ft. Two annual surveys on the project were completed. These surveys included 4809 panels. The number of cracked panels was 51 (1.1%) for the first year, and 96 (2.0%) for the second year after construction. Two of the 96 total cracks were surveyed in 2001 as transverse, mid-panel cracks. The remaining 94 cracks were all corner breaks similar to that shown in Figure 2.2. All cracks were of low severity, and no evidence of debonding was detected at this time.



*Figure 2.2: Panel Corner Break for Project 4*

Project 5 is a conventional whitetopping section that was completed during August 1998. The entire length of this project consisted of a conventional whitetopping with an overlay thicknesses of 5 to 6 in. These sections were sawn at a 10 to 15 degree skewed angle. Three annual surveys were completed for this test section. Cracks and distresses were not detected on this section.

Project 6 included conventional whitetopping sections with an overlay thickness of 5 in. It was completed in October 2000. Due to the length of this project, one experimental test section and one control section were selected for evaluation. One annual survey was completed on each section. The experimental section included all of the panels with 5.5-ft skewed transverse joints and 5.5-ft longitudinal joints. This section is approximately 2,630 ft long. The control section includes 100 panels with 11-ft skewed transverse joints. This section is approximately 550 feet long. Nine cracks were found in the experimental section, all of which were corner breaks. The corner breaks occurred at the corner of the panel where the skewed transverse joint formed an acute angle with the edge of the pavement. The cracks were all rated as low severity cracks. No cracks were found in the control section.

Project 7 section was completed in September 2001. This entire project is a conventional whitetopping with an overlay thickness of 5.75 in. Transverse joints were sawn at intervals of 5.5 ft and longitudinal joints sawn at intervals of 6.0 ft. The transverse saw joints were skewed at an angle of 10 to 15 degrees. A 6-month survey was completed in May 2002. Each experimental test section contains 120 rows of panels (480 total panels), and is approximately 660 ft long. Four panels had low severity transverse cracks.

Table 2.2 gives information on the pertinent construction costs for all of the whitetopping projects. Smaller panel sizes will increase the overall cost of the project due to the increased saw cutting cost.

**Table 2.2: Project Construction Cost Information**

Construction Item	Cumberland County – County Highway 2 (2001)	Piatt County – County Highway 4 (2000)	Clay County – County Highway 3 (1998)	Tuscola – U. S. Highway 36 (1999)	Carbondale – U. S. Highway 51 & Pleasant Hill Road (1998)	Decatur – U. S. Highway 36 & Country Club Road (1998)	Decatur – U. S. Highway 36 & Oakland Avenue
Pavement Milling 1.5 inches (sq. yds.)			\$0.17 (102,283)				
Pavement Milling 3.0 inches (sq. yds.)	\$1.11 (50,207)	\$1.61 (63,490)					
Pavement Milling 3.5 inches (sq. yds.)					\$6.86 (2,147)	\$7.23 (2,563)	\$7.23 (537)
Concrete Placement 2.5 inches (sq. yds.)						\$18.72 (1,216)	
Concrete Placement 3.5 inches (sq. yds.)					\$24.87 (2,147)	\$21.20 (1,347)	\$21.20 (537)
Concrete Placement 5.0 inches (sq. yds.)		\$13.85 (63,490)	\$12.56 (94,502)				
Concrete Placement 5.75 inches (sq. yds.)	\$15.84 (50,207)						
Concrete Placement 6.0 inches (sq. yds.)			\$13.89 (6,478)				
Concrete Placement Various (sq. yds.)				\$17.69 (10,626)			
Saw Joints Partial-Depth (feet)	*	*	*	\$0.72 (36,394)			
Saw Joints Full-Depth (feet)	*	*	*	\$2.65 (7,710)			
Saw Joints Combined (feet)					\$1.83 (9,921)	\$1.15 (9,200)	\$1.15 (2,267)
Total Cost (Per Square Yard)	\$16.95	\$15.46	\$12.73 (5") \$14.06 (6")	\$22.08	\$40.19	\$30.08 (2.5") \$32.56 (3.5")	\$33.28

\* Indicates this item was included with the cost of concrete placement.

A summary of this section is as follows:

- 1) The initial performance data of the seven projects listed show that ultra-thin whitetopping may manifest panel movement. This panel movement indicates poor or no aggregate interlock.
- 2) Ninety-four out of the 96 cracks found in Project 4 were all corner breaks. Most of the distresses in the whitetopping were mid-panel cracks or corner cracks.
- 3) Overall early performance of whitetopping in Project 1 was satisfactory. From the given information, smaller panel sizes will increase the overall cost of the project due to the increased saw cutting cost.

## 2.2 Minnesota

Three ultra-thin whitetopping (UTW) and three thin whitetopping pavement test sections were constructed, and extensive field testing was conducted at the Minnesota Road Research System (MnROAD) in 1997. Field performance data was provided. The ultra-thin whitetopping test sections were designated as test cells 93, 94, and 95. Three whitetopping test cells were also constructed, but will not be considered in this study.

Table 2.3 describes slab thickness, panel size, and fiber type of the UTW test cells. Traffic loading of test cells consisted of approximately 26,400 annual average daily traffic (AADT) with 14% heavy commercial annual average daily traffic (HCAADT). These test cells were constructed in 1997 and had carried approximately 6 million equivalent single axle loads (ESALs) in the right driving lane, in addition to 1.5 million ESALs in the passing lane as of June 2004. This report presents the performance history for the UTW test cells.

**Table 2.3: Ultra-thin Whitetopping test cell design features**

Test Cell Number	Concrete Slab Thickness, In (mm)	Panel size, ft (m)	Fiber Type
93	4 (102)	4 × 4 (1.2 × 1.2)	Polypropylene
94	3 (76)	4 × 4 (1.2 × 1.2)	Polypropylene
95	3 (76)	5 × 6 (1.5 × 1.8)	Polyolefin

Figures 2.3 through 2.5 show the ride quality history for test cells 93, 94, and 95 respectively. Indices used in the ride quality are present serviceability rating (PSR) and the International Roughness Index (IRI), in m/km. The PSR is a subjective “seat of the pants” measure of pavement roughness determined by a group of people riding in similar vehicles. The IRI is a measure of the cumulative rise and fall of the pavement surface. It is determined using a laser device mounted on a special testing vehicle. The PSR is calculated from the IRI rating by Equation 2.1.

$$PSR = 6.634 - (2.813)\sqrt{IRI} \quad (2.1)$$

The PSR has a scale of 0 (poor) to 5 (excellent), and a pavement is declared to have terminal serviceability when it declines to a value of 2.5 and below. As shown in Figures 2.3 through 2.5, the driving lane had reached values far below 2.5 in the spring of 2004. The cause of the low PSR was due to the distressed UTW surface. Figure 2.6 shows that cell 94, in particular, was experiencing punchout type distress in the corners of the interior panels near the wheelpaths. It is interesting to note the difference in performance between the driving and passing lanes in the UTW test cells.

The performance of UTW is clearly related to the volume of traffic loading. Other factors affecting the performance of UTW include the degree of bonding, the presence of moisture, and the geometry of the panels in relation to traffic loading. The types and quantities of cracking distress are summarized in Table 2.4.

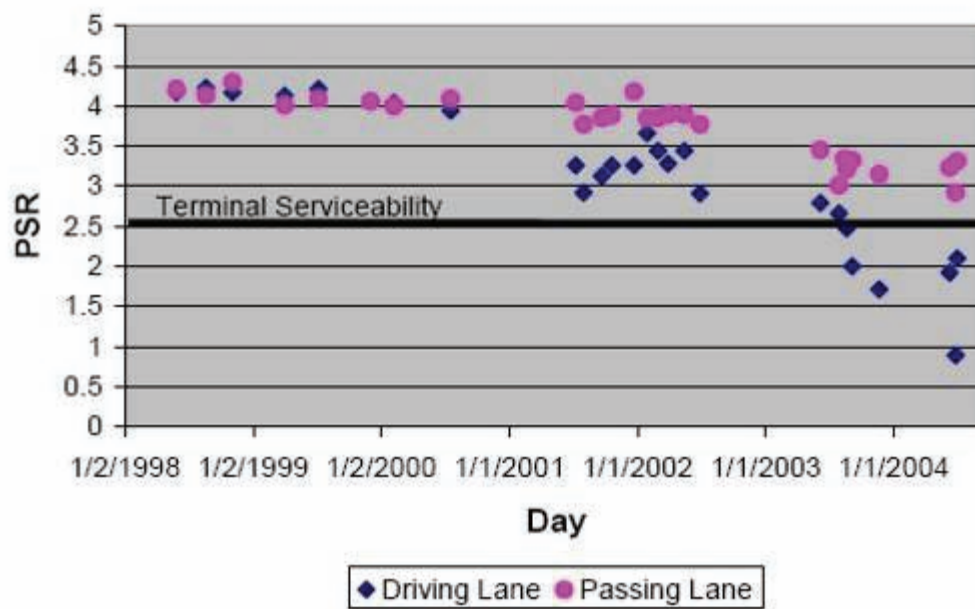


Figure 2.3: Ride Quality History for Test Cell 93

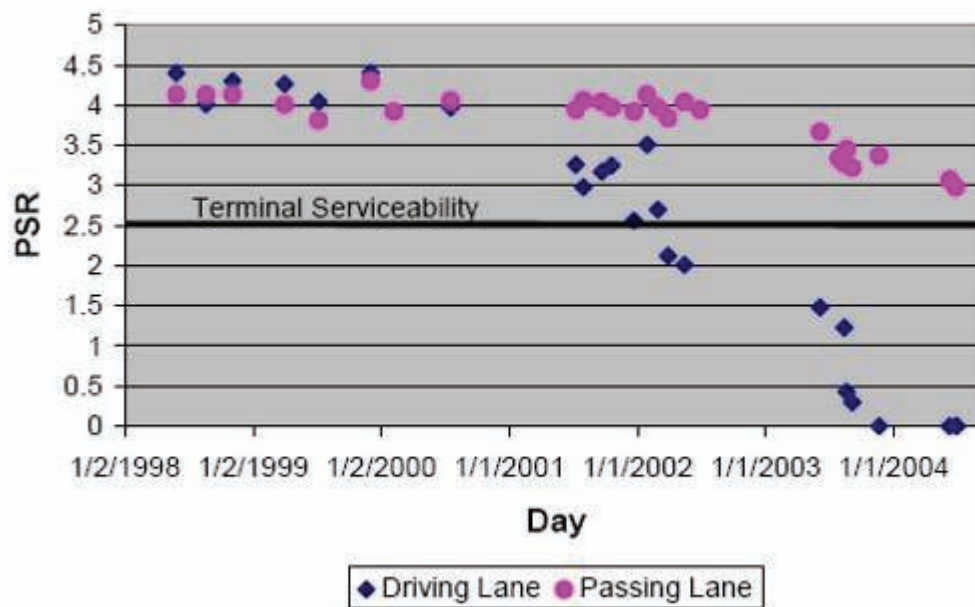


Figure 2.4: Ride Quality History for Test Cell 94



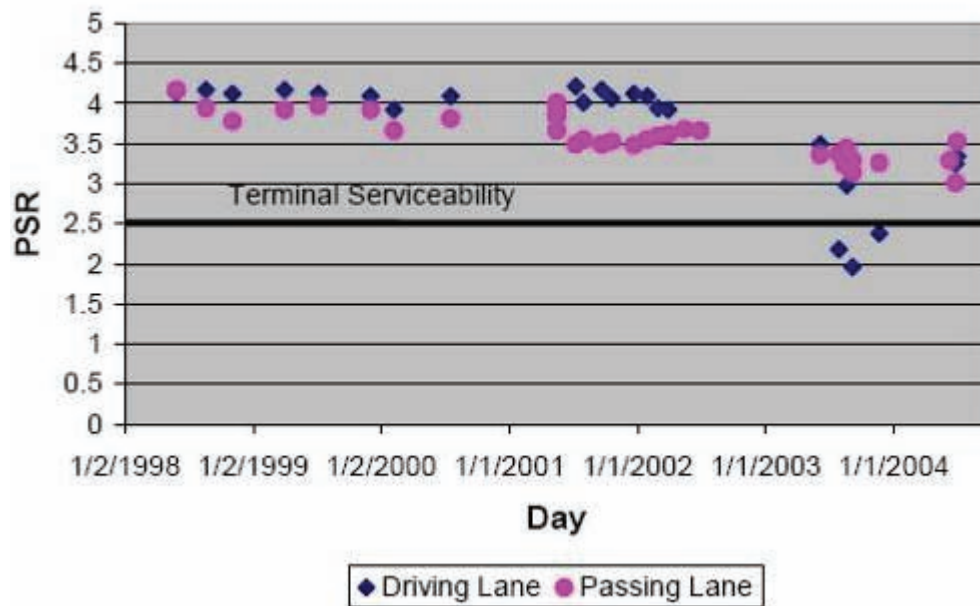


Figure 2.5: Ride Quality History for Test Cell 95



Figure 2.6: Corner cracked areas beginning to punch out in test cell 94

**Table 2.4: Type and quantities of distress for UTW test cells**

Test Cell	Corner cracks		Transverse cracks		Panels cracked (%) Panels repaired in 2001 not included	
	Driving Lane	Passing Lane	Driving Lane	Passing Lane	Driving Lane	Passing Lane
93	43	6	9	4	23	4
94	391	84	8	8	94	34
95	30	16	5	2	32	16

Test cell 93 consisted of a 4-in. thick UTW over 9-in. of hot-mix asphalt. This test cell experienced most surface distress in the form of corner cracking on the inside edge of the outer panels in the driving lane. Cracking was predominantly located on the approach side of the panels, nearest to the outside wheelpath of the driving lane. Figures 2.7 and 2.8 show examples of the distress before and after patching done by the Minnesota Department of Transportation (MnDOT) maintenance crews. The other predominant distresses in test cell 93 were reflective cracking (due to the bond with the HMA) and load-related cracking. All but a few of these distresses were located in the outer panels of the driving lane, nearest to the shoulder (Figures 2.9 through 2.11).



*Figure 2.7: Corner cracks near outside wheelpath in test cell 93*





*Figure 2.8: Patched corner crack areas near outside wheelpath of test cell 93 driving lane*



*Figure 2.9: Cracks from underlying asphalt layer reflected through UTW overlay in test cell 93*



*Figure 2.10: Load-related cracking and surface depression (punchout) near existing transverse crack of test cell 93*



*Figure 2.11: Load-related cracking and large surface depression of test cell 93 driving lane*

Test cell 94 consists of a 3-in. thick UTW over 10-in. of hot-mix asphalt. This test cell experienced most surface distress in the form of corner cracking near the longitudinal joints of the center panels in the driving lane. Corner cracking was very extensive leading to center panels having diamond-shaped punchouts near the corners. In some cases, the corner cracks were connected to the corner cracks in adjacent panels as shown in Figure 2.12. Figure 2.13 shows



how extensive the corner crack patching was in the summer of 2004. The thinner panels of test cell 94 demonstrated more load-related transverse cracking than test cell 93. By November 2003, the inside wheelpath of the passing lane in test cell 94 was starting to exhibit similar distress as the driving lane. As shown in Figure 2.14, the ride quality of the driving lane became so low (PSR=0) that interstate traffic was removed (for safety reasons) from the MnROAD mainline test sections on June 14, 2004.



*Figure 2.12: Extensive corner cracking of test cell 94, November 2003*



*Figure 2.13: Asphalt patching on nearly every panel in the driving lane of test cell 94, September 2004*



*Figure 2.14: Passing lane of test cell 94, November 2003*

Similar to test cell 94, test cell 95 consists of a 3-in. thick UTW over 10 in. of hot-mix asphalt. However, this test cell experienced much less surface distress than test cell 94. The major difference is attributed to the larger panel size in test cell 95. Moving the wheel path away from the longitudinal edges allows the thin 3-in. section to handle loads more efficiently. According to common theory in whitetopping design, if panel sizes are small, curling stresses will be reduced and the panels will deflect uniformly downward under the load. The performance of test cells 93 and 94 clearly demonstrate that a panel size of 4-ft by 4-ft is not a good design for high-volume traffic applications. Test cell 95 exhibited a fair amount of corner cracking on panel corners nearest the shoulder. This was true for both the driving and passing lanes. As shown in Figure 2.15 and 2.16, the corner cracking is always initiated on the approach side of the panel. Test cell 95 also had a small number of reflective cracks that grew large enough to warrant patching.



*Figure 2.15: Corner cracking on the outside edge of test cell 95, for driving lane, November 2003*



*Figure 2.16: Corner cracking on the outside edge of test cell 95, for passing lane, November 2003*

The performance history of different UTW test cells at MnROAD shows some variation in distress type and distress level. Test cells 93 and 94 developed severe corner cracking under the wheelpaths on the driving lane. Test cell 95 developed most cracking in the panels on the driving lane near the shoulder. Reflective and load-related cracking were common on all test cells. All three test cells provided over 5 years of serviceability before reconstruction.

Findings related to performance analysis for MnDOT test cells show that joint spacing has a significant effect on performance. Additionally, corner cracking appears to be the primary



failure mode, and fatigue cracking is believed to be the primary failure mechanism. Analysis also shows that bonding is an important factor to long-term performance. Ultra thin whitetopping provides small joint spacing to minimize restraint stress. However, joint locations and traffic loading should be given significant consideration. In the stress-reduction mechanism by bonding, debonding between layers always occurred near panel edges or cracks. The bond between layers was found to be intact near the center of panels.

## **2.3 Colorado**

Four thin whitetopping test sections were constructed between 1996 and 2001 in Colorado. The first two were constructed on US 85 and SH 119 in 1996. The third was constructed on US 287 in 1997 and the fourth section was constructed on SH 121 in 2001. Many variables were considered in the Colorado DOT test sections. These variables include concrete thickness, slab size, asphalt thickness, asphalt surface preparation and the use of dowel and tie bars. Each site had multiple test sections and test slabs. Field testing was conducted at four different sites between 1996 and 2003. The tests were carried out to verify and revise design guidelines for bonded whitetopping pavement systems. The evaluation of the existing asphalt pavement condition prior to the thin whitetopping construction was performed including a visual condition survey, rutting measurements, coring, and falling weight deflectometer (FWD) testing.

Table 2.5 presents a summary of the test sections and certain section characteristics. Approximate traffic levels of AADT (Annual Average Daily Traffic) were used for each test section. The AADT level included 1,500 (25% truck), 19,760 (8% truck), 2,287 (59% truck), and 44,562 (3% truck) for US 85, SH 119, US 287, and SH 121, respectively.

**Table 2.5: Test Slab Characteristics and Test Results**

Site	Test Slab	PCC Thickness, in	AC Thickness, in	Long. Joint Spacing, in	Trans. Joint Spacing, in	AC Resilient Modulus	AC Surface Condition	Subgrade Modulus, pci
US 85 Santa Fe	1	4.7	4.5	60	60	350,000	New	150
	2	5.8	5.9	60	60		New	
	3	6.0	5.4	60	60		New Milled	
SH 119 Longmont	1	5.1	3.3	72	72	800,000	Existing	340
	2	5.4	4.6	120	144		New	
	3	6.3	3.4	72	72		New	
	4	7.3	3.4	72	144		Existing Milled	
	5	6.8	2.8	144	144		Existing Milled	
US 287 Lamar	B	7.4	7.6	144	120	800,000	Existing Milled	225
	E	6.8	6.6	72	72			
	F	5.6	6.6	72	72			
SH 121 Wadsward	1	4.1	5.3	48	48	398,000	Existing Milled	500
	2	4.4	5.5	72	72	288,000		
	3	7.0	4.6	72	108	334,000		
	4	6.3	5.0	72	72	394,000		

Three test sections, out of four, were examined for overall pavement performance during June 2003, after 7 years of service. The task included crack mapping, core sampling, faulting measurements, joint width measurements, photographs, and FWD testing.

The overall condition of the US 85 test section was very good. Isolated longitudinal cracks were observed and a few corner cracks and transverse shrinkage cracks appeared to be located over longitudinal joint tie bars. Figures 2.17 and 2.18 present typical pavement conditions and a distressed area for US 85 test section.



*Figure 2.17: Typical Pavement Condition*



*Figure 2.18: Distressed Area at Stop Sign Approach*



One hundred thirty-one panels were surveyed on the SH 119 test section, 107 of which suffered some cracking. These cracks were filled with asphalt sealant. In addition to the longitudinal panel cracks in Section No. 2 of the SH 119 test section, the most frequent distress observed was minor joint spalling at various locations along the test sections. However, the overall ride quality was qualitatively rated as excellent and the overall pavement condition was very good. Figures 2.19 and 2.20 present typical pavement condition, including slab cracking in section No. 2.



*Figure 2.19: Typical Pavement Condition*



*Figure 2.20: Slab Cracking Filled with Asphalt Sealant*

The most frequent distress observed in the US 287 test section was minor transverse joint spalling. In addition, isolated longitudinal cracking was observed in one of the 6-ft by 6-ft slab test sections. Approximately 33 of the 200 slabs surveyed were cracked. Many of the cracks observed in this section appeared to be located in the outside wheel path. The overall ride quality was qualitatively rated as excellent, and the overall condition was also very good. Figures 2.21 and 2.22 show typical pavement conditions and cracked slabs.



*Figure 2.21: Typical Pavement Condition*



*Figure 2.22: Cracked Slabs*

## **2.4 Summary of Distress**

Based on the study findings, partially bonded systems should be considered in the whitetopping design procedure. A good bond between concrete and asphalt is essential for successful whitetopping performance. It is recommended that joint spacing for thin whitetopping pavements be 6 ft in both directions. At joint spacings greater than 4 ft, the temperature gradient in the concrete layer increases the load-induced tensile stress. Dowel bars at transverse contraction joints are not critical to attain satisfactory thin whitetopping pavement performance based on the performance of existing Colorado thin whitetopping test sections. Long-term monitoring is needed to determine the effect of load transfer devices.



## Chapter 3. In-Depth Literature Review on Design Procedures

### 3.1 Colorado Design Procedure

The Colorado design procedures for whitetopping and UTW were published in 1998 and 2004. The reports describe a slightly thicker slab (4 to 8 in.) and wider joint spacing (up to 12 ft) than thin whitetopping. The reports suggest a guideline for the thickness design of bonded whitetopping pavement in the state of Colorado. In this report, the Colorado Department of Transportation (CDOT) performed laboratory testing and field testing at three different sites.

The objectives of the field testing were to identify the critical load location, the effects of AC surface preparation, the response of whitetopping pavements to traffic loading, the interface bonding strength, the effect of pavement age on load-induced stresses, and the calibration of design guidelines developed. Laboratory tests were conducted on compressive strength, modulus of elasticity, and flexural strength after casting concrete cylinders and beams at test sites. Cores were used to measure thickness. Direct shear testing was performed to determine the interface shear strength between the concrete and asphalt layers.

#### 3.1.1 Determination of Critical Load Location

The critical load location was determined by comparing the stress data collected for each load position. The highest tensile stress was determined when the load was centered along a longitudinal free-edge joint. Figure 3.1 shows the location of load resulting in maximum stress.

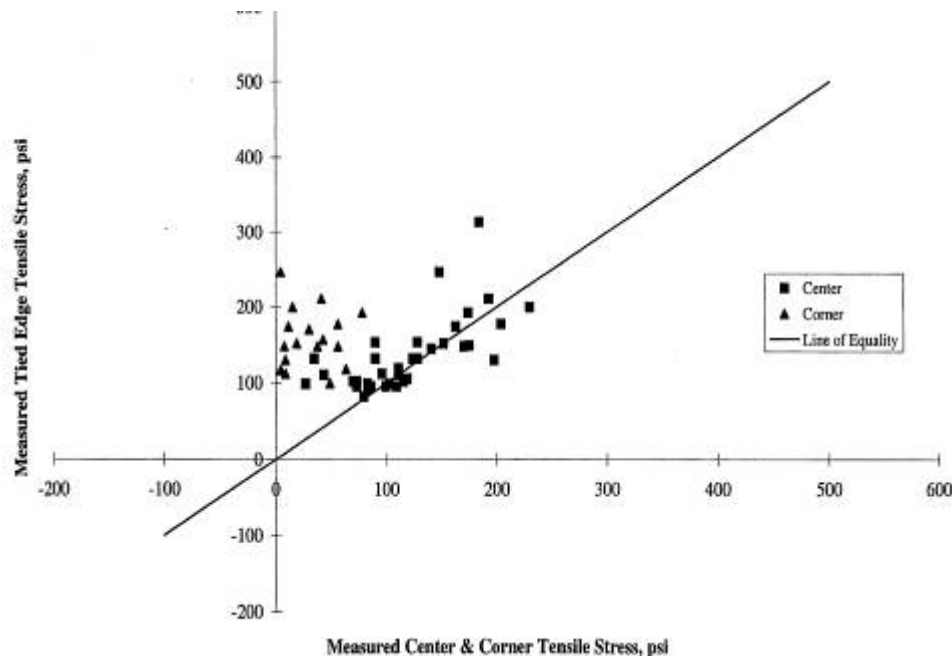


Figure 3.1: Location of Load Resulting in Maximum Stress

### 3.1.2 Determination of Load-Induced Stress at Zero Temperature Gradient

Zero temperature gradient stresses were compared with theoretically derived stresses. This comparison was to allow for a partial bond calibration factor to be applied to fully bonded theoretical stresses.

#### *Analysis of the Effect of Bond Interface on Load-Induced Concrete Stress*

Stresses caused by loads at mid-joint and slab corner were computed using the finite element computer program ILLISLAB (ILSL2), assuming fully bonded concrete-asphalt interface. Partial bond stresses were measured at tied edges. These stresses were greater than theoretically calculated stresses. Equations 3.2 and 3.3 represent the original and revised models respectively, while Figure 3.2 show the calculated stresses using both the original and revised models.

$$\text{1998 Original Model } \sigma_{ex} = 1.65 \times \sigma_{th} \quad (3.2)$$

$$\text{2004 Adjusted Model } \sigma_{ex} = 1.51 \times \sigma_{th} \quad (3.3)$$

where,

$\sigma_{ex}$  = the experimental stress, and

$\sigma_{th}$  = the theoretical stress.

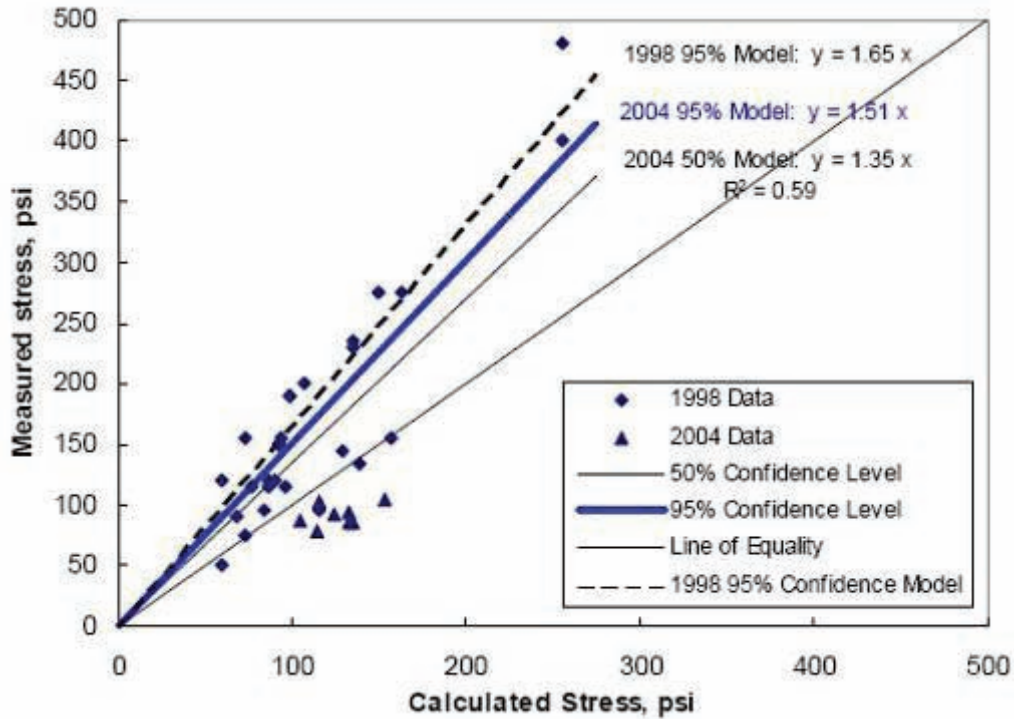


Figure 3.2: Increase in Critical Load Stress Due to Partial Bonding Condition

### 3.1.3 Analysis of the Effect of Interface Bond on Load-Induced Asphalt Strain

Prior to construction, strain gages were placed at the surface of the asphalt and the bottom of the concrete. There is approximately a 10% loss of strain transfer from the concrete to the asphalt due to the partial bond between the layers. This shows a decrease of 15% from the readings determined in the original study. Figure 3.3 shows a comparison of asphalt and concrete strains for the tied edge loading case. The equations representing the loss of strain are as follows:

$$1998 \text{ Original Model } \varepsilon_{ac} = 0.842 \times \varepsilon_{pcc} \quad (3.4)$$

$$2004 \text{ Adjusted Model } \varepsilon_{ac} = 0.897 \times \varepsilon_{pcc} - 0.776 \quad (3.5)$$

where,

$\varepsilon_{ac}$  = measured asphalt surface strain, microstrain, and

$\varepsilon_{pcc}$  = measured concrete bottom strain, microstrain.

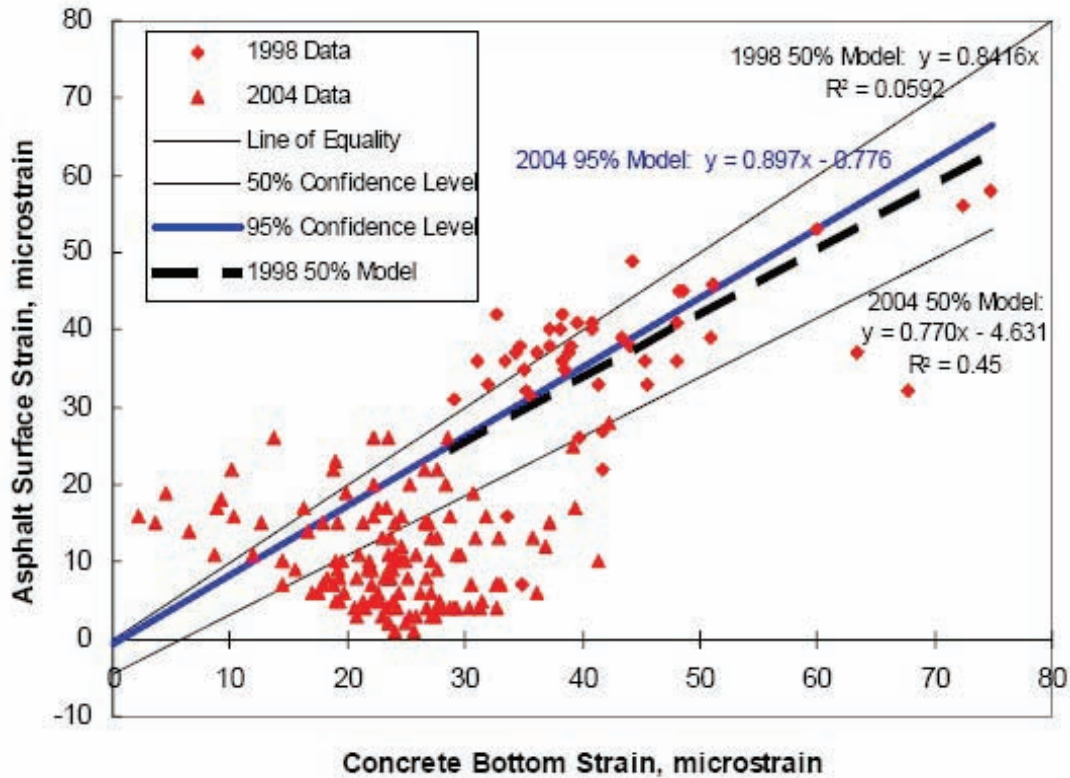


Figure 3.3: Asphalt Surface Strain vs. Concrete Bottom Strain

### 3.1.4 Analysis of Temperature Effects on Load-Induced Stresses

Temperature gradients throughout load testing ranged from -2 to 6° F/in. Figure 3.4 shows the percent change in measured stress over the range of temperature gradients tested. The relationships derived between the change in stress and measured temperature gradient are as follows:

$$1998 \text{ Original Model } \sigma_{\%} = 4.56 \times \Delta_T \quad (3.6)$$

$$2004 \text{ Adjusted Model } \sigma_{\%} = 3.85 \times \Delta_T \quad (3.7)$$

where,

$\sigma_{\%}$  = percent change in stress from zero gradient, and

$\Delta_T$  = the change in temperature.

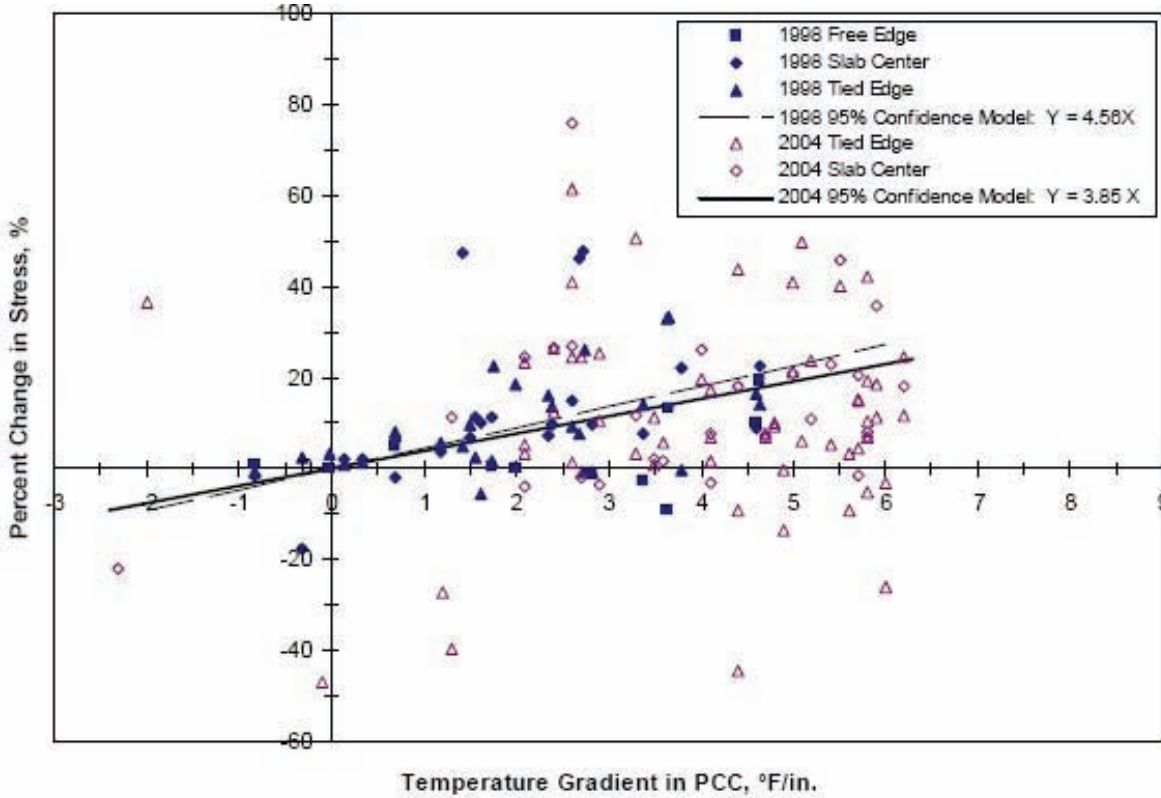


Figure 3.4: Increase in Load Stress Due to Curling Loss of Support

### 3.1.5 Development of Revised Design Equations

Stress calculations were conducted using the finite element program ILLISLAB (ILSL2). Curling and warping restraint stresses were not incorporated into the parametric analysis. Prediction equations were derived for computing design concrete flexural stresses and asphalt flexural strains. Table 3.1 lists the combinations of parameters. The derived equations and revised equations were as follows:

#### 1998 Original Prediction Equations for Design Stresses and Strains

Concrete Stress for 20-kip single axle load (SAL)

$$\sigma_{pcc} = 919 + \frac{18492}{l_e} - 575.3 \log k + 0.000133 E_{ac} \quad (3.8)$$



Concrete Stress for 40-kip tandem axle load (TAL)

$$\sigma_{pcc} = 671.2 - 0.000099E_{ac} - 437.1 \log k + \frac{1.582 \times 10^4}{l_e} \quad (3.9)$$

Asphalt Strain for 20-kip SAL

$$\frac{1}{\epsilon_{ac}} = 8.51114 \times 10^{-9} E_{ac} + \frac{0.008619 l_e}{L} \quad (3.10)$$

Asphalt Strain for 40-kip TAL

$$\frac{1}{\epsilon_{ac}} = 9.61792 \times 10^{-9} E_{ac} + \frac{0.009776 l_e}{L} \quad (3.11)$$

where,

- $\sigma_{pcc}$  = maximum stress in the concrete slab, psi
- $\epsilon_{ac}$  = maximum strains at bottom of asphalt layer, microstrain
- $E_{pcc}$  = concrete modulus of elasticity, assumed 4 million psi
- $E_{ac}$  = asphalt modulus of elasticity, psi
- $t_{pcc}$  = thickness of the concrete layer, in.
- $t_{ac}$  = thickness of the asphalt layer, in.
- $\mu_{pcc}$  = Poissons ratio for the concrete, assumed 0.15
- $\mu_{ac}$  = Poissons ratio for the asphalt, assumed 0.35
- $k$  = modulus of subgrade reaction, pci
- $l_e$  = effective radius of relative stiffness for fully bonded slabs, in.

$$l_e = \sqrt[4]{\frac{E_{PCC}(t_{PCC}^3/12 + t_{PCC}(NA - t_{PCC}/2)^2)}{k(1 - \mu_{PCC}^2)} + \frac{E_{AC}(t_{AC}^3/12 + t_{AC}(t_{PCC} - NA + t_{AC}/2)^2)}{k(1 - \mu_{AC}^2)}}$$

$NA$  = neutral axis from top of concrete slab, in.

$$NA = \frac{E_{PCC} \frac{t_{PCC}^2}{2} + E_{AC} t_{AC} (t_{PCC} + \frac{t_{AC}}{2})}{E_{PCC} t_{PCC} + E_{AC} t_{AC}}, \text{ and}$$

$L$  = joint spacing, in.

#### 2004 Revision of the Stresses and Strain Prediction Design Equations

Concrete Stress for 20-kip SAL

$$(\sigma_{pcc})^{1/2} = 18.879 + 2.918 \frac{t_{pcc}}{t_{ac}} + \frac{425.44}{l_e} - 6.955 \times 10^{-6} E_{ac} - 9.0366 \log k + 0.0133L \quad (3.12)$$

Concrete Stress for 40-kip TAL

$$(\sigma_{pcc})^{1/2} = 17.669 + 2.668 \frac{t_{pcc}}{t_{ac}} + \frac{408.52}{l_e} - 6.455 \times 10^{-6} E_{ac} - 8.3576 \log k + 0.00622L \quad (3.13)$$

Asphalt Strain for 20-kip SAL

$$(\epsilon_{ac})^{1/4} = 8.224 - 0.2590 \frac{t_{pcc}}{t_{ac}} - 0.04419 l_e - 6.898 \times 10^{-7} E_{ac} - 1.1027 \log k \quad (3.14)$$

### Asphalt Strain for 40-kip TAL

$$(\epsilon_{ac})^{1/4} = 7.923 - 0.2503 \frac{t_{pcc}}{t_{ac}} - 0.04331 l_e - 6.746 \times 10^{-7} E_{ac} - 1.0451 \log k \quad (3.15)$$

where,

- $\sigma_{pcc}$  = maximum stress in the concrete slab, psi,
- $\epsilon_{ac}$  = maximum strains at bottom of asphalt layer, microstrain,
- $E_{pcc}$  = concrete modulus of elasticity, assumed 4 million psi,
- $E_{ac}$  = asphalt modulus of elasticity, psi,
- $t_{pcc}$  = thickness of the concrete layer, in,
- $t_{ac}$  = thickness of the asphalt layer, in,
- $\mu_{pcc}$  = Poissons ratio for the concrete, assumed 0.15,
- $\mu_{ac}$  = Poissons ratio for the asphalt, assumed 0.35,
- $k$  = modulus of subgrade reaction, pci,
- $l_e$  = effective radius of relative stiffness for fully bonded slabs, in,

$$= \sqrt[4]{\frac{E_{PCC}(t_{PCC}^3/12 + t_{PCC}(NA - t_{PCC}/2)^2)}{k(1 - \mu_{PCC}^2)} + \frac{E_{AC}(t_{AC}^3/12 + t_{AC}(t_{PCC} - NA + t_{AC}/2)^2)}{k(1 - \mu_{AC}^2)}}$$

$NA$  = neutral axis from top of concrete slab, in,

$$= \frac{E_{PCC} \frac{t_{PCC}^2}{2} + E_{AC} t_{AC} (t_{PCC} + \frac{t_{AC}}{2})}{E_{PCC} t_{PCC} + E_{AC} t_{AC}}, \text{ and}$$

$L$  = joint spacing, in.

**Table 3.1: Combinations of Parameters**

Parameters	Original 1998	Adjusted 2004
Joint spacing	48, 72, and 144 in.	48, 72, and 144 in.
Concrete slab thickness	4, 5, and 6 in.	4, 5, 6, and 7 in.
Asphalt thickness	3, 6, and 9 in.	3, 6, and 9 in.
Concrete elastic modulus	4 million psi	4 million psi
Asphalt elastic modulus	0.05, 0.5, and 1 million psi	0.05, 0.25, 0.5, 0.75 and 1 million psi
Concrete Poisson's ratio	0.15	0.15
Asphalt Poisson's ratio	0.35	0.35
k-value	75, 200, and 400 pci	50, 150, 300, and 500 pci
Truck axle configuration	SAL and TAL	SAL and TAL
Slab loading locations	Corner & Long. Edge	Corner & Long. Edge

### 3.1.6 Mechanistic Whitetopping Thickness Design Procedure

The design of whitetopping pavement should be determined considering material properties and design parameters. The design procedure is explained in 12 steps. Parameters required include percentage fatigue life of the existing asphalt pavement and assumed concrete slab thickness. Also, material properties needed are the existing modulus of subgrade reaction, temperature differential (temperature gradient; °F/in.), joint spacing, modulus of elasticity, thickness, and Poisson's ratio of asphalt and concrete, and modulus of rupture of concrete. A brief summary for thickness design procedures follows.

- (1) Design parameters,  $l_e$  and  $L/l_e$  are determined, then the load-induced critical concrete stresses and asphalt strains are calculated using developed equation for anticipated 20-kip single axle loads (SAL) and 40-kip tandem axle loads (TAL).
- (2) Computed fully bonded concrete stresses and asphalt strains are adjusted using equations for the partial bond condition. The adjusted concrete stresses are computed for the loss of support due to temperature-induced concrete slab curling again.
- (3) Fatigue analyses for concrete stresses and asphalt strains are conducted separately.
- (4) Concrete thickness and joint spacing are determined so that they meet the fatigue failure criteria. If not, the previous steps are repeated until they satisfy fatigue failure criteria.

Figure 3.5 exhibits the flow chart of the concrete thickness design procedure developed in Colorado.

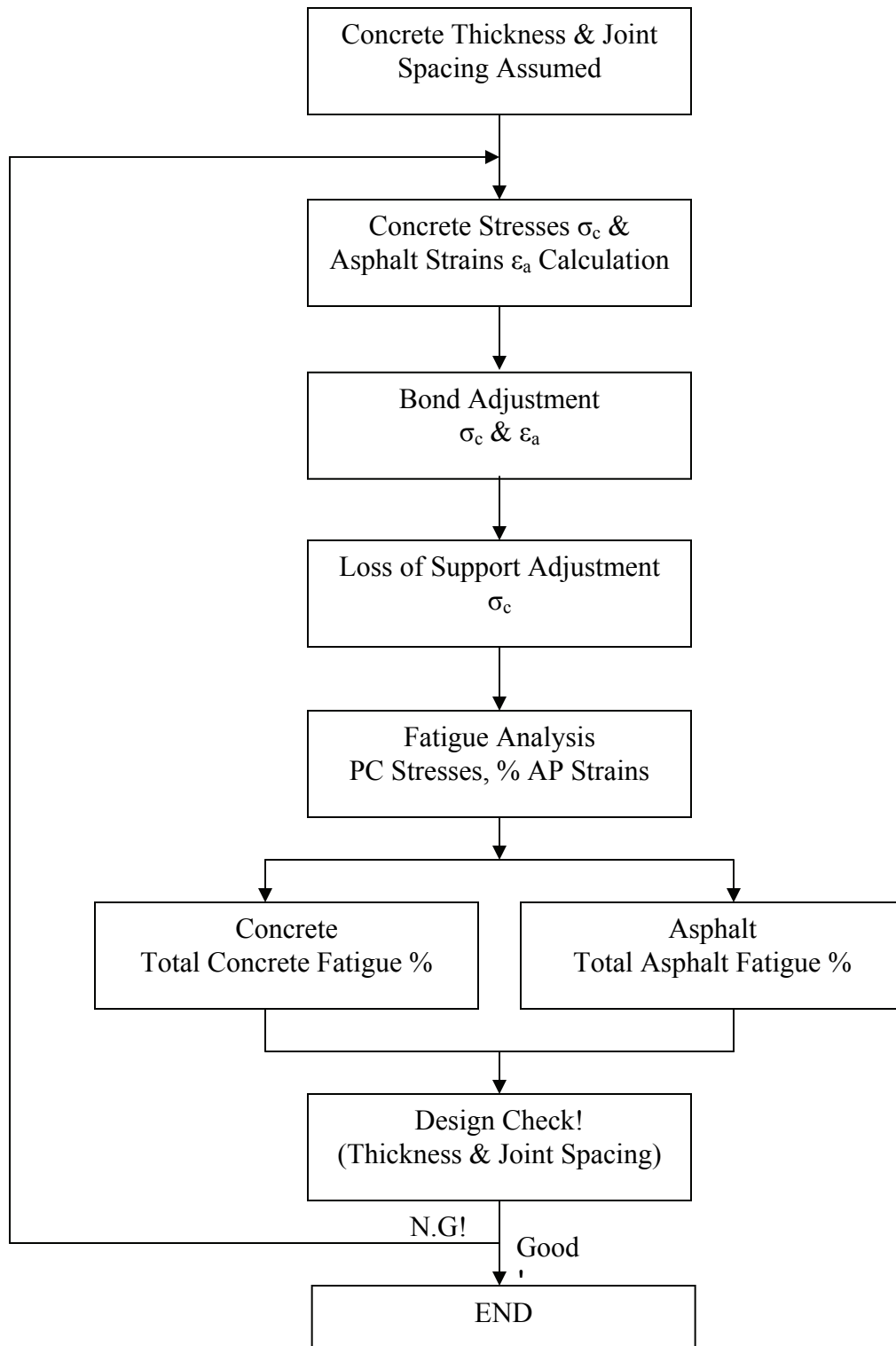


Figure 3.5: Flow Chart for Colorado Design Procedure

### **3.1.7 Sensitivity Analysis**

Sensitivity analyses were conducted for asphalt thickness, modulus of subbase/subgrade reaction, asphalt modulus of elasticity, concrete flexural strength and the expected number of 18-kip equivalent single axle loads (ESALs).

The 1998 study was sensitive to the modulus of subbase/subgrade reaction, but the 2004 study is much less sensitive to subgrade modulus. The 1998 study appeared to be fairly sensitive at very low asphalt moduli (50,000 psi), and there appeared to be a minimum asphalt thickness of about 5 inches. However, the 2004 sensitivity analysis shows more consistency with the general relationship than is expected between concrete thickness and asphalt modulus.

The thickness is slightly sensitive to the flexural strength of concrete. The thickness, however, was not sensitive to anticipated concrete temperature gradients. Required concrete thicknesses based on the 1998 study were not sensitive to the number of ESALs above 1 million except under various levels of asphalt modulus of elasticity. The 2004 revised design procedure is more sensitive to traffic levels for each of the design variables.

## **3.2 ACPA Design Procedure**

The design and construction of conventional whitetopping and ultra-thin whitetopping are presented in this report. Four factors are considered in the structural design of concrete pavement, including the following: supporting strength of the existing asphalt pavement; flexural strength of the concrete; design period (the expected service life of the pavement before any major structural rehabilitation is required); and amount of truck traffic expected.

### **3.2.1 Support provided by the existing asphalt pavement**

The support at the top of asphalt is determined by the k-value of the subgrade ( $k_s$ ), the thickness of granular or cement-treated base, and the layer thickness of the existing asphalt. Figures 3.6 and 3.7 show the chart to estimate the k-value on top of the existing asphalt pavement according to base types.

The k-value of the subgrade ( $k_s$ ) is usually determined by a plate load test, but can be calculated with a falling weight deflectometer (FWD). Also, approximate k-values for soil types are shown in Table 3.2.

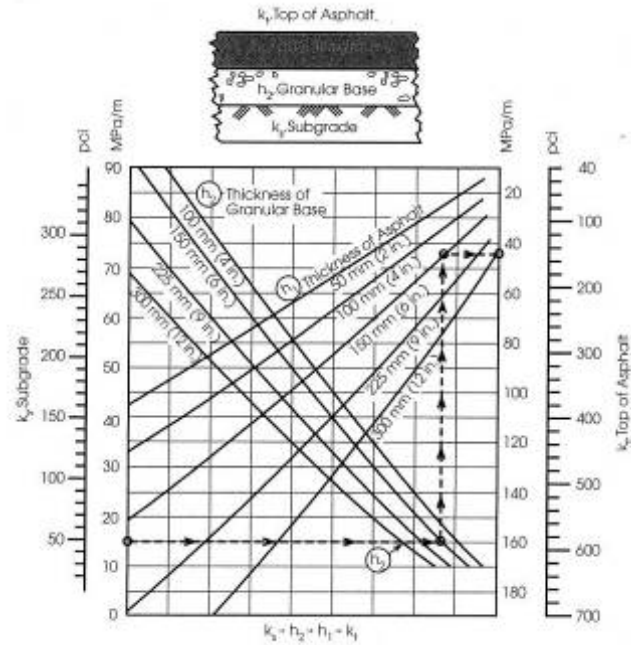


Figure 3.6: K-value on top of asphalt pavement with granular base

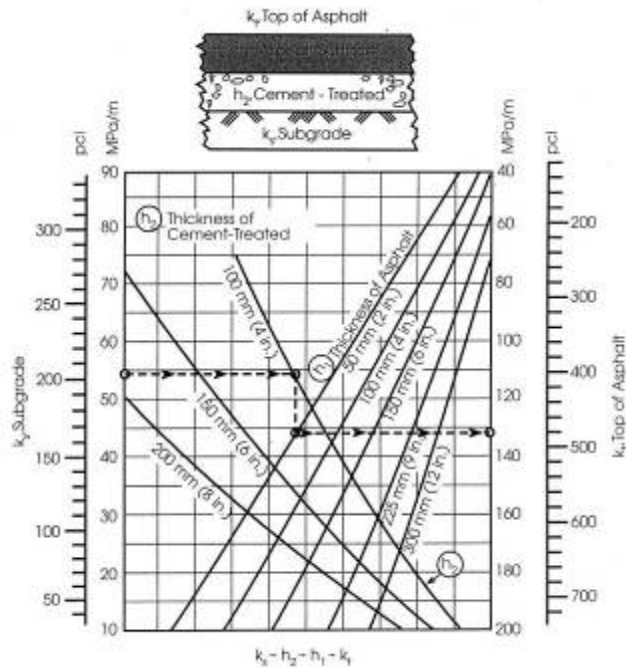


Figure 3.7: K-value on top of asphalt pavement with cement-treated base.

**Table 3.2: Subgrade Soil Types and Approximate k-value**

<i>Type of Soil</i>	<i>Support</i>	<i>k, MPa (pci)</i>	<i>CBR, %</i>	<i>R</i>
Fine-grained soils in which silt and clay-size particles predominate	Low	20-30 (75-120)	2.5 – 3.5	10 - 22
Sand and sand-gravel mixtures with moderate amount of silt and clay	Medium	35-45 (130-170)	4.5 – 7.5	29 - 41
<b>Sand and sand-gravel mixtures relatively free of plastic fines</b>	High	50-60 (180-2200)	8.5 - 12	45 - 52

CBR = California Bearing Ratio, ASTM D 1183

R = Resistance R-Value, ASTM D2844

### 3.2.2 Flexural Strength Design Value for Concrete

Flexural strength design value for concrete pavement is considered to be the value measured at 28 days. However, if the compressive strength of concrete is tested, the following equation, which is an approximate relationship between flexural and compressive strength, may be used.

$$f_r = C(f_{cr}')^{0.5} \quad (3.16)$$

where,

$f_r$  = flexural strength (modulus of rupture) MPa (psi),

C = a constant, 0.75 metric (9 U.S.), and

$f_{cr}$  = compressive strength, MPa (psi).

### 3.2.3 Truck Traffic

Truck traffic considered in the design is the weight and number of daily repetitions. Other vehicles in the traffic stream are not considered. In the design table, the number of trucks, expressed as “trucks per day per lane,” indicates how many load repetitions per day are applied on the pavement.

### 3.2.4 Design Period

Design period is generally considered 20 years; it may be longer or shorter depending on the expected use of the facility. In this publication, the design period is 20 years.

### 3.2.5 Determination of Pavement Thickness

Slab thickness is determined by the amount of truck traffic, flexural strength of concrete, and support strength (k-value) on top of existing asphalt pavement. The ACPA design procedure is represented in Tables 3.3 and 3.4 for two traffic categories. One is for light to medium truck traffic. The other is for heavy truck traffic. The table shows that if the flexural strength of concrete and traffic are constant, then the slab thickness depends on the support reaction on top of existing asphalt pavement. Therefore, it is important to determine an accurate support reaction k-value of the existing asphalt pavement.

**Table 3.3: Slab Thickness, Light to Medium Truck Traffic**

Trucks per day per lane	Design flexural strength, psi (average)	k-value, pci									
		700		500		300		200		100	
2	650	4.5	(4.0)	4.5	(4.0)	5.0	(4.0)	5.5	(4.5)	6.0	(5.0)
	600	4.5	(4.0)	5.0	(4.0)	5.5	(4.5)	5.5	(4.5)	6.0	(5.0)
	550	5.0	(4.0)	5.5	(4.5)	5.5	(5.0)	6.0	(5.0)	6.5	(5.5)
10	650	4.5	(4.0)	5.0	(4.0)	5.5	(4.5)	5.5	(4.5)	6.0	(5.0)
	600	5.0	(4.0)	5.0	(4.5)	5.5	(4.5)	6.0	(5.0)	6.5	(5.5)
	550	5.5	(4.5)	5.5	(4.5)	6.0	(5.0)	6.5	(5.5)	7.0	(6.0)
40	650	5.0	(4.0)	5.0	(4.5)	5.5	(4.5)	6.0	(5.0)	6.5	(5.5)
	600	5.0	(4.5)	5.5	(4.5)	6.0	(5.0)	6.0	(5.0)	7.0	(6.0)
	550	5.5	(4.5)	6.0	(5.0)	6.5	(5.5)	6.5	(5.5)	7.5	(6.0)

Dowels are not required

( ) = pavement with edge support

Min. thickness = 4 in

**Table 3.4: Slab Thickness, Heavy Truck Traffic**

Trucks per day per lane	Design flexural strength, psi (average)	k-value, pci									
		700		500		300		200		100	
80	650	7.0	(6.0)	7.0	(6.0)	7.5	(6.5)	<b>8.0</b>	(7.5)	<b>9.0</b>	(7.5)
	600	7.0	(6.5)	7.5	(6.5)	<b>8.0</b>	(7.0)	<b>8.5</b>	(7.5)	<b>9.5</b>	(8.0)
	550	7.5	(6.5)	<b>8.0</b>	(7.0)	<b>8.5</b>	(7.5)	<b>9.0</b>	(8.0)	<b>10.0</b>	(8.5)
400	650	7.5	(7.0)	<b>8.0</b>	(7.0)	<b>8.0</b>	(7.5)	<b>8.5</b>	(7.5)	<b>9.5</b>	(8.0)
	600	7.5	(7.0)	<b>8.0</b>	(7.0)	<b>8.5</b>	(7.5)	<b>9.0</b>	(8.0)	<b>10.0</b>	(8.5)
	550	<b>8.0</b>	(7.0)	<b>8.5</b>	(7.5)	<b>9.0</b>	(8.0)	<b>9.5</b>	(8.5)	<b>10.5</b>	(9.5)
1200	650	<b>7.5</b>	(7.5)	<b>8.0</b>	(8.0)	<b>8.5</b>	(8.0)	<b>9.0</b>	(8.0)	<b>9.5</b>	(8.5)
	600	<b>8.0</b>	(7.5)	<b>8.5</b>	(8.0)	<b>9.0</b>	(8.5)	<b>9.5</b>	(8.0)	<b>10.5</b>	(9.0)
	550	<b>8.5</b>	(7.5)	<b>9.0</b>	(8.0)	<b>9.5</b>	(8.5)	<b>10.0</b>	(8.5)	<b>11.0</b>	(9.5)

**Bold = doweled joint**, normal = undoweled joint

( ) = pavement with edge support



### **3.3 New Jersey Design Procedure**

The objective of this research study was to identify and address important factors that contribute to the performance of the UTW pavement system. The field testing of a UTW ramp that was constructed in New Jersey began in 1994. The testing was conducted using a Heavy Weight Deflectometer (HWD), Falling Weight Deflectometer (FWD), and Dynamic Cone Penetrometer (DCP). In addition, a visual survey was conducted and pavement cores were tested. The performance of this UTW pavement was studied using a 3-Dimensional Finite Element Model (FEM). An interim design procedure was developed based on the experiences gained from field testing and the Finite Element Model.

#### **3.3.1 Field Testing**

Ultra-thin whitetopping pavement was constructed by New Jersey DOT (NJDOT) in August of 1994. Preparatory measures included milling the distressed bituminous surface. An average of three inches of milling was made prior to the placement of UTW. The panel sizes were 3-ft by 3-ft, 4-ft by 4-ft, and 6-ft by 6-ft.

Non-destructive testing using HWD and FWD was performed on a total of 45 locations—29 locations on 3-ft by 3-ft panels, 10 locations on 4-ft by 4-ft panels, and 6 locations on 6-ft by 6-ft panels. Deflection data was analyzed in order to determine the in-situ layer stiffnesses and load transfer capability of the saw cut joints. Dynamic Cone Penetrometer (DCP) testing was performed to obtain a continuous reading of California Bearing Ratio (CBR) with depth.

A visual survey was carried out in order to determine the areas of significant distress. The survey revealed that the major forms of visual distress for the pavement structure are cracking and corner breaking. ARAN equipment with automatic video was used to survey the pavement and measure its roughness. The data obtained was not available for review and may be used in conjunction with other findings in the field in the future.

A total of 10 pavement cores were taken. The thickness of UTW and AC for each core was recorded. Three of the extracted cores were debonded at the interface. Other cores showed a strong bond at the interface but were broken in the AC layer presumably due to the coring operation. The average UTW thickness was 3.8 in.

#### **3.3.2 Finite Element Analysis and Verification**

The modeling and analysis were performed by the SAP2000 structural analysis program. Figures 3.8 to 3.9 show the finite element modeling. The model describes a four-layer pavement consisting of the UTW, AC base, granular subbase, and the subgrade. Parameters investigated and their ranges are shown in Table 3.5.

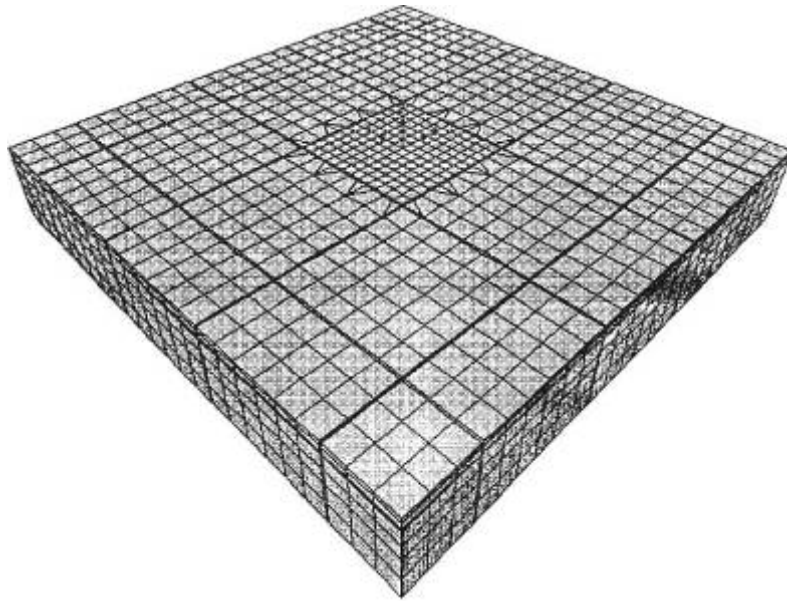


*Figure 3.8: Finite Element Model*

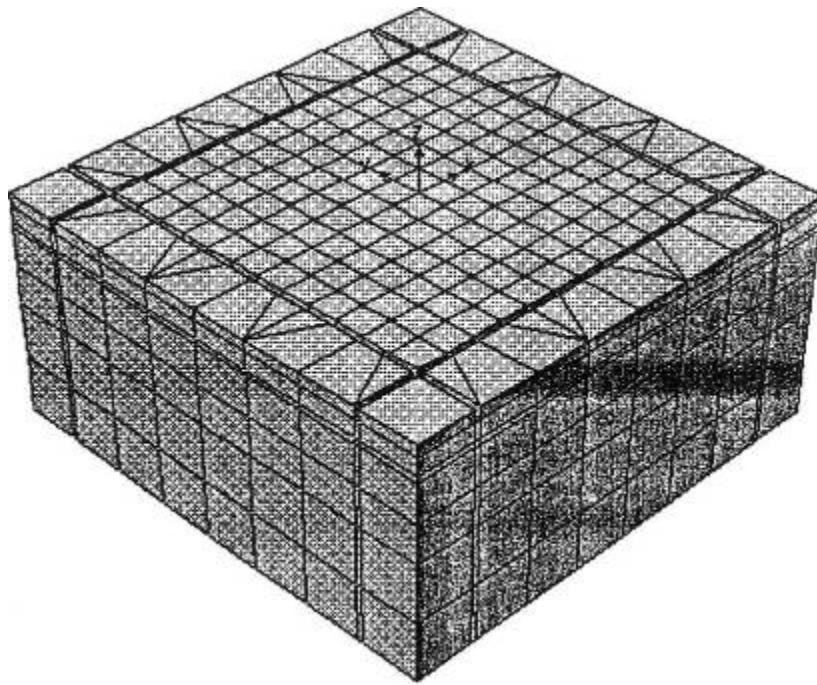


*Figure 3.9: Detail of the finite element model*

**Table 3.5: Parameters Investigated**

<i>Parameters</i>	<i>Range</i>
<b>UTW thickness</b>	3 to 5 in
<b>AC thickness</b>	4 to 8 in
<b>AC modulus of elasticity</b>	880 to 1660 ksi
<b>Subbase modulus of elasticity</b>	4.2 to 16.8 ksi
<b>Modulus of subgrade reaction</b>	145 to 580 pci
<b>UTW slab size</b>	3-ft×3-ft, 4-ft×4-ft
<b>Interface bonding</b>	from fully bonded to unbonded
<b>Joint width and depth</b>	0.5 in and 1/3 of the thickness

The Westergaard equation is used to verify the finite element model. The maximum flexural stress in the slab can be approximately expressed as:

$$\sigma = \frac{0.316P}{h^2} \left[ 4 \log \left( \frac{l}{b} \right) + 1.069 \right] \quad (3.17)$$

where,

$$\begin{aligned} P &= \text{the applied load,} \\ h &= \text{the slab thickness;} \\ b &= \text{the size of the resisting section of the slab} \\ &= \sqrt{1.6r^2 + h^2} - 0.675 && \text{if } r < 1.724h \\ &= r && \text{if } r \geq 1.724h \end{aligned}$$

Finally,  $l$  is the radius of relative stiffness.

$$l = \sqrt[4]{\frac{Eh^3}{12(1-\mu^2)k}} \quad (3.18)$$

where,

$$\begin{aligned} E &= \text{elastic modulus of concrete slab,} \\ \mu &= \text{Poisson's ratio of the slab, and} \\ k &= \text{the coefficient of subgrade reaction.} \end{aligned}$$

The results show that the maximum tensile stress for a 3-in. thick slab, modulus of 3400 ksi, Poisson's ratio of 0.15, subgrade reaction of 250 pci, and a 12,000-lb load with 50 psi air pressure is equal to 758 psi. The maximum tensile stress obtained from the finite element model is 785 psi.

### 3.3.3 Design Procedure

The following steps summarize the UTW design procedure.

#### *Step 1.*

Obtain the traffic data for the project and find the number of equivalent 18-kip single axle loads. The traffic data, which is a combination of different vehicles, is converted to an equivalent 18-kip single axle to be used in fatigue equations. Equations 3.19 and 3.20 are used for single axles and tandem axles, respectively.

$$W_{18} = \left( \frac{W_{SAL}}{18} \right)^{3.3} \quad (3.19)$$

where,

$W_{SAL}$  = the weight of single axle load, and

$W_{18}$  = the factor to convert a single axle weighing  $W_{SAL}$  to an equivalent 18-kips single axle load.

$$W_{18} = \left( \frac{TW_{TAL}}{2 \times 18} \right)^{3.3} \quad (3.20)$$

where,

$W_{TAL}$  = the weight of tandem axle load,

$T$  = tandem axle stress factor, and

$W_{18}$  = the factor to convert a tandem axle weighing  $W_{TAL}$  to an equivalent 18-kips single axle load.

It is recommended by AASHTO (1993) to use a safety factor by increasing the number of design ESALs based on the standard deviation of errors in traffic prediction and pavement performance in addition to the required design reliability.

$$W_D = 10^{-Z_R S_0} W_{18} \quad (3.21)$$

where,

$S_0$  = the overall standard deviation of errors in design, and

$Z_R$  = the standard normal deviate associated with design reliability.

#### *Step 2.*

Obtain the elastic modulus and thickness of the existing asphalt pavement, as well as the coefficient of the subgrade reaction using methods such as FWD.

#### *Step 3.*

Calculate the allowable tensile stress in AC using the fatigue equation developed by the Asphalt Institute and Portland Cement Association.

$$N = 0.058 \frac{E_a^{2.437}}{\sigma^{3.291}} \quad (3.22)$$

where,

- $N$  = the number of load repetition before failure (10% cracking),
- $E_a$  = asphalt elastic modulus (psi), and
- $\sigma$  = maximum tensile stress in asphalt (psi).

*Step 4.*

Assume a thickness for UTW and find the maximum tensile stress in AC using Equations 3.23 and 3.24 for both bonded and unbonded conditions. Based on the composite beam concept, the prediction equations for maximum tensile stress in AC with or without bond case were developed as follows.

$$\sigma_B^{AC} = \frac{CP(N.A. - h)}{I_B} \left[ C_1 \log\left(\frac{l}{b}\right) + C_2 \frac{N.A.}{a} + C_3 \right] \quad (3.23)$$

$$\sigma_U^{AC} = \frac{CPa}{2I_U} \left[ C_1 \log\left(\frac{l}{b}\right) + C_2 \frac{a}{h} + C_3 \right] \quad (3.24)$$

where,

- $\sigma_B^{AC}$  = maximum tensile stress in AC for boned condition (psi),
- $\sigma_U^{AC}$  = maximum tensile stress in AC for unbonded condition (psi),
- $P$  = applied load (lbs)
- $C$  = construction joint factor,
- $C_1, C_2, C_3$  = calculation constants,
- $N.A.$  = depth of the neutral axis from the top surface (in.),
- $h$  = total thickness (in.),
- $l$  = radius of relative stiffness (in.),
- $b$  = slab width (in.),
- $a$  = asphalt thickness (in.),
- $I_B$  = section moment of inertia for bonded section (in.<sup>3</sup>),
- $I_U$  = section moment of inertia for unbonded section (in.<sup>3</sup>),

*Step 5.*

Compare the maximum tensile stress in AC against the allowable stress from Step 3.

*Step 6.*

Repeat Steps 4 and 5 until the allowable stress and maximum tensile stress are equal.

Step 7.

Calculate the maximum tensile stress in UTW due to both axle load and temperature differentials from the following equations.

$$\sigma_B^{UTW} = \frac{CPn(N.A. - c)}{I_B} \left[ C_1 \log\left(\frac{l}{b}\right) + C_2 \frac{N.A.}{c} + C_3 \right] \quad (3.25)$$

$$\sigma_U^{UTW} = \frac{CnPc}{2I_U} \left[ C_1 \log\left(\frac{l}{b}\right) + C_2 \frac{c}{h} + C_3 \right] \quad (3.26)$$

$$\sigma_T = CE_c \alpha \Delta T \left[ C_4 \frac{c}{l} + C_5 \right] \quad (3.27)$$

where,

- $\sigma_B^{UTW}$  = maximum tensile stress in UTW for bonded condition (psi),
- $\sigma_U^{UTW}$  = maximum tensile stress in UTW for unbonded condition (psi),
- $\sigma_T$  = stress due to temperature differentials (psi),
- $P$  = applied load (lbs),
- $N$  = the ratio of elastic modulus of concrete to that of asphalt,
- $C$  = construction joint influence factor (about 1.1),
- $C_1, C_2, C_3, C_4, C_5$  = calculation constants,
- $c$  = thickness of concrete (in.),
- $N.A.$  = depth of the neutral axis from the top surface (in.),
- $h$  = total thickness (in.),
- $l$  = radius of relative stiffness (in.),
- $b$  = slab width (in.),
- $\alpha$  = coefficient of thermal expansion (°F/in/in),
- $I_B$  = section moment of inertia for bonded section (in<sup>3</sup>), and
- $I_U$  = section moment of inertia for unbonded section (in<sup>3</sup>).

Step 8.

Obtain the stress ratio SR in the UTW and determine the maximum allowable number of load repetitions using the following equations.

$$SR > 0.55, N = 10^{12.1(0.972 - SR)} \quad (3.28)$$

$$SR > 0.45, N = \left( \frac{4.258}{SR - 0.4325} \right)^{3.268} \quad (3.29)$$

where,

- $N$  = allowable number of load repetitions to failure, and
- $SR$  = maximum stress ratio.

*Step 9.*

If the UTW fatigue criterion indicates a smaller number of ESALs than  $W_D$ , increase the UTW thickness and repeat Steps 4 to 9.

*Step 10.*

Choose the final UTW thickness by comparing bonded and unbonded design process.

### **3.4 PCA Design Procedure**

The Portland Cement Association design procedure was developed by the Construction Technology Laboratories, Inc. In order to develop this design procedure, a three-dimensional finite element method developed. The model was calibrated and verified from field data collected in Missouri and Colorado. The Three-dimensional Finite Element Method (3D FEM) was used to correct factors used in the Two-dimensional Finite Element Method (2D FEM) and, therefore, to simplify the derived prediction equations. This collaboration procedure is explained in the following subsections.

#### **3.4.1 Development of the 3D FEM**

The model was developed using the NISA STATIC finite element package. A total of nine slabs were simulated in a 3 by 3 arrangement. Spring elements were used at the UTW joints to simulate load transfer and interface between the HMA and the UTW. In order to assess the sensitivity of the model inputs, a parametric evaluation was performed—including center and edge loading conditions with and without cracks—in the HMA layer (the fully bonded, partially bonded, and unbonded cases).

#### **3.4.2 Verification of the 3D FEM**

In order to verify the developed model, field data from Missouri and Colorado were used. The measured stresses in the UTW in unbonded slabs were approximately 14 to 34% higher than the fully bonded 3D FEM simulation. It should be noted that only one correction was made to the FEM model to account for partial bonding.

#### **3.4.3 Development of a Modified 2D FEM and Prediction Equations**

The ILSL2 2D finite element program was used to simplify the development of the design procedure. Multiple linear regression was used to derive relationships between the measured response from the 2D and 3D models. The developed equations for the prediction of the responses are stated as follows:

$$\log_{10}(\epsilon_{HMA,18kSAL}) = 5.267 - 0.927 \times \log_{10}(k) + 0.299 \times \log_{10}\left(\frac{L_{adj}}{l_e}\right) - 0.037 \times l_e \quad (3.30)$$

$$\log_{10}(\epsilon_{HMA,36kTAL}) = 6.070 - 0.891 \times \log_{10}(k) - 0.786 \times \log_{10}(l_e) - 0.028 \times l_e \quad (3.31)$$

$$\log_{10}(\sigma_{PCC,18kSAL}) = 5.025 - 0.465 \times \log_{10}(k) + 0.686 \times \log_{10}\left(\frac{L_{adj}}{l_e}\right) - 1.291 \times \log_{10}(l_e) \quad (3.32)$$

$$\log_{10}(\sigma_{PCC,36kTAL}) = 4.898 - 0.559 \times \log_{10}(k) + 1.395 \times \log_{10}\left(\frac{L_{adj}}{l_e}\right) - 0.963 \times \log_{10}(l_e) - 0.088 \times \left(\frac{L_{adj}}{l_e}\right) \quad (3.33)$$

$$\Delta\epsilon_{HMA,\Delta T} = -28.698 + 2.131 \times \alpha_{PCC} \times \Delta T + 17.692 \times \left(\frac{L_{adj}}{l_e}\right) \quad (3.34)$$

$$\Delta\sigma_{PCC,\Delta T} = 28.037 - 3.496 \times \alpha_{PCC} \times \Delta T + 18.382 \times \left(\frac{L_{adj}}{l_e}\right) \quad (3.35)$$

where,

$\epsilon_{HMAC,18kSAL}$  = HMA bottom strain due to a 18-kip single axle load,

$\epsilon_{HMAC,36kTAL}$  = HMA bottom strain due to a 36-kip tandem axle load,

$\sigma_{PCC,18kSAL}$  = UTW corner (top) stress due to a 36-kip tandem axle load (psi),

$\sigma_{PCC,36kTAL}$  = UTW corner (top) stress due to a 36-kip tandem axle load (psi),

$\Delta\epsilon_{HMA,\Delta T}$  = additional HMA bottom strain due to temperature gradient,

$\Delta\sigma_{PCC,\Delta T}$  = additional UTW corner (top) stress due to temperature gradient (psi),

$\alpha_{PCC}$  = thermal coefficient of expansion of the PCC,

$\Delta T$  = temperature gradient in UTW (°F),

$l_e$  = the effective radius of relative stiffness for fully bonded slab (in.),

and

$L_{adj}$  = adjusted slab length (in.).

$L_{adj}$  is adjusted slab length (in.), defined as:

$$L_{adj} = 12 \times (8 - 24 / (L / 12 + 2)) \quad (3.36)$$

where,

$L$  = joint spacing (in.).

### 3.4.4 Fatigue Model

The final step of the design procedure is to calculate the predicted fatigue damage. Fatigue of the PCC at the corner of the UTW and fatigue at the bottom of the HMA were considered as follows:



*Fatigue of the PCC by PCA fatigue equation*

$$SR > 0.55, N = 10^{12.1(0.972-SR)} \quad (3.37)$$

$$0.45 < SR \leq 0.55, N = \left( \frac{4.258}{SR - 0.4325} \right)^{3.268} \quad (3.38)$$

$$SR \leq 0.45, N = \text{unlimited} \quad (3.39)$$

where,

$N$  = allowable number of load repetitions to failure, and

$SR$  = maximum stress ratio.

*Fatigue damage of the HMA by the Asphalt Institute equation*

$$N_{HMA} = 0.0795 \times \left( \frac{1}{\epsilon_{HMA}} \right)^{3.29} \times \left( \frac{1}{E_{HMA}} \right)^{0.854} \quad (3.40)$$

where,

$N_{HMA}$  = the fatigue life for the hot mixed asphalt pavement,

$\epsilon_{HMA}$  = maximum strain of hot mixed asphalt, and

$E_{HMA}$  = elastic modulus of hot mixed asphalt (psi).



## Chapter 4. Field Testing Program

### 4.1 Overview

In order to develop design guidelines for whitetopping pavement systems, full-scale field load testing was conducted. The following list briefly itemizes the main objectives of the field testing program.

- 1) Measurement of the response of whitetopping pavement under static and repetitive traffic loading using instrumentation
- 2) Establishment of the fatigue relationship of whitetopping pavement using full-scale fatigue testing data
- 3) Calibration of the developed mechanistic design procedure to develop design guidelines
- 4) Evaluation of the current specification requirements for implementation.

### 4.2 Full-Scale Whitetopping Pavement

#### 4.2.1 Test Pavement

A full-scale whitetopping pavement system, which consisted of natural subgrade, aggregate base, existing asphalt concrete (AC) pavement, and portland cement concrete (PCC) slab, was constructed and tested in this study. The dimensions of the full-scale concrete slab were 18 ft by 18 ft by 6 in. with 6-ft joint spacing and the slab was placed on top of a 4-year-old existing asphalt concrete pavement system. Figure 4.1 shows the cross-section of the pavement structure.

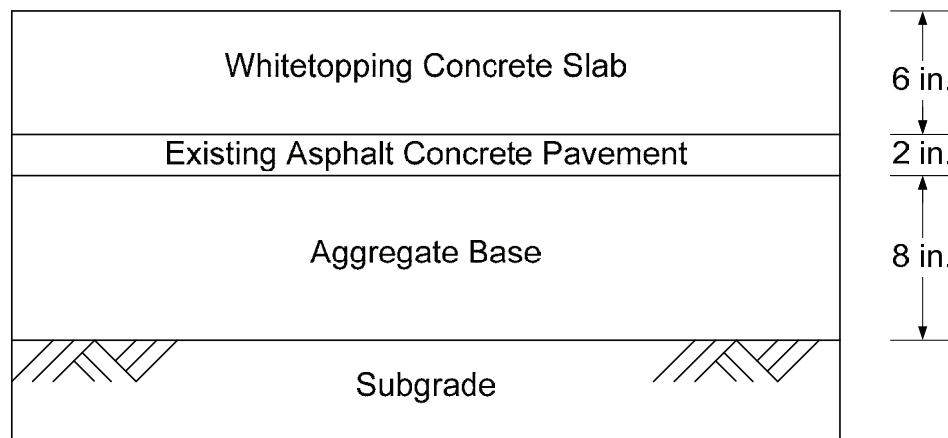


*Figure 4.1: Cross-section of the whitetopping pavement system*

#### 4.2.2 Mixture Proportion

The concrete mixture designs used in the full-scale whitetopping slab were typical concrete paving mixtures used in the state of Texas. The concrete mixtures used in this study are summarized in Table 4.1.

**Table 4.1: Mixture proportion for whitetopping**

Material Constituent	Quantities per yd <sup>3</sup> of Concrete	Remark
Cement (lbs)	470	Type I/II, 5 sack mix
Water (lbs)	205	4.9 gal/sack
Coarse Aggregate (lbs)	1998	
Fine Aggregate (lbs)	1301	
Air Content (%)	5	
Air Entraining Agent (fl. oz)	1.2	0.25 oz/c.w.t.
Retarder (fl. oz)	18.8	4.0 oz/c.w.t.
Water-Cementitious ratio	0.45	

#### 4.2.3 Construction of Full-Scale Whitetopping Slab

A full-scale whitetopping concrete slab was constructed at the Pickle Research Campus of The University of Texas at Austin on May 3, 2007. A ready-mixed concrete company supplied the concrete in two separate 5-yd<sup>3</sup> loads for the slab and specimens. Once the slab was placed and finished, the curing compound was applied on the top surfaces in accordance with TxDOT specifications. Saw cuts with 2-in. depth were made at the age of 12 hours to induce 6-ft spacing joint. Figures 4.2 and 4.3 illustrate the construction of whitetopping and saw cuts.

The test slab was instrumented with vibrating wire gages, dynamic strain gages, linear variable differential transformers (LVDTs), and a stress meter for monitoring slab behavior due to both environmental and traffic loading. The detail of gage locations will be described later in this report.

#### 4.2.4 Mechanical Properties of Whitetopping Concrete

To determine the mechanical properties of the concrete mixture used in the field slab, 4-in. by 8-in. cylinders and 6-in. by 6-in. by 20-in. beams were cast at the time of slab casting. All cylinders and beams were cured in a wet sand bed adjacent to the slab testing site and also cured under the standard 100% moisture condition. The temperature histories of specimens were monitored to compare the maturity values with field slabs. The recorded temperature differences between the temperature at the middle of the slab and the temperature of the specimens in the wet sand bed were negligible (less than  $\pm 3^{\circ}$  F). Conservatively, it was assumed that the strengths from the sand-cured specimens were the strengths corresponding to the full-scale slab. Specimens were tested at the age of 1, 3, 7, 14, 28, and 90 days and the results are shown in Table 4.2.

**Table 4.2: Mechanical properties of whitetopping concrete**

Test Age (days)	Compressive Strength (psi)	Modulus of Rupture (psi)	Elastic Modulus (million psi)
Standard Curing (73° F, 100% moisture)			
1	1688	288	2.258
3	2820	-	3.575
7	3551	542	4.941
14	4150	-	5.189
28	4972	643	5.514
90	6062	703	5.522
Wet Sand Bed Curing			
1	1688	288	2.258
3	3198	-	3.809
7	3983	557	4.976
14	4173	-	5.296
28	5155	666	5.394
90	6112	720	5.544



*(a) Installation of instrumentations before slab casting*



*(b) Concrete placement and compaction*



*(c) Application of curing compound*



*(d) Fabrication of strength specimens*

*Figure 4.2: Construction of the full-scale whitetopping slab*



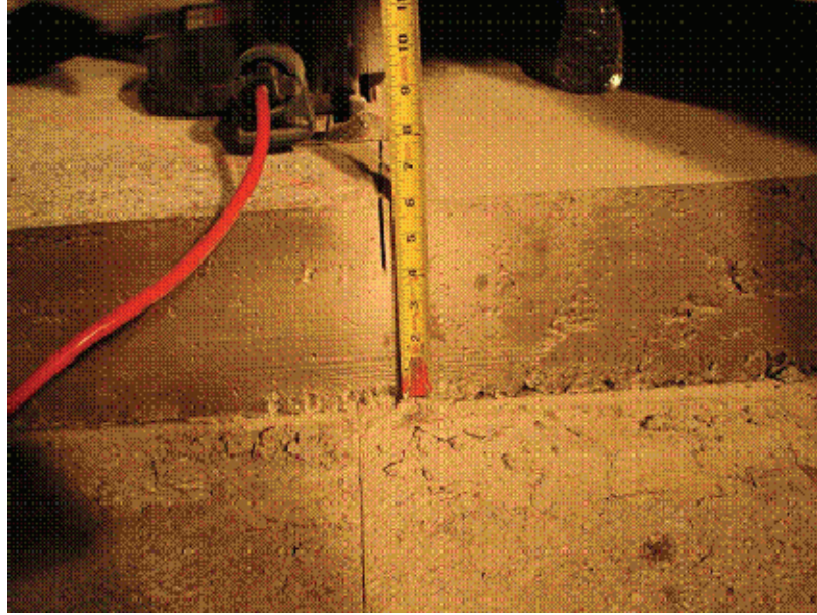


*Figure 4.3: Saw cut (2-in. depth, 6-ft spacing) at the age of 12 hours*

### **4.3 Foundation Properties**

To facilitate the determination of the applied stress levels during the accelerated testing on the field pavement system, the foundation properties were investigated prior to the field load testing. Three in-situ tests were performed to evaluate foundation properties: 1) falling weight deflectometer (FWD), 2) dynamic cone penetrometer (DCP), and 3) plate load test to evaluate modulus of subgrade reaction (k-value).

#### **4.3.1 Falling Weight Deflection test**

The falling weight deflection test was performed at the 108 locations on a 3-ft grid before the casting of the whitetopping slab. The objectives for the FWD tests were to 1) check the uniformity of the supporting condition at the testing site and 2) obtain the elastic modulus of each layer. The modulus of the 2-in. HMA cannot be back-calculated and it must be assumed. The elastic modulus of the AC layer was assumed to be constant for use in the back-calculation software. Figure 4.4 illustrates the field testing and the FWD displacement contour at sensor no. 1 with a 9-kip load. The dotted line in Figure 4.4 (b) is the selected location of the whitetopping slab. The average back-calculated elastic moduli of each layer from testing results are shown in Table 4.3.



**Table 4.3: Average back-calculated elastic modulus from FWD testing**

Layer	Average Elastic Modulus (psi)	Standard Deviation (psi)	Coefficient of Variance (%)	Remark
Asphalt Concrete	485,000	0.0	0.0	Result from assumed value
Aggregate Base	38,400	9.5	24.6	
Subgrade	27,100	2.9	10.7	

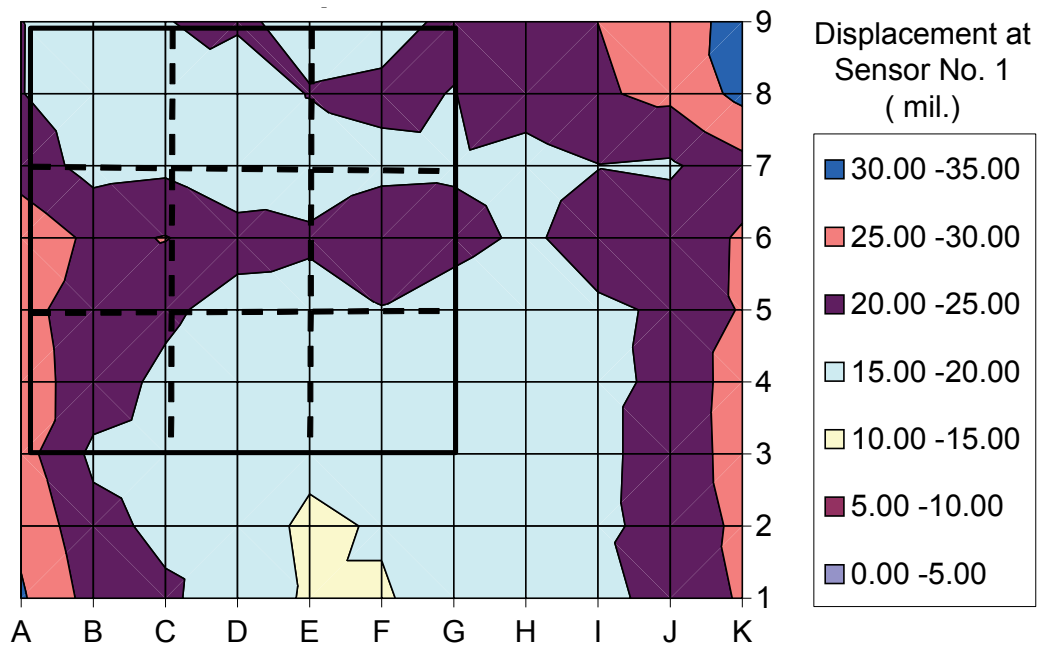
#### **4.3.2 Dynamic Cone Penetrometer (DCP) test**

The dynamic cone penetration (DCP) tests for 10 locations were performed before casting the whitetopping slab in order to investigate subgrade conditions. The DCP consists of upper and lower shafts. The upper shaft has a 17.6-lb drop hammer with a 22.6 in drop height and is attached to the lower shaft through the anvil. The lower shaft contains an anvil and a cone attached at the end of the shaft. The cone is replaceable and has a 60 degree cone angle. In order to run the DCP test, three operators were required. One person held the upper shaft, another person dropped the hammer, and the other recorded measurements. The DCP test procedure is as follows:

- 1) Assemble upper shaft and lower shaft containing cone tip.
- 2) Put the cone tip assembled with the shafts on the testing surface.
- 3) Execute a seating drop to stabilize the equipment due to the disturbed loose state of the ground surface and the self-weight of the device.
- 4) The value of the initial reading is counted as the initial penetration corresponding to blow zero.
- 5) Hammer blows are repeated and the penetration depth is measured for each hammer drop.
- 6) This process is continued until a desired penetration depth is reached or the anvil approaches the surface of the structure.



(a) FWD field testing



(b) FWD displacement contour at sensor no. 1 with 9-kip load

Figure 4.4: FWD testing

Figure 4.5 shows the DCP testing at the foundation of whitetopping test slab.



Figure 4.5: DCP testing

From the DCP results, the California bearing ratio (CBR) and the corresponding elastic subgrade modulus were calculated using Equations 4.1 and 4.2.

$$CBR = 292 / DCP^{1.12} \quad (4.1.a)$$

where,

$CBR$  = California bearing ratio, and

$DCP$  = DCP index (mm/blow).

$$M_R = 1500 \times CBR \quad (4.1.b)$$

where,

$M_R$  = resilient modulus = elastic modulus (psi).

Combining Equations 4.1.a and 4.1.b,

$$M_R = \frac{438,000}{DCP^{1.12}} \quad (4.2)$$

where,

$M_R$  = resilient modulus = elastic modulus (psi), and

$DCP$  = DCP index (mm/blow).

An average subgrade elastic modulus of 20,200 psi was obtained with a 31% coefficient of variation. Figure 4.6 shows the comparison of the back-calculated subgrade modulus results from the DCP and FWD tests. As shown in Figure 4.6, the correlation between DCP and FWD results is rather poor. One of the possible reasons for the poor correlation might be that the FWD back-calculation process requires certain assumptions regarding layer characteristics and bed rock depth, which are not always known. Also, the FWD tends to evaluate deep subgrade. For subgrade modulus, data from the DCP tests were used in this study.

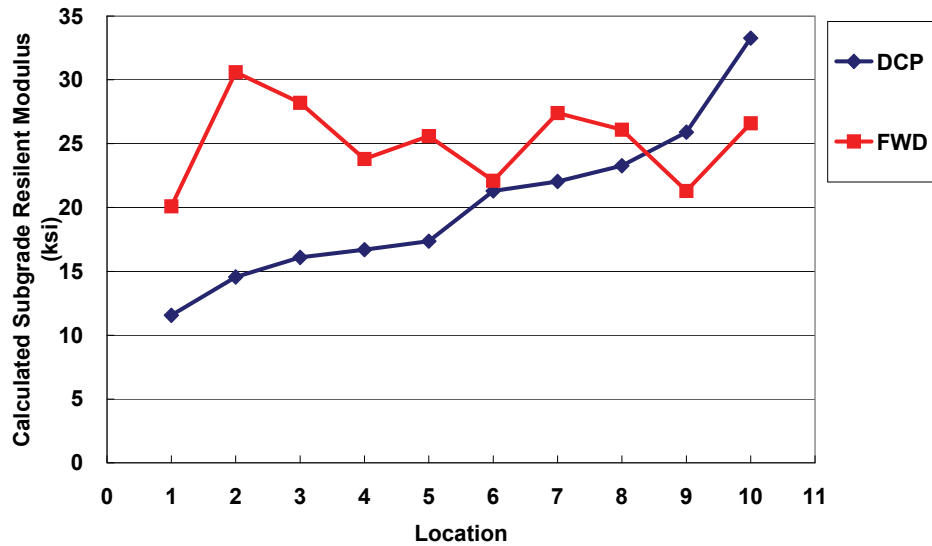


Figure 4.6: Comparison of DCP and FWD results

After the completion of the modulus of subgrade reaction testing, explained in the next section, three additional DCP locations were selected for the comparison of foundation properties. Figure 4.7 shows the DCP testing results at the k-value test locations.

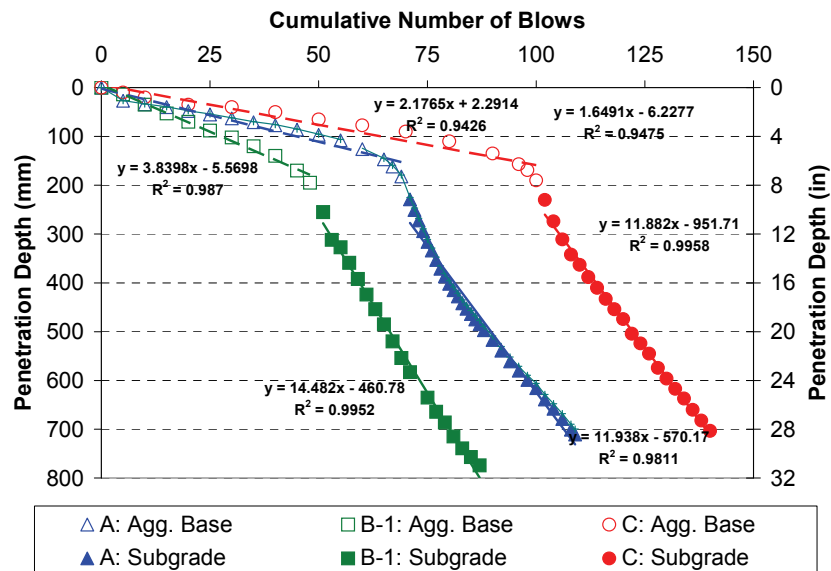


Figure 4.7: DCP results for k-value testing locations

### 4.3.3 Modulus of Subgrade Reaction (k-value) Test—Plate Load Test

An actual field plate load test to determine the modulus of subgrade reaction (k-value) using a fully loaded dump truck and load bearing plates was performed at the testing site. Exact k-values from this test can provide design values for the subgrade and base with significantly higher accuracy compared to other back-calculation methods.

The schematic diagram of the plate loading test is illustrated in Figure 4.8 while the actual testing equipment is shown in Figures 4.9 and 4.10. Sand was put on the test surface to level the test location and seat the steel bearing plate. On the 12-in. diameter steel bearing plate, 9-in. and 6-in. diameter steel plates were stacked up and carefully centered with a pyramid shape. All plates have a 1-in. thickness. A load cell was located to measure load on the top steel plate. A hydraulic jack was inserted between the reaction frame and the load cell to apply the test load. A fully loaded dump truck was used as the reaction equipment with a gross weight of 48,000 lbs.

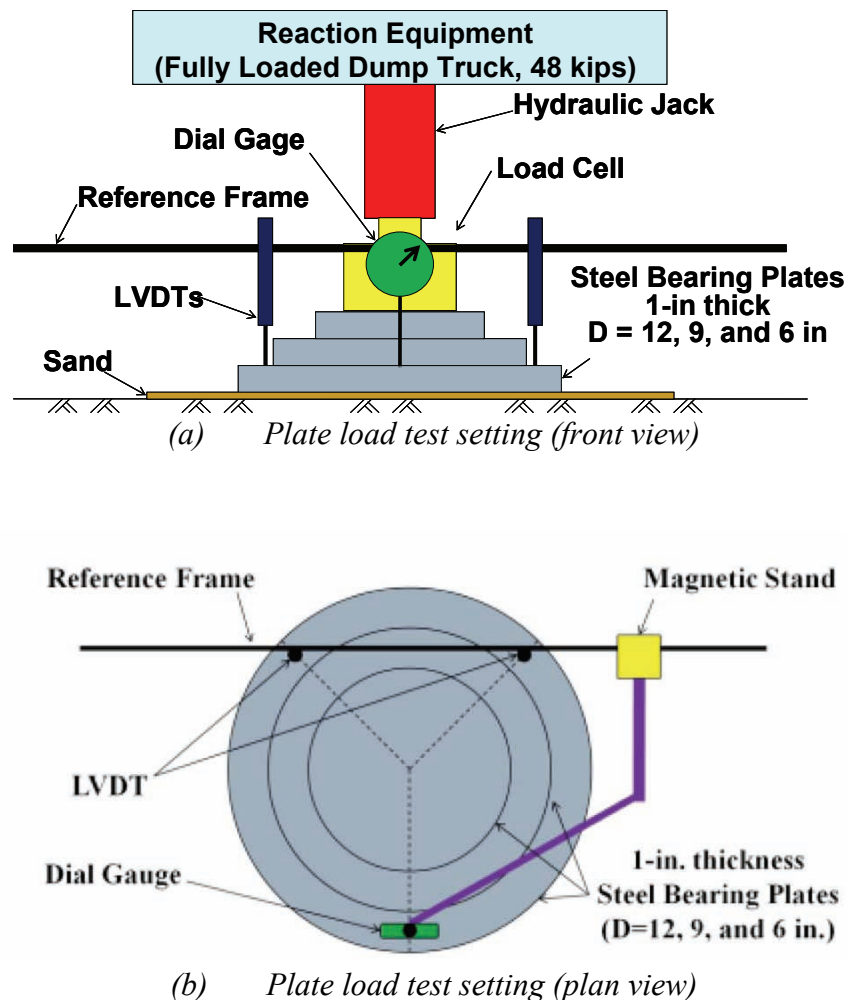


Figure 4.8: Schematic diagram of plate load test



(a) Sand for leveling



(b) Loading plates with pyramid shape



(c) Load plates and reference bar



(d) LVDTs

Figure 4.9: Plate load testing apparatus

To measure vertical displacement of the ground surface due to loading, two linear variable differential transformers (LVDTs) and a dial gage were installed. All displacements were measured with respect to a 9-ft long reference frame. The test procedures were as follows:

- 1) After all the equipment had been properly arranged, an initial load for seating was applied.
- 2) Preload was released until the displacements were stable.

The load was applied at a moderately rapid rate in uniform displacement increments. In this field test, a 0.005-in. displacement increment was applied. After each increment of load, the corresponding displacements were measured after the rates of measured deflection were stabilized (less than 0.001 in./min). This process was continued until the total deflection was more than 0.05 in. For all cases, more than 6 load-deflection points were obtained.

Three test locations were selected based on FWD data as shown in Figure 4.11 and Table 4.4. One location (B and B-1), which had the medium FWD displacements, was selected for the plate loading test on top of the asphalt as well as the aggregate base. After completion of the plate load test on location B, the asphalt surface was removed and the k-value test was performed again. At this location (B-1), the repetitive plate load test was performed after removal of asphalt surface as shown in Figure 4.12.





*(a) Plate load test using fully loaded dump truck*



*(b) Loading equipments*

*Figure 4.10: Plate load test at testing site*

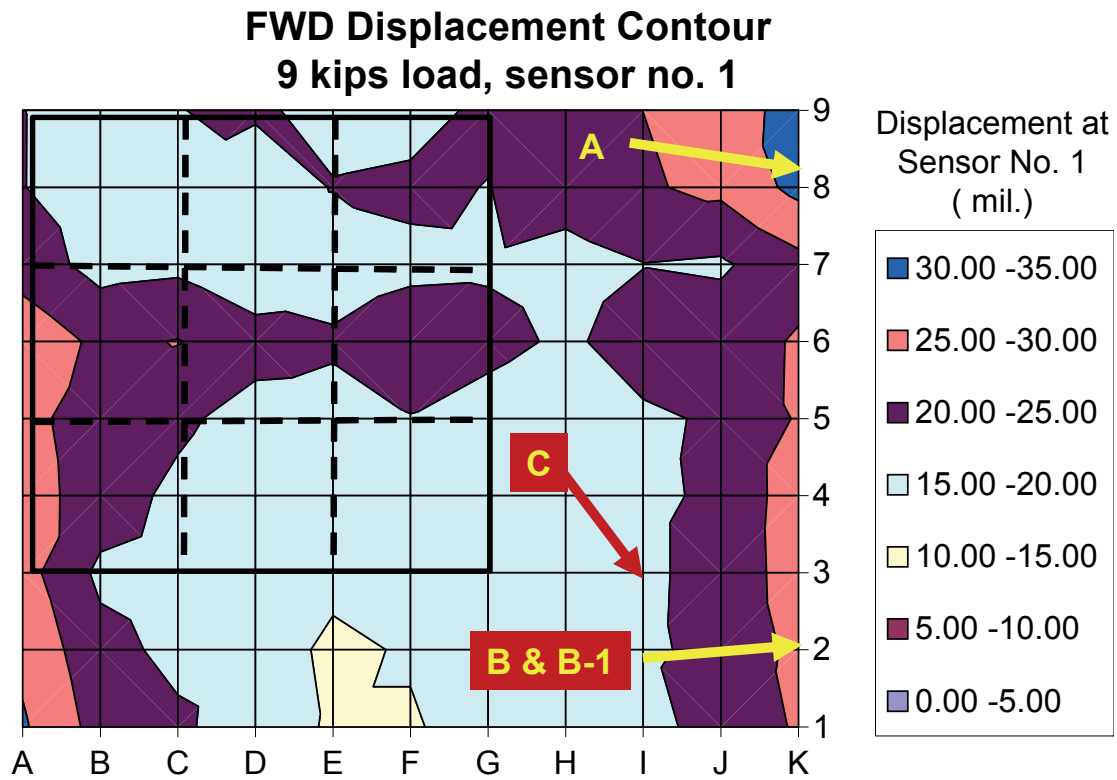


Figure 4.11: Selected *k*-value test locations based on FWD results

**Table 4.4: *k*-value test locations**

Location	Coordinate	9-kip FWD displacement At sensor no.1 (mils.)	Expected <i>k</i> -value Remark
A	K8	31.4	Low modulus
B	K2	26.5	Medium modulus
C	I3	19.6	High modulus
B-1	K2	-	- Test location B again - After removal of asphalt surface - Repetitive testing



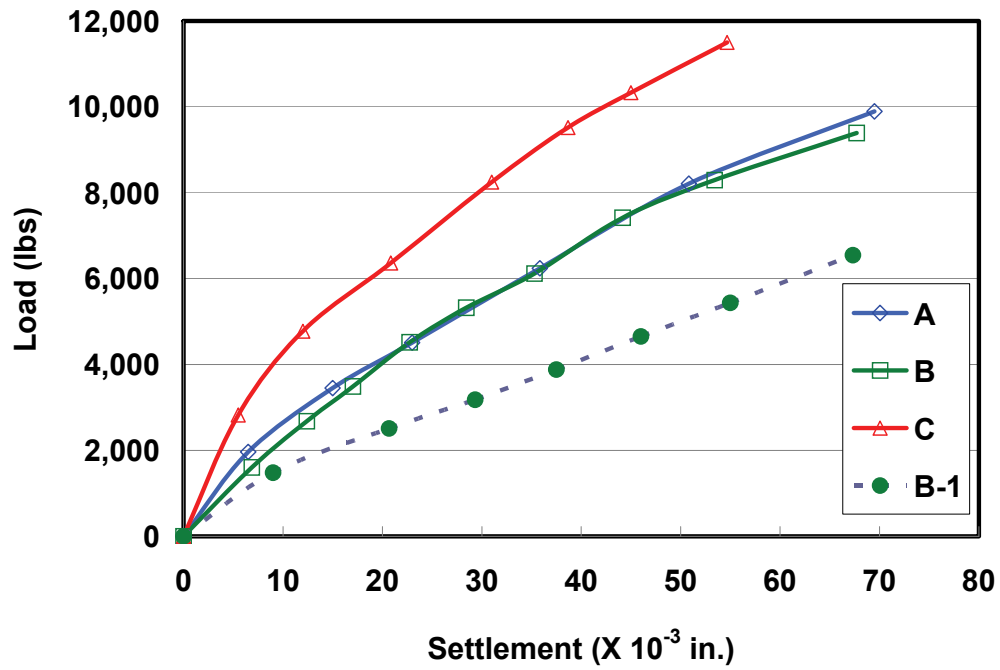


*Figure 4.12: Removal of asphalt surface*

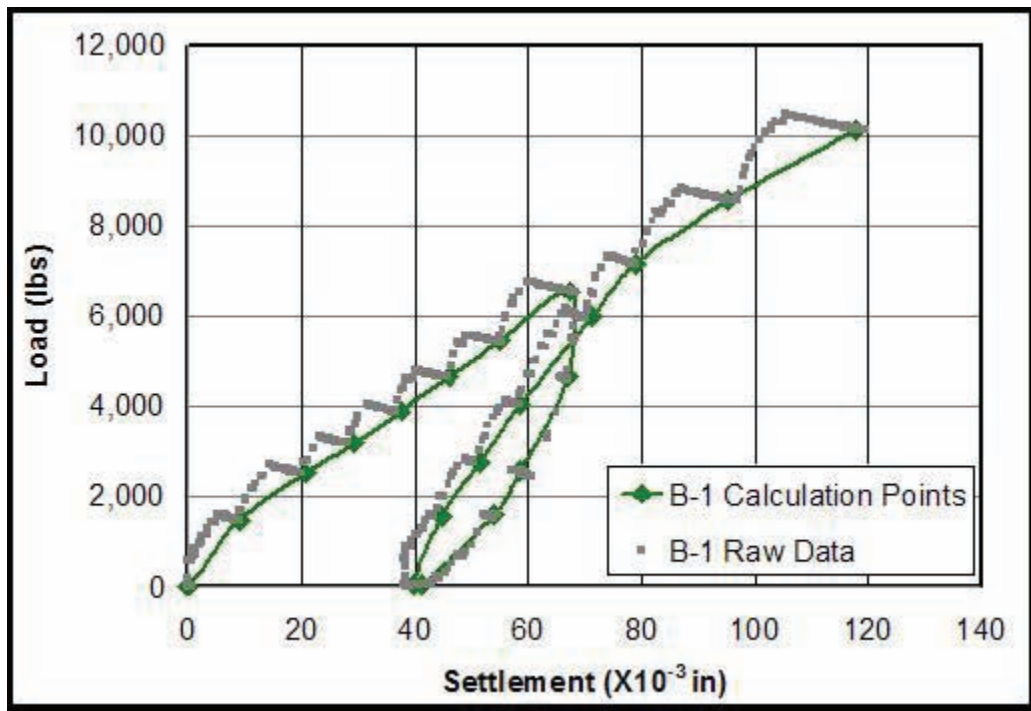
The k-value test results are shown in Table 4.5 with corresponding FWD and DCP test results, while the load-displacement plots are illustrated in Figure 4.13.

**Table 4.5: k-value test results with corresponding DCP values**

Location	9-kip FWD displacement. at sensor no.1 (mils.)	DCP Index (mm/blow)		k-value (psi/in)	Remark
		Aggregate Base	Subgrade		
A	31.4	2.18	11.94	1360	
B	26.5	-	-	1340	
C	19.5	1.65	11.88	1840	
B-1	-	3.84	14.48	840	Removal of asphalt surface



(a) Non-repetitive testing



(b) Repetitive testing

Figure 4.13: Load-settlement curves from  $k$ -value tests

The field plate load test results were compared with the calculated values from a layered program, ELSYM5 software, which is one of the most widely used evaluation programs in pavement design. The input values are shown in Figure 4.14.

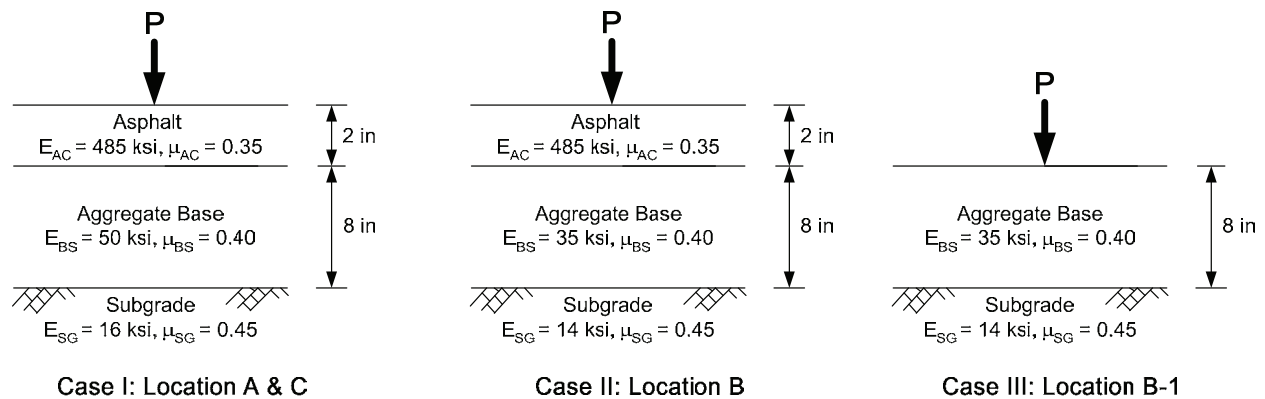


Figure 4.14: ELSYM5 inputs

Figure 4.15 shows the comparison of field test and ELSYM5 results. In all the locations, the calculated k-values using ELSYM5 showed a much higher magnitude compared to k-values from field tests. From this limited information, ELSYM5 tends to overestimate the modulus of subgrade reaction by two fold or higher than the plate load test values. When estimating the modulus of subgrade reaction from a layered elastic program using the estimated modulus value of each layer, the k-value should be reduced by half.

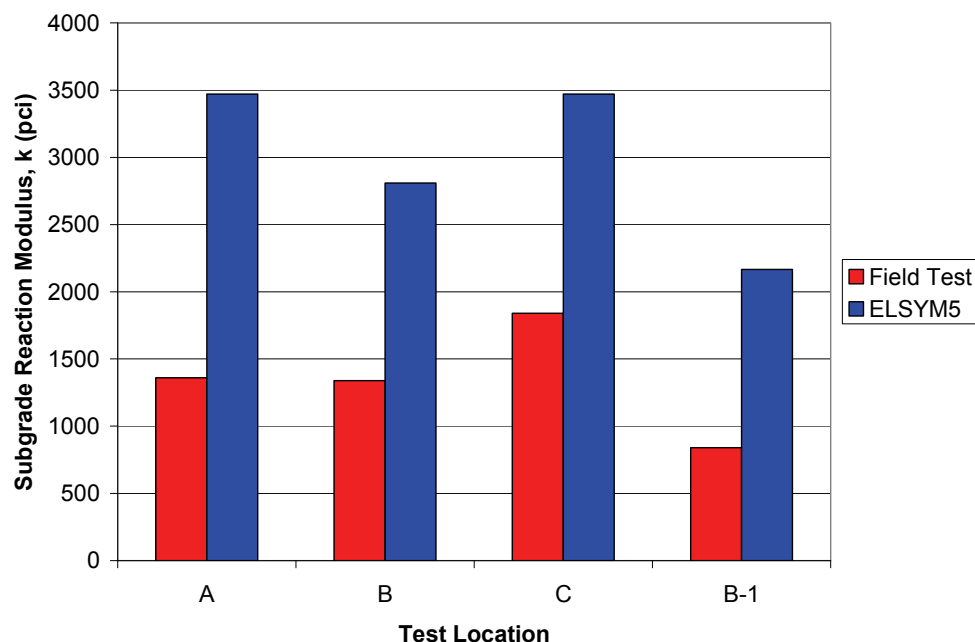
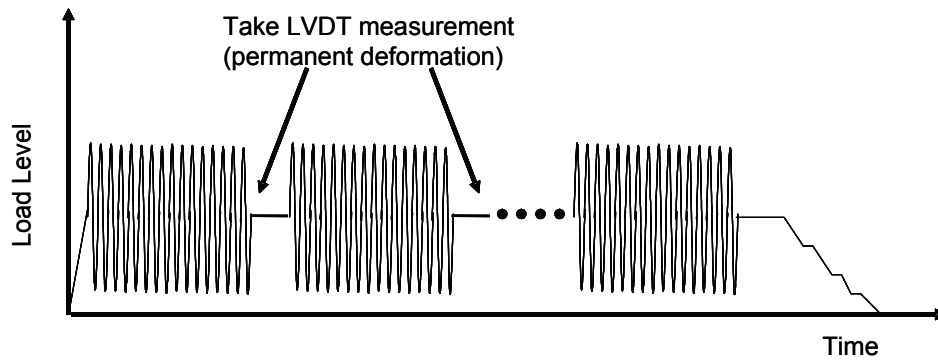


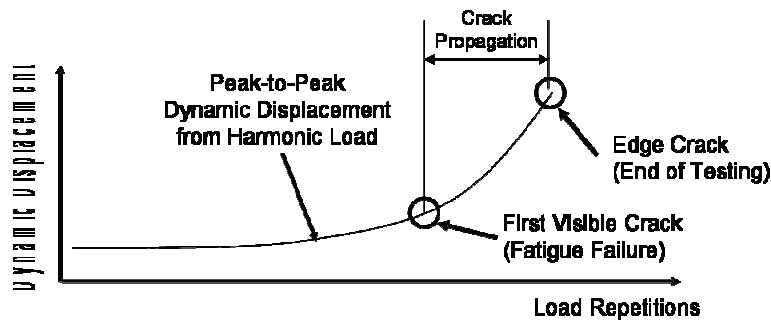
Figure 4.15: Comparison of  $k$ -values from field test and ELSYM5

#### 4.4 Super Accelerated Testing

The definition of super-accelerated pavement (SAP) testing is the application of one million load repetitions to a full-scale pavement system in a short time, on the order of 0.5 to 2 days, in nominal terms (Stokoe et al., 2000). The test is conducted by applying cyclic loads generated by an external loading system through a loading frame placed on the pavement surface. The dynamic loads are created by the servo-hydraulic actuator that generates sinusoidal harmonic loads at a pre-selected frequency as illustrated in Figure 4.16(a). In the case of rigid pavements, the difference between the maximum and minimum displacements during dynamic loading was found to best represent the elastic response of the concrete slab by Roesler and Barenberg (1999, 1999). The variation of dynamic displacements during super-accelerated testing was found to be the main indicator to characterize the fatigue behavior of a rigid pavement system. In this study, fatigue failure of a full-scale slab was defined as the occurrence of the first visible crack. This occurrence was generally accompanied by abrupt changes in dynamic displacement. The conceptual diagram for the representation of pavement performance is illustrated in Figure 4.16(b). To investigate the propagation of cracks and stress redistribution, cyclic loading was applied until full depth cracking at the edges or joints of the pavement occurred.



(a) Sequence of load repetitions



(b) Changes of dynamic displacement with increasing number of load repetitions

Figure 4.16: Illustrations of SDD testing method

#### 4.4.1 Description of the Stationary Dynamic Deflectometer (SDD)

Researchers at The University of Texas at Austin first developed the Rolling Dynamic Deflectometer (RDD) in the early 1990s (Bay et al., 1995; Bay et al., 1999). In the stationary mode, the device becomes a Stationary Dynamic Deflectometer (SDD). The SDD is a mobile accelerated pavement testing device, which can apply sinusoidal loads at a range of load levels and load frequencies.

The hydraulic system of the SDD can apply both a static hold-down force and a dynamic force to the test slab. The repeated dynamic force is applied to the slab using a loading frame with a steel loading pad.

#### 4.4.2 Super-Accelerated SDD Slab Testing Procedure

The super-accelerated SDD testing on the whitetopping slab was performed 90 days after the placement of concrete slab. Initially, saw cuts with a 2-in. depth were performed at the age of 12 hours to induce 6-ft joint spacing. Because the saw cuts had not propagated to the bottom of the slab even after 90 days since placement, additional 3-in. saw cuts were made just prior to the super-accelerated SDD testing as shown in Figure 4.17. The total saw cut depth was 5 in. while the thickness of the whitetopping slab was 6 in.



*(a) Additional saw cut work*



*(b) 5-in. total saw cut*

*Figure 4.17: Additional saw cut*

Figure 4.18 shows the SDD testing plans for the whitetopping slab. To obtain the fatigue relationship (S-N curve), three panels were tested under constant cyclic load. The stress levels

for each testing panel were determined using the static failure testing result, which was done on one of the panels.

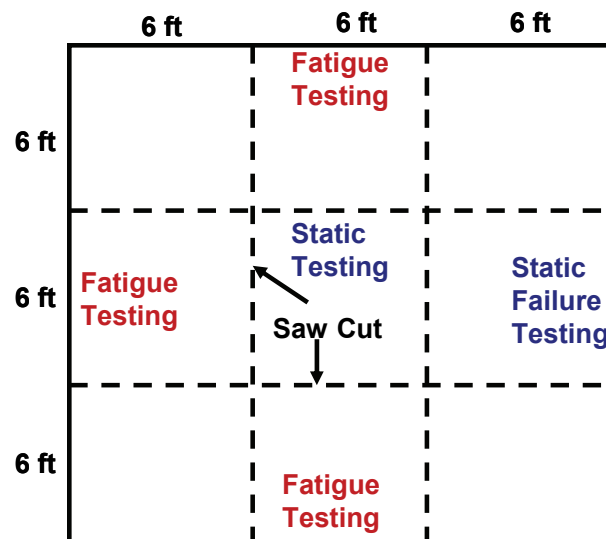


Figure 4.18: Super-accelerated SDD testing plan

The static and dynamic loads from the SDD were applied at the edge of the concrete pavement through a loading frame. The field arrangement of the super-accelerated testing is illustrated in Figures 4.19.



Figure 4.19: Field testing arrangement

To determine the ultimate strength of a panel, one of the panels was statically tested to failure using an edge loading condition. Based on the ultimate static failure load, three different



stress levels were examined in the SDD fatigue testing: 65, 80, and 90% of the ultimate static load, respectively.

To avoid potential instability of the SDD system, a minimum hold-down force was always required. An initial static hold-down force was applied, and then the continuous dynamic force was applied at a rate of 1200 cycles per minute (20 Hz). A load cell connected the SDD to the loading frame, and it was used to measure both the applied static and dynamic forces. The displacement history was captured during the entire test period using two types of sensors. First, three LVDTs were installed at the top, middle, and bottom edges of the slab to measure the dynamic motion of the pavement. Second, a dynamic strain gage was installed at the bottom of the loading position for all three fatigue testing cases. The installed displacement measuring devices are shown in Figure 4.20.



*Figure 4.20: Arrangement of loading frame and LVDTs*

The number of cycles to the appearance of the first visible crack was used for the definition of the number of load repetition to failure (N). Even after the occurrence of a visible crack, each test panel was loaded continuously until the visible crack propagated to the other edge of the concrete slab, full-depth. If a full-depth edge crack could not be observed after 200,000 cycles of load repetition was applied, the testing was terminated. After testing each panel, the dynamic displacement data from the instrumentation were plotted against the number of applied load repetitions. In general, the dynamic displacement increased rapidly as the concrete slab approached failure.

#### 4.4.3 Super-Accelerated Full-Scale Concrete Slab Testing Results

Most fatigue studies incorporated the use of a stress level ( $S$ ) concept (Okamoto, 1999). Use of a stress level normalizes the number of load repetitions (typically using logarithm) to fatigue failure with concrete strength. The number of repeated loads until failure ( $N$ ) varies inversely with the stress level ( $S$ ). Several concrete fatigue curves from previous research studies are presented in Table 4.6.

**Table 4.6: Summary of concrete fatigue curves from other researchers**

Researcher (Study)	Derived from	Failure criteria	Computed stress due to load
Kesler	Laboratory beam	Beam failure	Linear elastic beam stress
PCA	Laboratory beam	Beam failure	Linear elastic beam stress
Vesic	AASHTO Road Test	Terminal serviceability, $p_t = 2.5$	Westergaard interior
Thompson & Barenberg (NCHRP 1-26)	COE and AASHTO test track data	50% cracked slabs	Westergaard edge stress with 25% transfer

In addition to the effect of stress level ( $S$ ), the fatigue behavior of concrete is highly influenced by the minimum-to-maximum stress ratio,  $R$ . A slight increase of  $R$  decreases the fatigue life of concrete significantly. Shi et al. (1993) proposed a concept of equivalent fatigue life ( $EN$ ) to overcome this problem. The equivalent fatigue life ( $EN$ ) is defined as follows:

$$EN = N^{1-R} \quad (4.3)$$

where,

$EN$  = equivalent fatigue life,

$N$  = number of cycles to failure, and

$R$  = applied minimum-to-maximum stress ratio.

The super-accelerated full-scale whitetopping slab testing results are summarized in Table 4.7. The maximum and minimum stress levels were based on the static ultimate failure testing result shown in panel no. 4. In the case of a relatively lower stress level ( $S=0.65$ ), no visible cracks were observed although the testing slab definitely showed an increase in dynamic displacement with the increase in the number of load repetition cycles.

The fatigue life data ( $N$ ) from this study can be converted to the equivalent fatigue life ( $EN$ ) by applying Equation 4.3 as shown in Table 4.7.



**Table 4.7: Super-accelerated full-scale whitetopping test results**

Panel No.	Stress Level, $S$	Min/Max Stress, $R$	First Visible Crack, $N$	Equiv. fatigue life, $EN = N^{(1-R)}$	Termination of Test, cycles	Remark
1	0.90	0.14	19,000	4,783	49,000	
2	0.80	0.16	53,000	9,298	173,000	
3	0.65	0.15	Est. 210,000	33,411	462,000	No visible crack Estimated N
4	Static Failure	-	-	-	-	Failure load = 38 kips

*Failure Mode*

For all slabs with visible cracks, the first visible crack was initiated at the bottom of the loading edge and propagated upward about 2/3 of the distance to the top surface. Once the initial crack propagated to this location, the initiation of secondary semi-circular top surface cracks with a 2 to 2.5-ft radius was observed. The failure patterns with visible cracks are illustrated in Figure 4.21.

*Displacement Measurement*

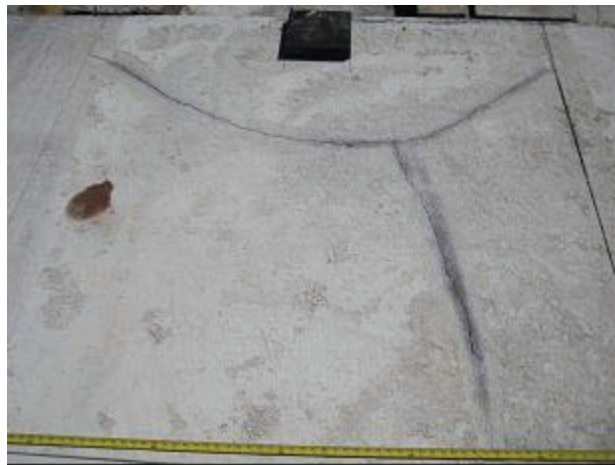
The dynamic displacement variations for test slabs are illustrated in Figure 4.22. The measured dynamic displacement data were normalized with respect to the initial dynamic displacement for comparison. For all test slabs, the dynamic displacements increased over the entire fatigue life. In general, the dynamic displacement after the first visible crack increased at a higher rate than before cracking. The increase in dynamic displacement before the first crack was due to the sum of the plastic deformation of the concrete slabs and permanent deformation of the foundation. The stress redistribution phenomenon was also observed. In spite of the slab's reduction in stiffness after the cracking, the full-scale rigid pavement system was still able to deliver stresses to the foundation (asphalt base and subgrade).



*(a)  $S= 0.90$ , fatigue failure*



*(b)  $S= 0.80$ , fatigue failure*



*(c) Static failure*

*Figure 4.21: Slab failure patterns*

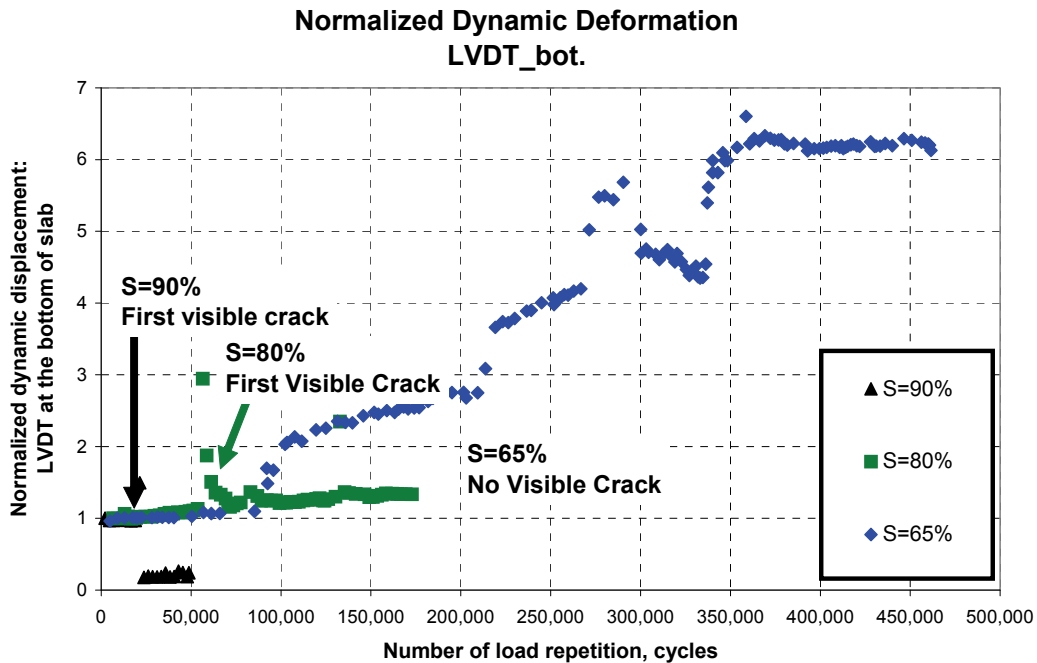


Figure 4.22: Variation of normalized dynamic displacement for full-scale slabs

#### *S-N Curve for Full-Scale Whitetopping Slab*

Figure 4.23 shows the comparison of several existing fatigue curves and full-scale field fatigue testing results. Kesler (1953) and PCA (1985) equations were developed based on laboratory testing, while the other two curves were derived from the field slab testing. The Vesic and Saxena (1969) fatigue equation was derived from the AASHTO Road Test data at a serviceability index equal to 2.5 as a function of the concrete strength and the induced stress in the pavement. The Thompson and Barenberg (1992) curve was based on results from Corps of Engineers' tests. The fatigue equation ( $S-N$  curve) derived in this study is very close to Thompson and Barenberg's  $S-N$  curve after the application of the equivalent fatigue life concept.

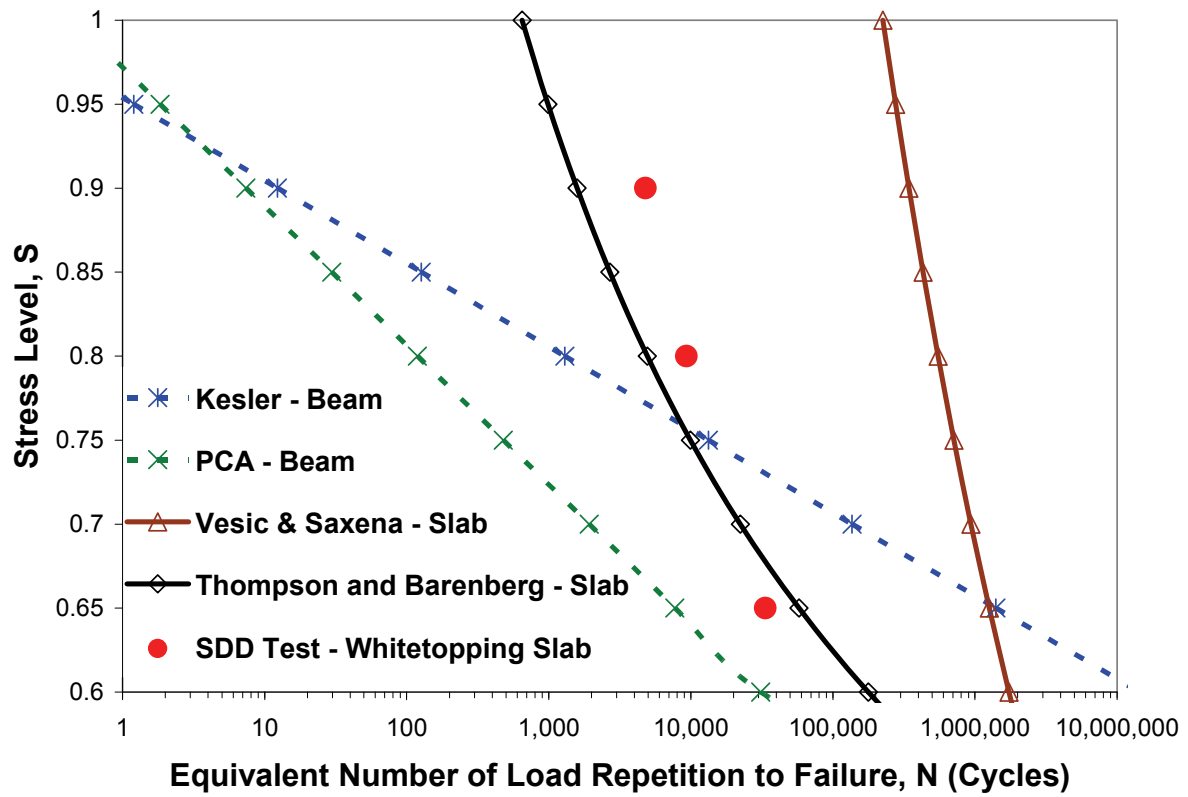


Figure 4.23: Comparison of existing fatigue curves and full-scale slab fatigue data

## Chapter 5. Development of Mechanistic Design Procedures

### 5.1 Design Logic

The behavior of thin whitetopping (TWT) differs from the behavior of full depth concrete pavement with contraction design (CPCD), primarily due to their joint spacing and load transfer mechanisms. Thin whitetopping has shorter joint spacing than regular CPCD. Thin whitetopping will behave more like a small independent slab, where stresses due to bending or warping/curling are relatively small compared with those in other concrete pavement types. However, failure modes and their analysis methodologies are similar for both pavement types. In this project, the same mechanistic analysis algorithms, except where indicated, were used for TWT and CPCD. Figure 5.1 shows the rehabilitation design logic for deteriorated asphalt pavement as originally presented in the initial proposal. During the course of the research, it was suggested that the AC overlay be removed from the scope of this project. Also, CRCP was removed because the primary applications of TWT will be at intersections or short stretches of highways, where the establishment of structural continuity required for CRCP may not be feasible. The resulting option was to develop a TWT design program, and if the thickness requires more than 7 in., then CPCD should be used.

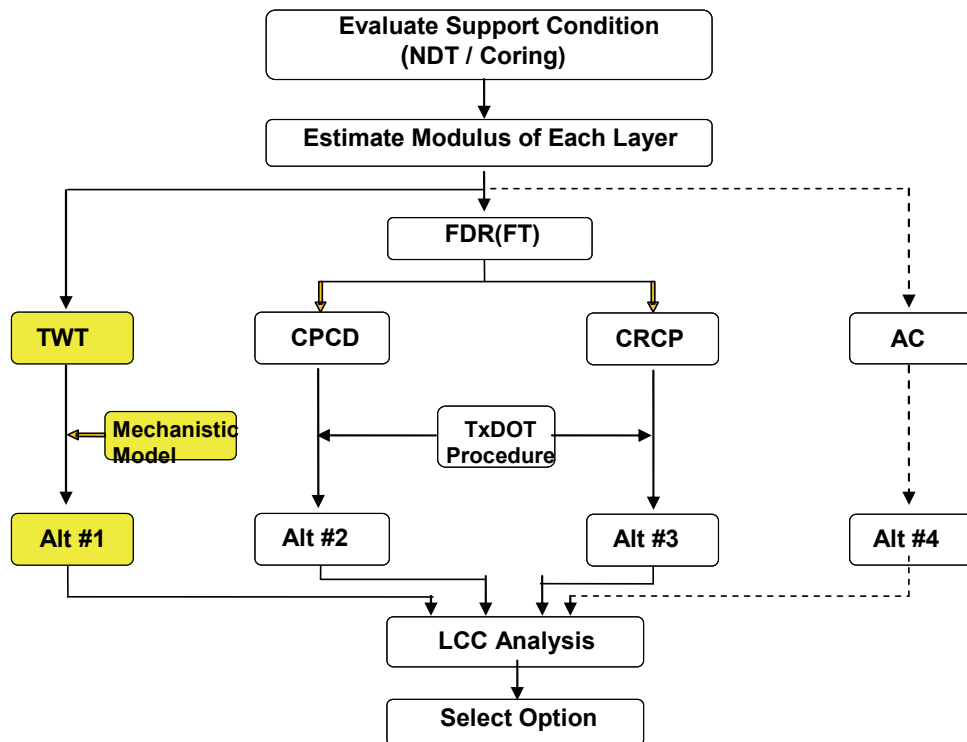


Figure 5.1: Flow diagram of design logic

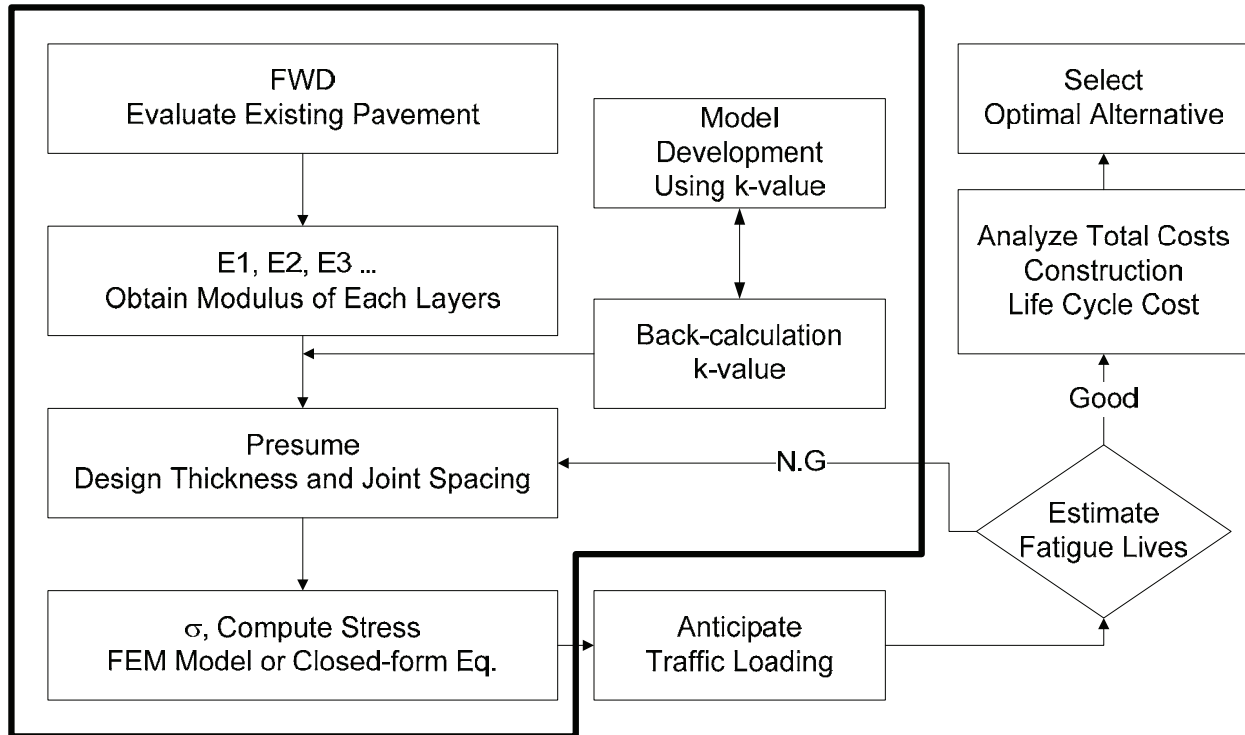


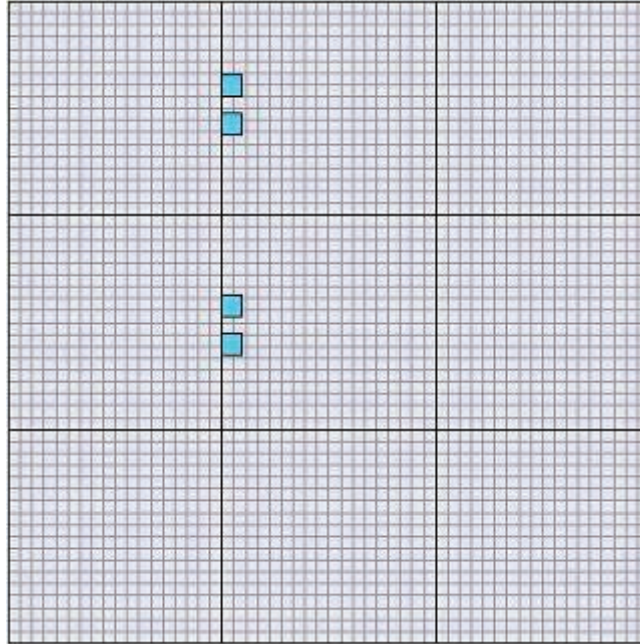
Figure 5.2: Flow diagram of mechanistic design procedure

## 5.2 Stress Computation Using ISLAB2000

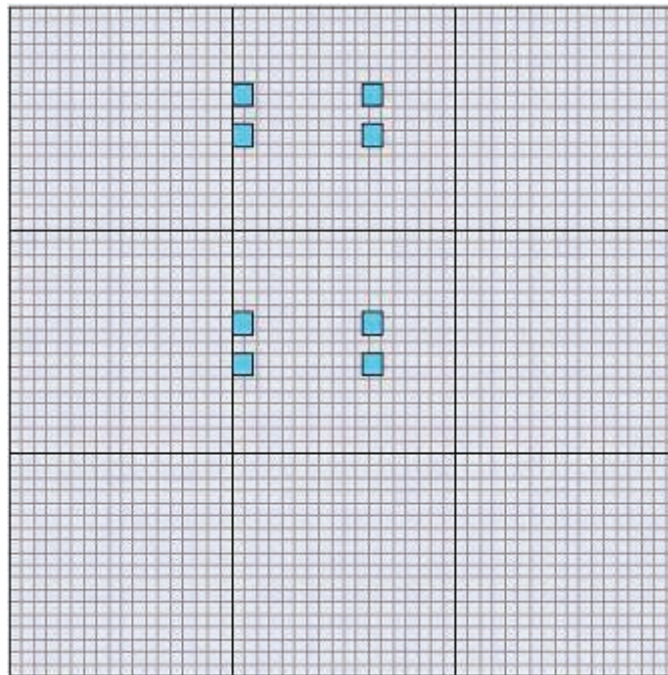
In order to develop the mechanistic design procedures for whitetopping pavement, the stress data under various loading conditions are essentially required. ISLAB2000, a 2.5-dimensional program, is a finite element program designed to model concrete pavement behavior under load. This program was used to develop a 2002 pavement design guide and its accuracy was verified by other researchers. Considering practical aspects, the ISLAB2000 software was selected for stress calculations in this project.

### 5.2.1 Input and Output

A series of numerical simulations using ISLAB2000 were performed considering various geometric and loading conditions and the results were analyzed. The pavement structure for all whitetopping models consisted of concrete topping, HMA, base, and subgrade. Each whitetopping slab has symmetrical 18-ft by 18-ft dimensions with 6-ft joint spacing. The edge loading at the center panel was assumed for maximum loading condition with a 20-kip single axle load (SAL) and 34-kip tandem axle load (TAL) as shown in Figure 5.3.



*(a) Single Axle Load*



*(b) Tandem Axle Load*

*Figure 5.3: Whitetopping model using ISLAB2000*

A total of 7,776 ISLAB2000 runs were executed to evaluate all combinations of all variables in an experimental design matrix. Ten design values were considered for the variables of the ISLAB2000 simulations. Each variable has values in a practical range to simulate possible field conditions. The values of each variable selected in this study are summarized in Table 5.1.

**Table 5.1: Summary of used input variables for ISLAB2000**

Variable	Selected Input Levels	Number of Cases
Traffic Load	20-kips SAL and 34-kips TAL	2
Bond Conditions	Bonded, Unbonded	2
Thickness of Concrete Layer (in.)	4, 6, and 8	3
Elastic Modulus of Concrete (million psi)	4 and 5	2
Thickness of Asphalt Layer (in.)	3, 6, and 9	3
Elastic Modulus of Asphalt (ksi)	200, 500, and 800	3
Thickness of Base Layer (in.)	5 and 10	2
Elastic Modulus of Base (ksi)	100 and 1000	2
Subgrade Reaction Modulus , k-value (pci)	50, 100, and 200	3
Load Transfer Efficiency - LTE (%)	1, 50, and 99	2
	Total Number of Run	7,776

Figures 5.4 through 5.11 show various actual input screens of ISLAB2000 with values used in this project. The mesh size used for this project was 4 in., and Totski's model was used for the interface between asphalt and base. The Winkler foundation model was used for subgrade, and load transfer efficiency (LTE) was adopted to consider joint stiffness. The typical ISLAB200 outputs for stresses and displacements are shown in Figures 5.12 through 5.16.



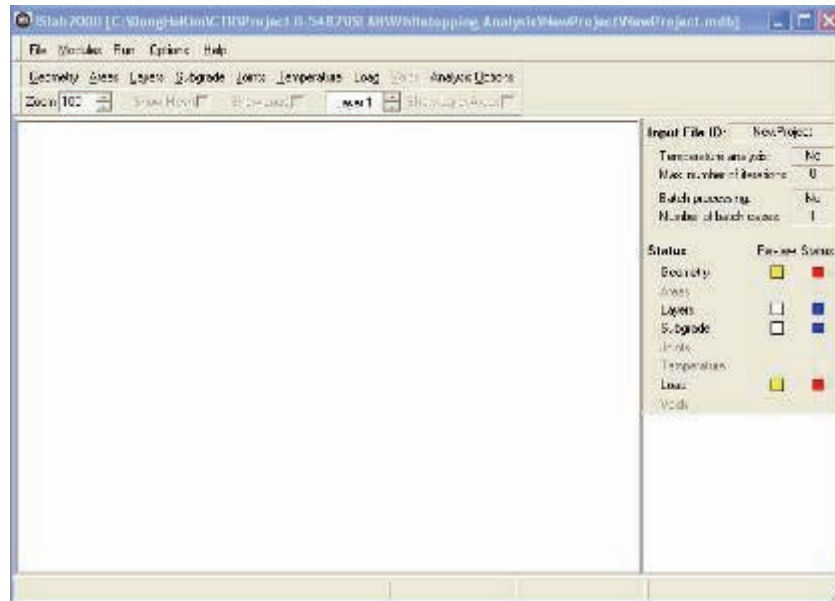


Figure 5.4: Initial input screen of program

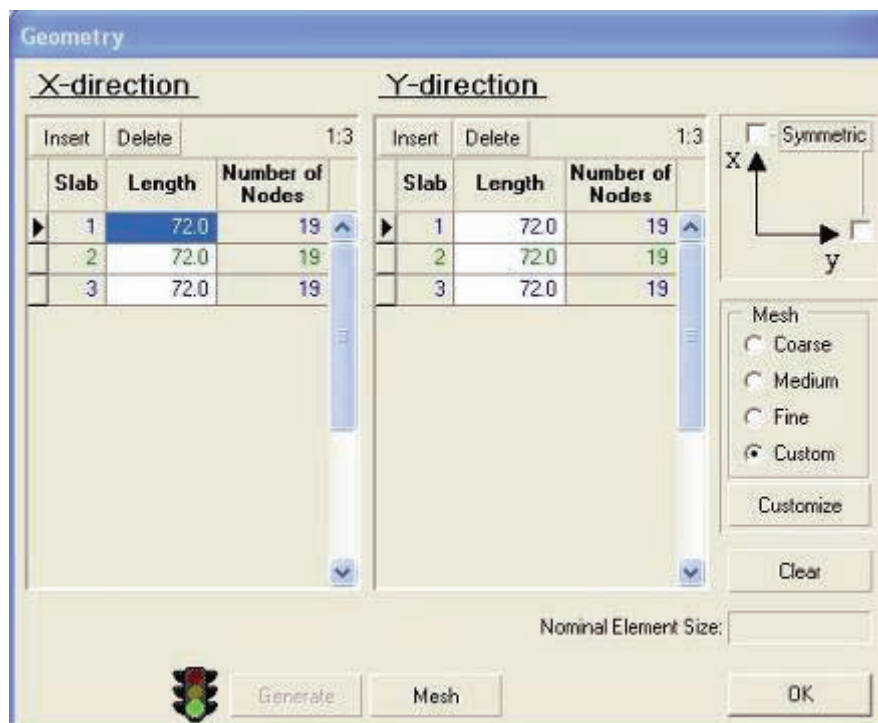


Figure 5.5: Geometry options

Layers

Number of layers: 3 Add Layer Delete Layer

Layer 1 | Layer 2 | Layer 3

Name: Concrete

Thickness: 4.000

Elastic Modulus:  $4.000 \times 10^5$

Poisson Ratio: 0.150

Coefficient of Thermal Expansion:  $4.00 \times 10^{-6}$

Unit Weight: 0.0670

Interface with above Layer: Disable for link layer

Interface K-value (Tolsti Model):

Description: Concrete

☒ Default ☐ Static ☐ Exceptions Edit Batch... Edit Exceptions...

☒ Uniform cross section ☐ Nonuniform cross section Edit Cross Section... OK

(a) Concrete

Layers

Number of layers: 3 Add Layer Delete Layer

Layer 1 | Layer 2 | Layer 3

Name: Asphalt

Thickness: 3.000

Elastic Modulus:  $2.000 \times 10^5$

Poisson Ratio: 0.350

Coefficient of Thermal Expansion:  $8.00 \times 10^{-6}$

Unit Weight: 0.0640

Interface with above Layer: Unbonded

Interface K-value (Tolsti Model):

Description: Asphalt

☒ Default ☐ Static ☐ Exceptions Edit Batch... Edit Exceptions...

☒ Uniform cross section ☐ Nonuniform cross section Edit Cross Section... OK

(b) Asphalt

Layers

Number of layers: 3 Add Layer Delete Layer

Layer 1 | Layer 2 | Layer 3

Name: Base

Thickness: 5.000

Elastic Modulus:  $1.000 \times 10^5$

Poisson Ratio: 0.450

Coefficient of Thermal Expansion:  $4.00 \times 10^{-6}$

Unit Weight: 0.0650

Interface with above Layer: Tolsti Model

Interface K-value (Tolsti Model):  $4.94 \times 14$

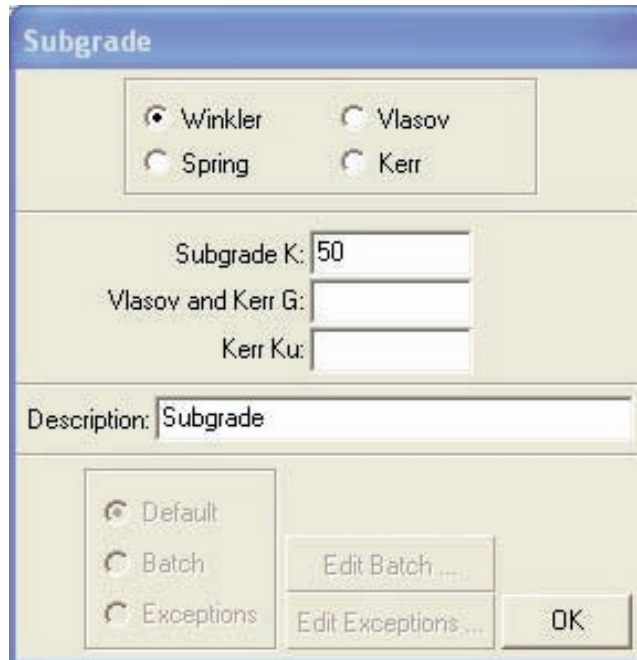
Description: Base

☒ Default ☐ Static ☐ Exceptions Edit Batch... Edit Exceptions...

☒ Uniform cross section ☐ Nonuniform cross section Edit Cross Section... OK

(c) Base

Figure 5.6: Input screens for each pavement layer



**Subgrade**

☒ Winkler      ☐ Vlasov  
☐ Spring      ☐ Kerr

Subgrade K:   
 Vlasov and Kerr G:   
 Kerr Ku:

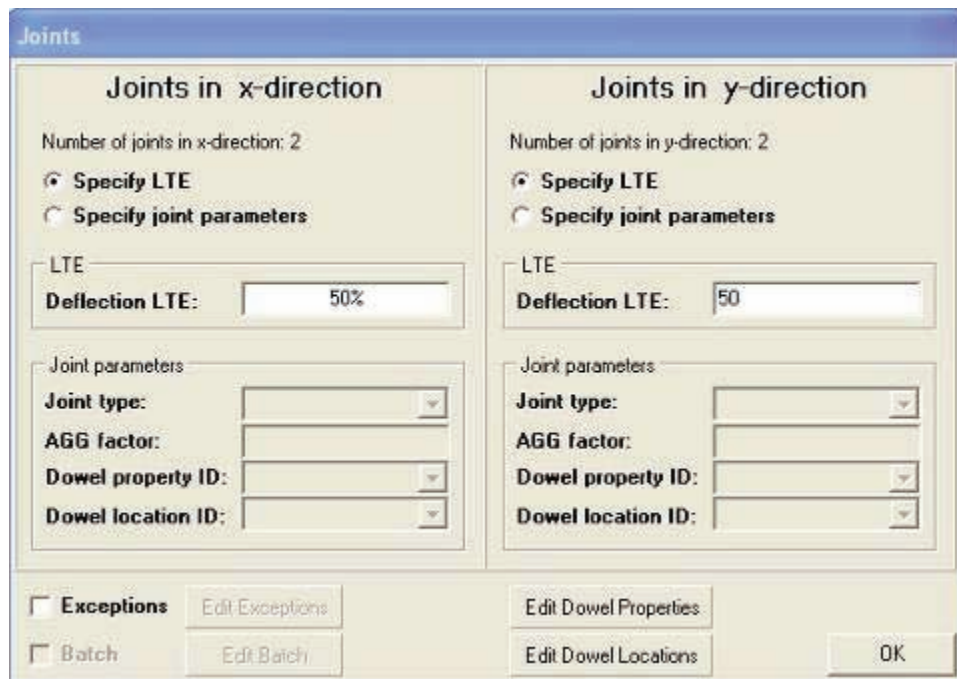
Description:

☒ Default  
☐ Batch  
☐ Exceptions

Edit Batch ...  
 Edit Exceptions ...

OK

Figure 5.7: Subgrade options



**Joints**

**Joints in x-direction**

Number of joints in x-direction: 2

☒ Specify LTE  
☐ Specify joint parameters

LTE

Deflection LTE:

Joint parameters

Joint type:   
 AGG factor:   
 Dowel property ID:   
 Dowel location ID:

**Joints in y-direction**

Number of joints in y-direction: 2

☒ Specify LTE  
☐ Specify joint parameters

LTE

Deflection LTE:

Joint parameters

Joint type:   
 AGG factor:   
 Dowel property ID:   
 Dowel location ID:

☐ Exceptions      Edit Exceptions  
☐ Batch      Edit Batch

Edit Dowel Properties  
 Edit Dowel Locations

OK

Figure 5.8: Joint options

**Layers Temperature Properties**

☒ Perform Temperature Analysis

		Temperatures					
Layer	Type	Difference	Top	Middle	Bottom	Reference	
▶ 1	Linear	12.00					<div> <div></div> <div></div> <div></div> <div></div> </div>
2	Linear	0.00					
3	Linear	0.00					

☐ Batch

Figure 5.9: Temperature properties of each layer

**Load**

☒ Place Axles
 ☐ Place Trucks

Axle Number	Reference Point	Axle Name	X-Location	Y-Location	Load
▶ 1	Bottom Left	SAL	96.5	72.0	20000

☐ Batch

Figure 5.10: Load options

**Analysis Options**

Problem description: SAL

Input file directory: C:\DongHoKim\CTR\Project 0-5482\SLAB\w\hitetopping

Input file ID: SAL

☒ Temperature analysis

☐ Batch processing

Maximum number of iterations: 10

Batch Parameters:

Total number of cases:	1
Name	Number of Cases

OK

Figure 5.11: Analysis options

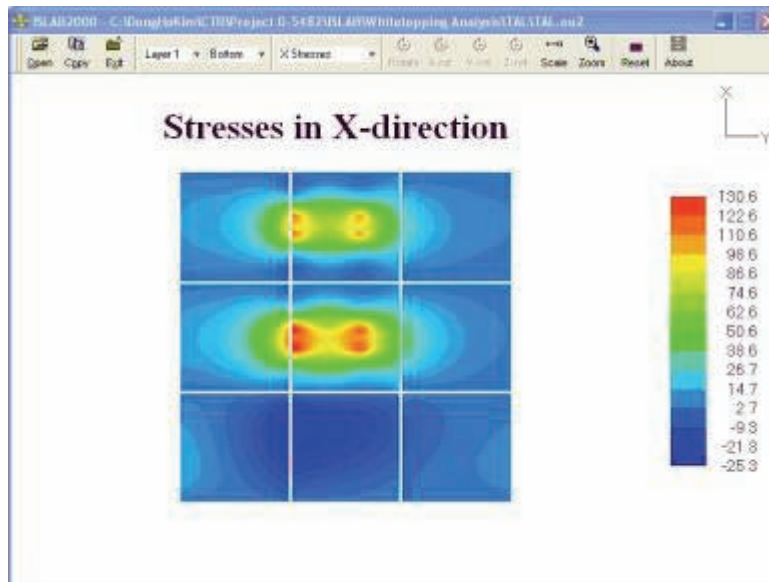


Figure 5.12: Stress contour in x-direction

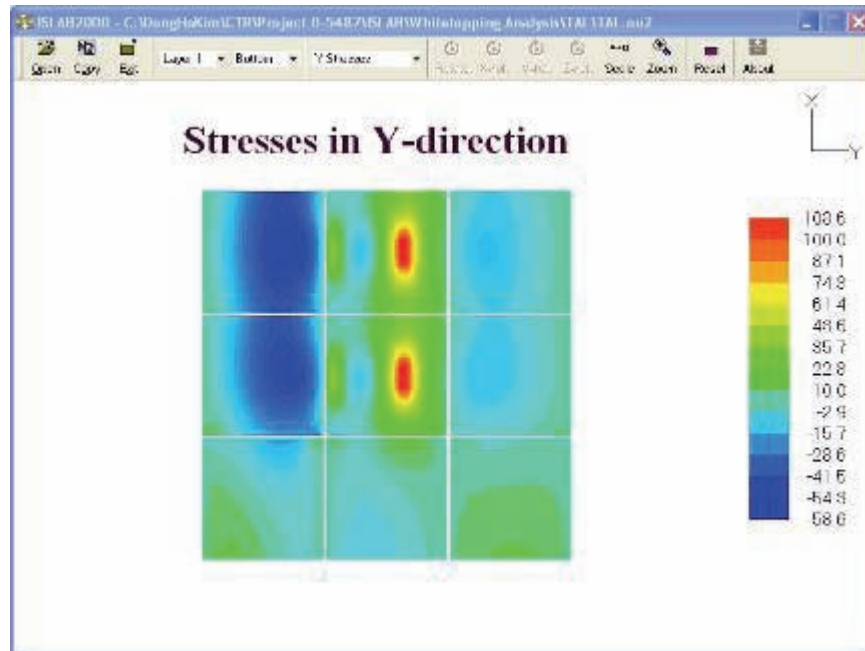


Figure 5.13: Stress contour in y-direction

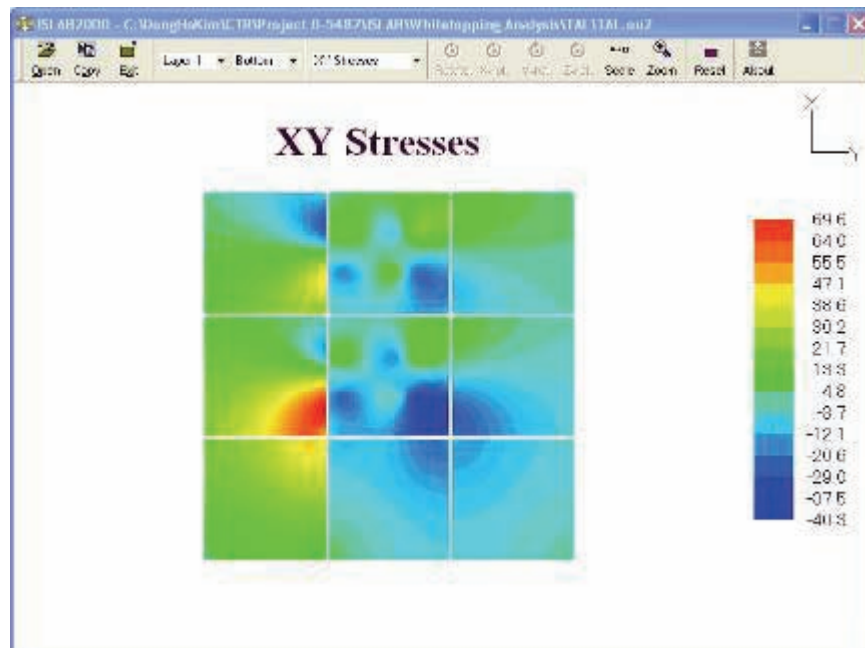


Figure 5.14: Shear stress contour



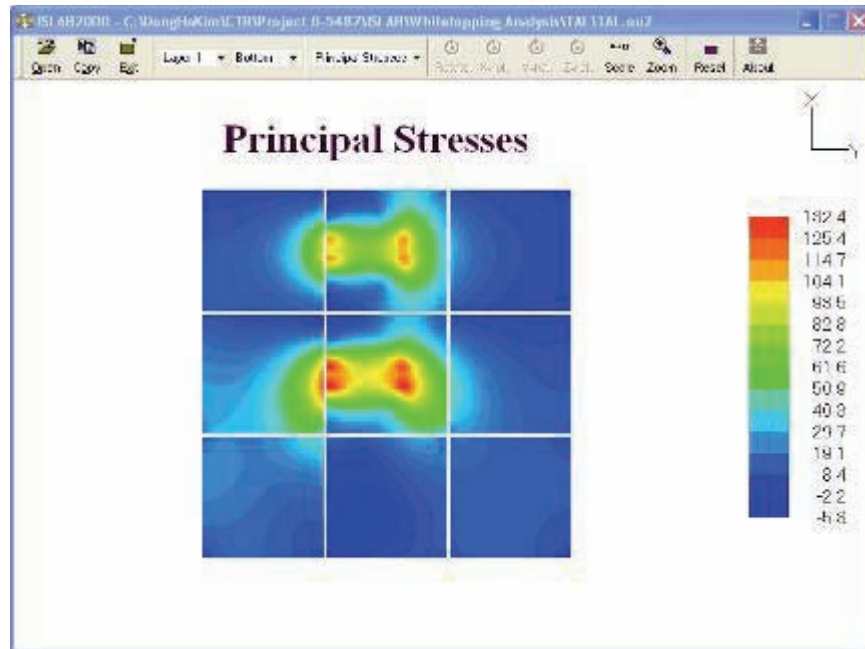


Figure 5.15: Principal stress contour

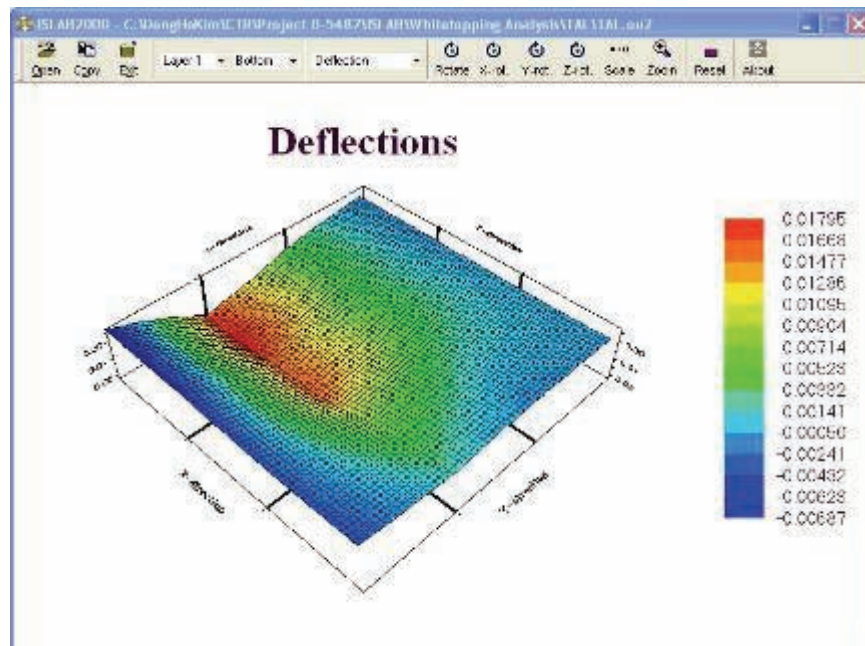


Figure 5.16: Deflection contour

### 5.2.2 Analysis of ISLAB2000 Output

#### *Effect of Interface Bond Conditions on Maximum Stress*

Figure 5.17 shows sample results of the comparison of the ISLAB2000 outputs for bond conditions for SAL and TAL loads, respectively. Although the unbonded case always showed the higher maximum stress due to loading, there was no clear mathematical relationship between the bonded and unbonded stresses. The correlation factor ( $R^2$ ) for these datasets ranged from 0.41 to 0.44 only. Colorado DOT (1998) performed an experiment on this issue and the following relationship was found by comparing the measured tied edge loading partial bond stresses and theoretical fully bonded edge stresses.

$$\sigma_{ex} = 1.65 \times \sigma_{th} \quad (5.1)$$

where,

$\sigma_{ex}$  = measured experimental partially bonded stress (psi), and

$\sigma_{th}$  = calculated fully bonded stress (psi).

It is almost impossible to estimate the interface bond conditions in the field and the conditions would vary with locations. To induce conservative results, the unbonded interface condition was selected to establish the design equation in this study. Equation 5.1 was used to predict stress in the proposed design equation model, which will be discussed later in this report.

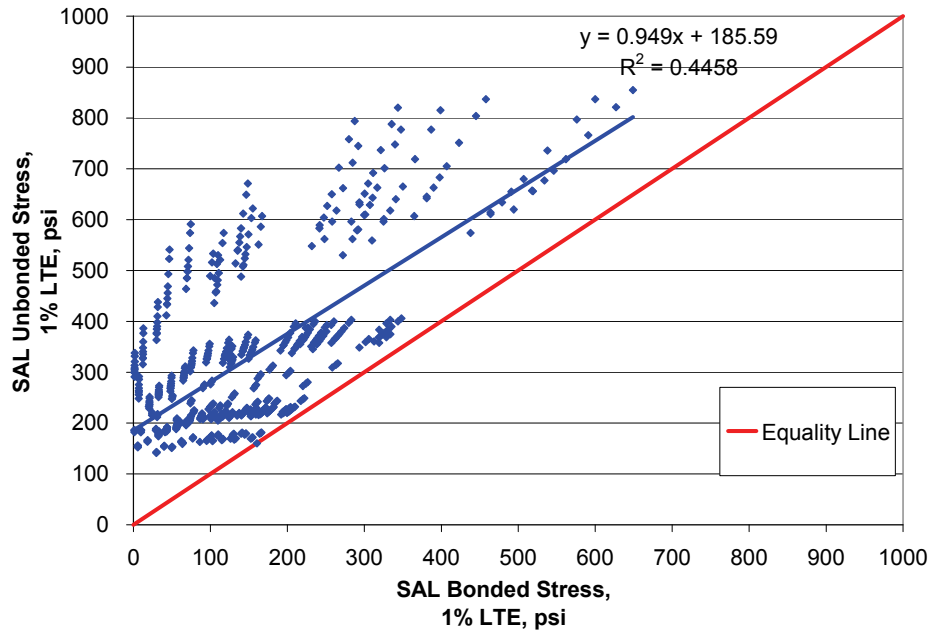
#### *Effect of LTE on Maximum Stress*

Three load transfer efficiency (LTE) levels were used as an input variable for numerical simulations in this project: 1, 50, and 99%. The ISLAB2000 output shows the very close relationship for all loading cases between LTE levels as shown in Figure 5.18. It is very difficult to estimate the LTE in the field; for conservative purposes, the 1% LTE data sets were selected for the prediction model.

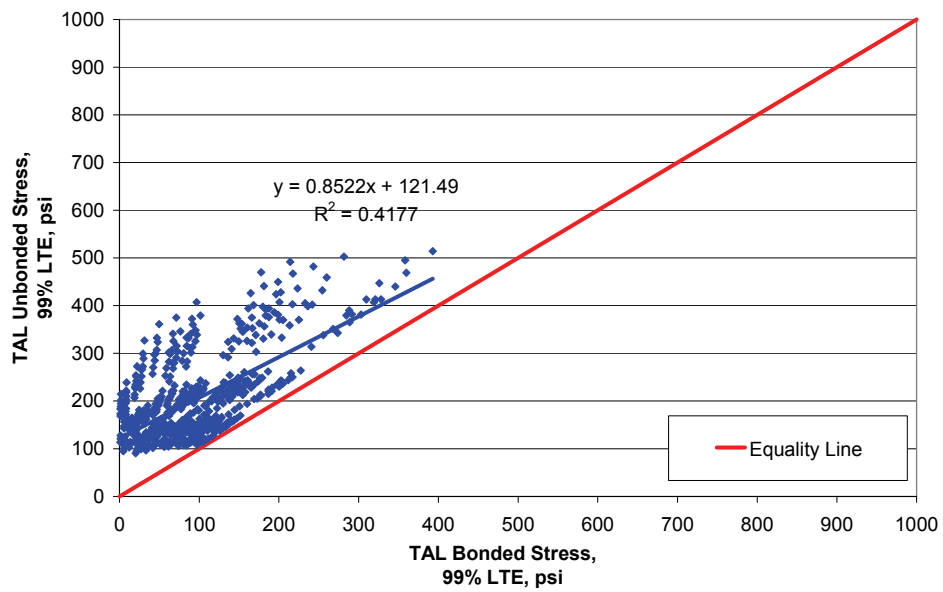
#### *Effect of Loading Type on Maximum Stress*

Figure 5.19 shows the effect of loading type on the maximum stress in the whitetopping concrete. The SAL loading conditions show about 5 to 10% higher stress values compared to the TAL loading conditions. For this research, SAL load stresses were selected for the development of the prediction model, which is a more conservative loading type.



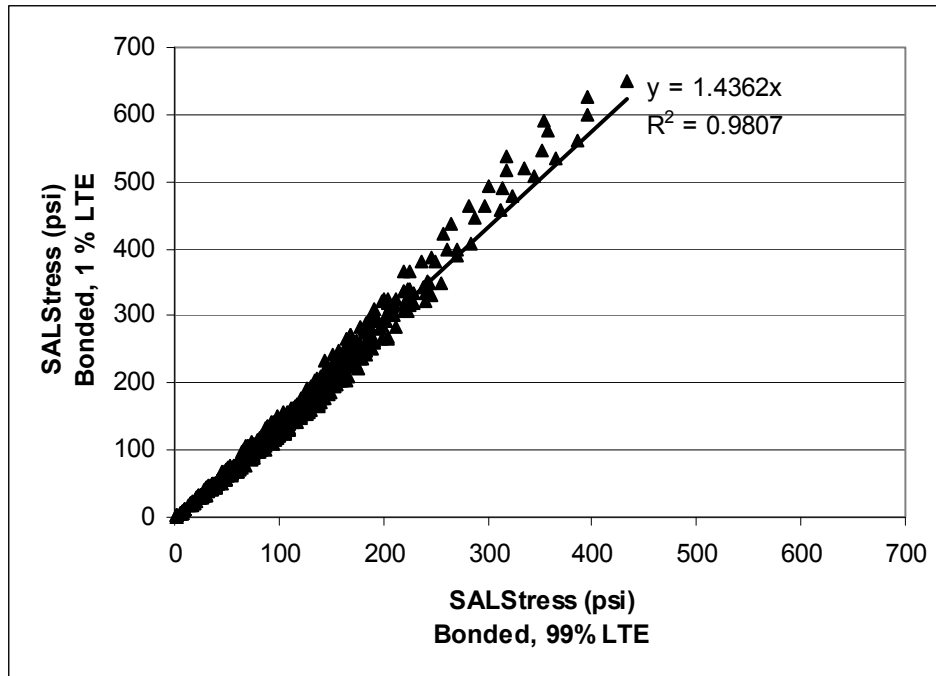


(a) SAL, 1% LTE

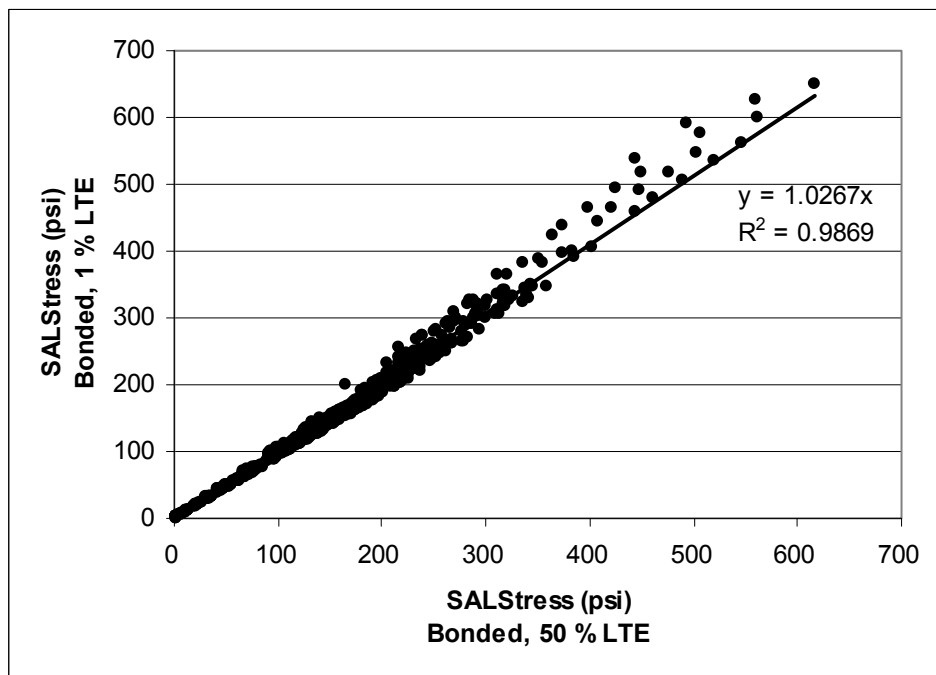


(b) TAL, 99% LTE

Figure 5.17: Effect of bond conditions on maximum stress

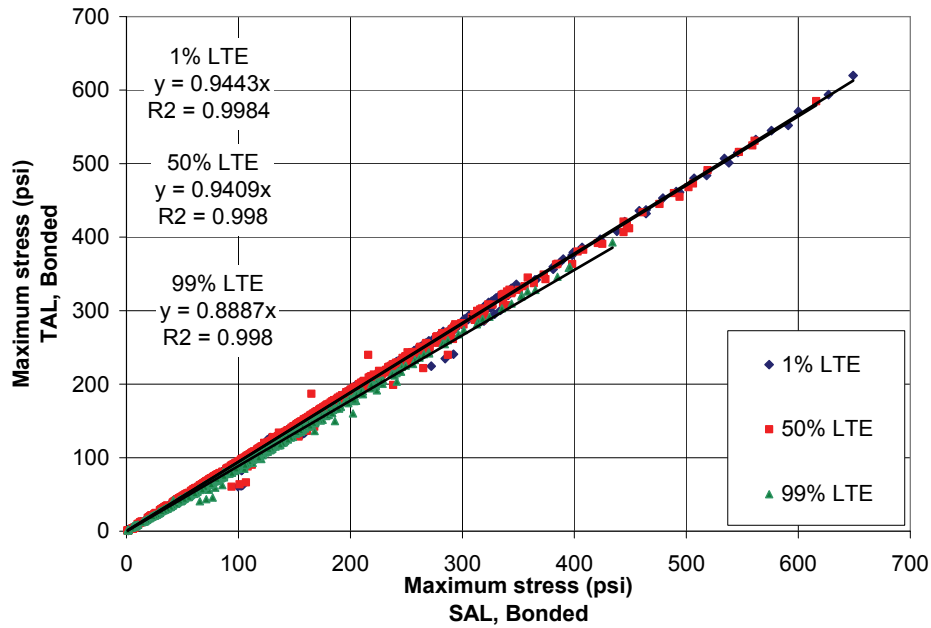


(a) 1% LTE vs. 99% LTE

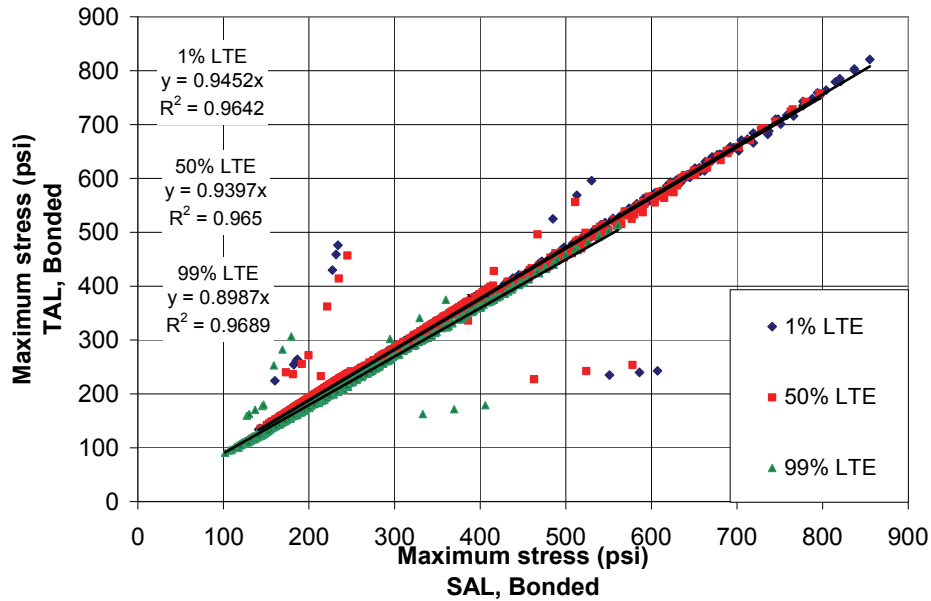


(b) 1% LTE vs. 50% LTE

Figure 5.18: Effect of LTE on maximum stress: SAL, bonded interface



(a) SAL vs. TAL: bonded interface



(b) SAL vs. TAL: unbonded interface

Figure 5.19: Effect of loading type on maximum stress

### 5.3 Regression Analysis

The ISLAB2000 calculation model generated a large number of data sets based on variable selections. To establish a statistically meaningful regression equation, a log-log expression was used for data analyses as shown in Equation 5.2.

$$\log(\sigma) = A + B\log(t_{PCC}) + C\log(E_{PCC}) + D\log(t_{AC}) + E\log(E_{AC}) + F\log(t_{BS}) + G\log(E_{BS}) + H\log(k) \quad (5.2)$$

where,

$A, B, C, D, E, F, G, H$  = regression coefficients,

$\sigma$  = maximum stress at the bottom fiber of whitetopping pavement,

$t_{PCC}$  = thickness of the concrete layer, in,

$E_{AC}$  = concrete modulus of elasticity, psi,

$t_{AC}$  = thickness of the asphalt layer, in,

$E_{AC}$  = asphalt modulus of elasticity, psi,

$t_{BS}$  = thickness of the base layer, in,

$E_{BS}$  = base modulus of elasticity, psi, and

$k$  = modulus of subgrade reaction, pci.

The stress output data for both bonded and unbonded interface conditions under SAL and 1% LTE loading were processed using regression analysis. The least squares linear regression analysis was used to determine the best fit for the coefficients in Equation 5.2.

Because the initial output data are very broadly scattered, the target data set was divided by three groups based on the output values: 1) low stress range (lower than 300 psi), 2) mid stress range (300 to 450 psi), and 3) high stress range (more than 450 psi). Table 5.2 shows the regression coefficients results for Equation 5.2 from regression analysis of the stress output data set under the bonded interface, SAL, and 1% LTE loading conditions.

**Table 5.2: Regression coefficients for Equation (5.2)—bonded, SAL, and 1% LTE**

Regression Coefficient	Low Stress Range (less than 300 psi)	Mid Stress Range (300 to 450 psi)	High Stress Range (more than 450 psi)
$A$	6.4598	3.3736	3.5706
$B$	-9.7900	-2.4642	8.4016
$C$	4.8760	0.6044	-6.8272
$D$	1.9640	0.9096	-1.0822
$E$	0.9297	-0.3078	0.0000
$F$	0.2838	-0.1945	-1.1155
$G$	-2.1592	-0.7195	1.0457
$H$	-0.7040	-0.2348	0.3328
Adjusted $R^2$	0.943	0.923	0.970

Figure 5.20 presents the comparison between the predicted stresses and ISLAB2000 output values calculated using the coefficients in Table 5.2. The developed regression equation generated practically conservative and acceptable stress results.

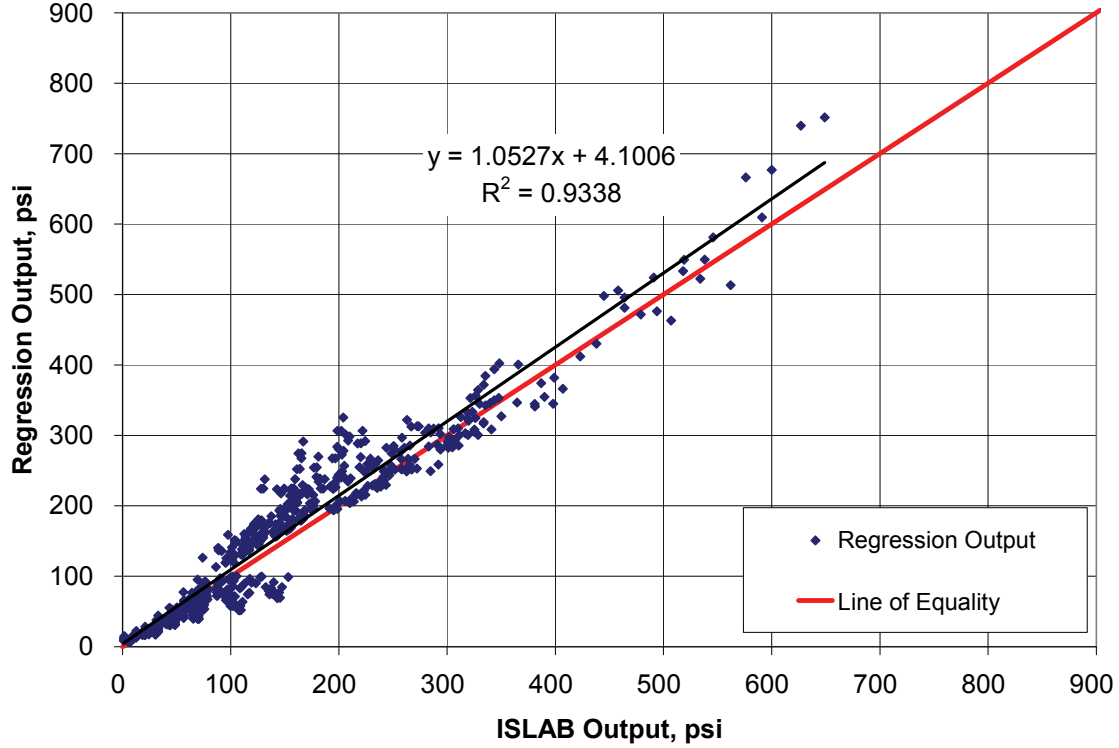


Figure 5.20: Regression output vs. ISLAB2000 output: bonded, SAL, 1% LTE

## 5.4 Development of TWT Design Equations

### 5.4.1 Stress Prediction of Unbonded Interface Conditions

The developed stress prediction equation shown in the previous section was limited to cases with bonded interface. For the unbonded interface cases, Equation 5.3 was used to calculate maximum stress as discussed in the previous sections.

$$\sigma_{unbonded} = 1.65 \times \sigma_{bonded} \quad (5.3)$$

where,

$\sigma_{unbonded}$  = maximum stress of whitetopping under unbonded interface condition, and

$\sigma_{bonded}$  = maximum stress of whitetopping under bonded interface condition.

### 5.4.2 Calibration of Stress Prediction using Fatigue Behavior of Whitetopping

The developed stress prediction equation shown in Equation (5.2) and Table 5.2 was calibrated using experimentally determined fatigue criterion for whitetopping. It is found that the fatigue equation (S-N curve) for whitetopping slabs derived in this study is very close to Thompson and Barenburg's S-N curve after the application of the equivalent fatigue life concept. Equation 5.4 presents Thomson and Barenburg's fatigue curve.

$$\log N = -1.7136 \frac{\sigma}{MR} + 4.284 \quad \left( \frac{\sigma}{MR} \geq 1.25 \right)$$

$$\log N = 2.8127 \left( \frac{\sigma}{MR} \right)^{-1.2214} \left( \frac{\sigma}{MR} \right)^{1.25} \quad (5.4)$$

where,

$N$  = number of load repetition to failure,  
 $\sigma$  = maximum stress of whitetopping, and  
 $MR$  = modulus of rupture of concrete.

### 5.4.3 Development of Thickness Prediction Equations

The thickness prediction equation for whitetopping concrete was developed combining Equations 5.2 through 5.4. The conversion factors from a 20-kip SAL to the 18-kip equivalent single axle load (ESAL) was considered as 1.0, which provides a little conservatism.

The derived final thickness prediction equation for thin whitetopping concrete pavement is the following:

$$\begin{aligned} \log(t_{PCC}) = & 3.5615 + 0.1017 \cdot \log(ESALs) + 0.4982 \cdot \log(E_{PCC}) \\ & - 0.7232 \cdot \log(t_{AC}) - 0.3624 \cdot \log(E_{AC}) - 0.2695 \cdot \log(t_{BS}) - 0.0891 \cdot \log(E_{BS}) \\ & - 0.0287 \cdot \log(k) - 1.2250 \cdot \log(MR) \end{aligned} \quad (5.5)$$

where,

$t_{PCC}$  = required thickness of the whitetopping concrete, in,  
 $ESALs$  = expected number of 18-kip ESALs,  
 $E_{PCC}$  = concrete modulus of elasticity, psi,  
 $t_{AC}$  = thickness of the asphalt layer, in,  
 $E_{AC}$  = asphalt modulus of elasticity, psi,  
 $t_{BS}$  = thickness of the base layer, in,  
 $E_{BS}$  = base modulus of elasticity, psi,  
 $k$  = modulus of subgrade reaction, pci, and  
 $MR$  = modulus of rupture of whitetopping concrete, psi.

Three factors of safety were incorporated into the prediction equations: 1) using the 18-kips ESAL as the standard load, while original ISLAB2000 outputs were based on 20-kip SAL, 2) using a 1% LTE data, which showed highest stress results compared to calculated stresses using higher LTE loading cases, 3) use of unbonded interface stress by Equation 5.3.

### 5.5 Sensitivity Analysis

Sensitivity analyses were conducted for calculated whitetopping thickness using the proposed prediction equations. Design variables included the expected number of 18-kip ESALs, concrete elastic modulus, asphalt thickness, asphalt elastic modulus, base thickness, base elastic modulus, and modulus of subgrade reaction.

The sensitivity analysis plots for the various design variables are presented in Figures 5.21 through 5.28. For the most cases, whitetopping thicknesses are not very sensitive to the number of expected load repetitions (ESALs), especially when projected ESALs exceed 2 million.

The geometric property (thickness of each layer) of the whitetopping pavement is more sensitive to the whitetopping thickness compared to the material properties (elastic modulus of each layer and k-value) except for the whitetopping concrete strength (modulus of rupture). The asphalt thickness is more sensitive to the whitetopping thickness than the base thickness as shown in Figures 5.21 and 5.22.

The asphalt elastic modulus has the most influence on the required whitetopping thickness compared to other material properties. The elastic modulus of concrete has a slight impact on the whitetopping thickness while the base elastic modulus and k-value shows minimal sensitivity to the whitetopping thickness.

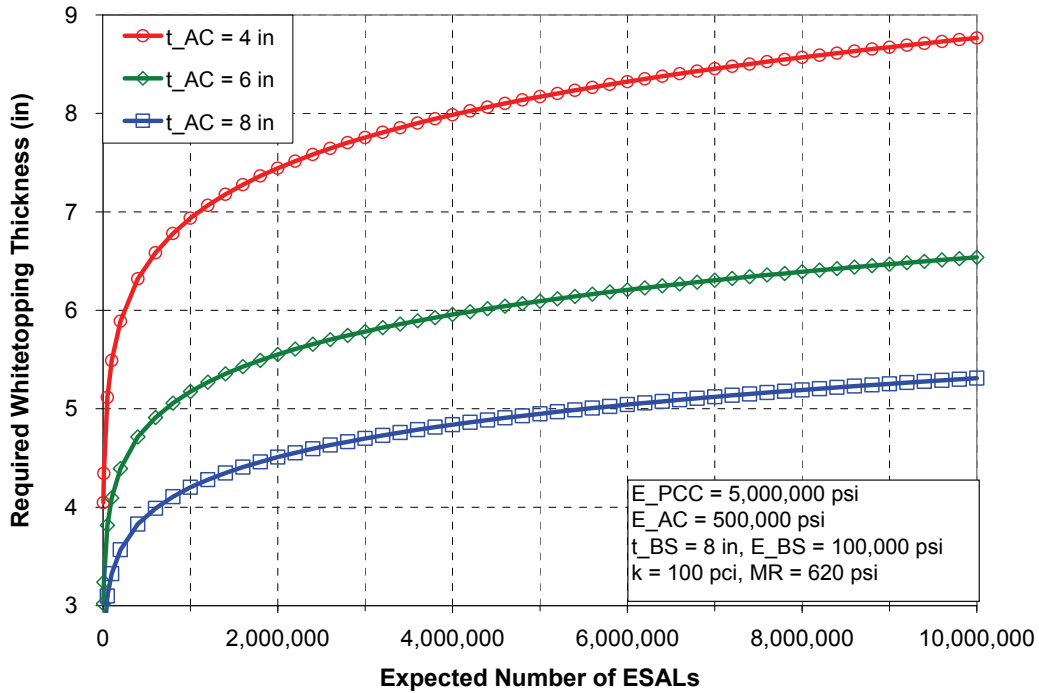


Figure 5.21: Whitetopping thickness sensitivity to asphalt thickness

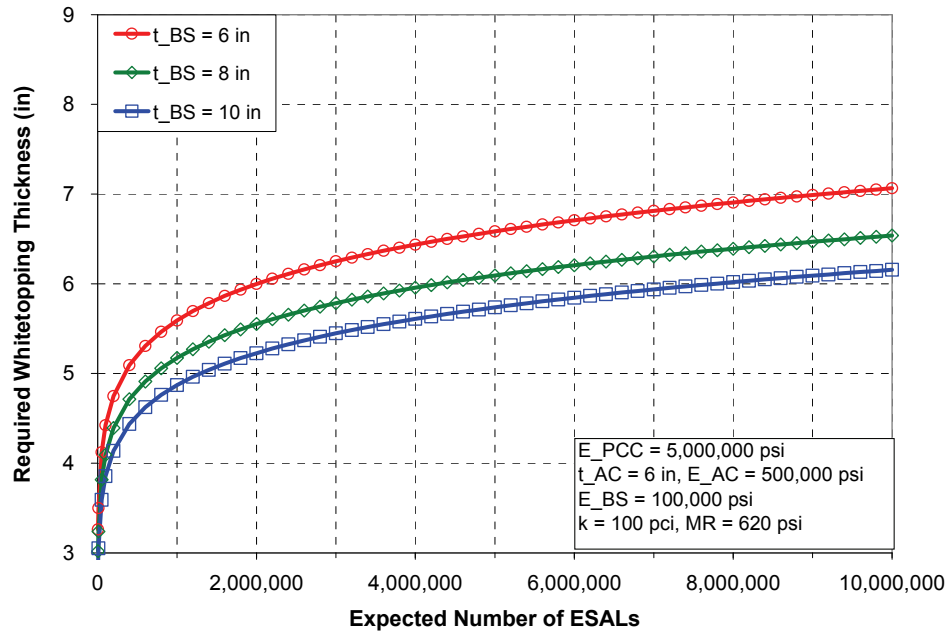


Figure 5.22: Whitetopping thickness sensitivity to base thickness

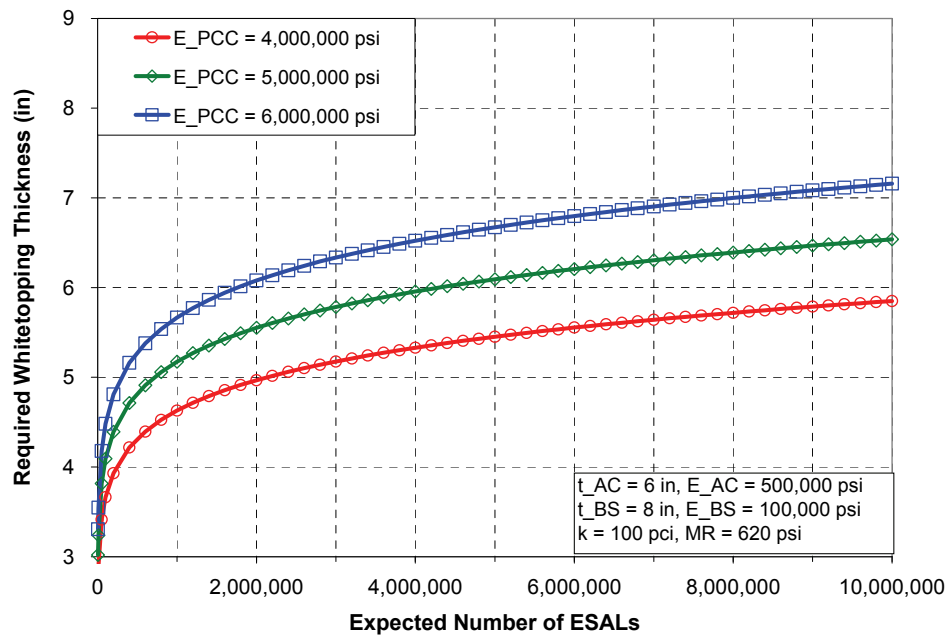


Figure 5.23: Whitetopping thickness sensitivity to concrete elastic modulus



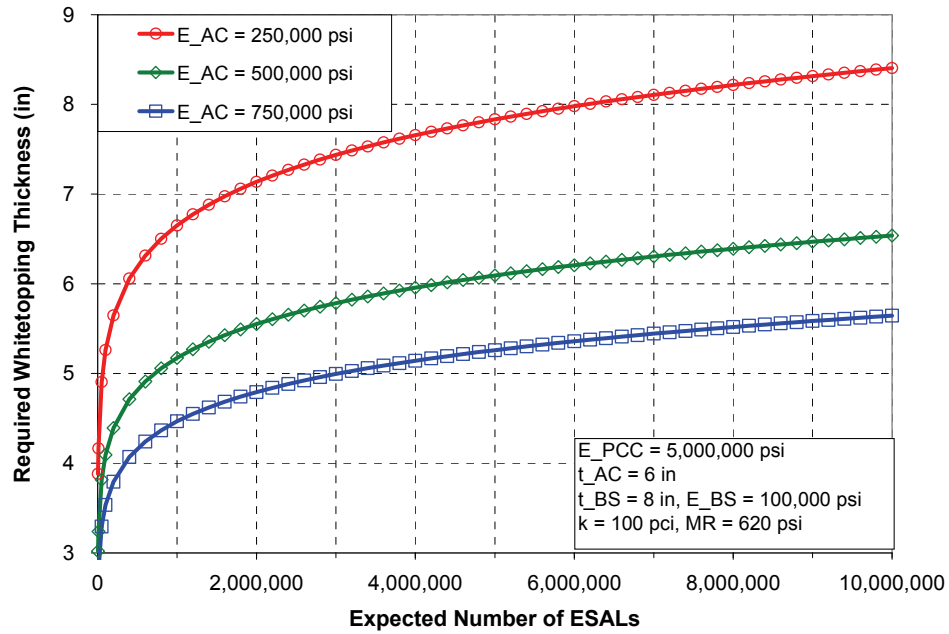


Figure 5.24: Whitetopping thickness sensitivity to asphalt modulus

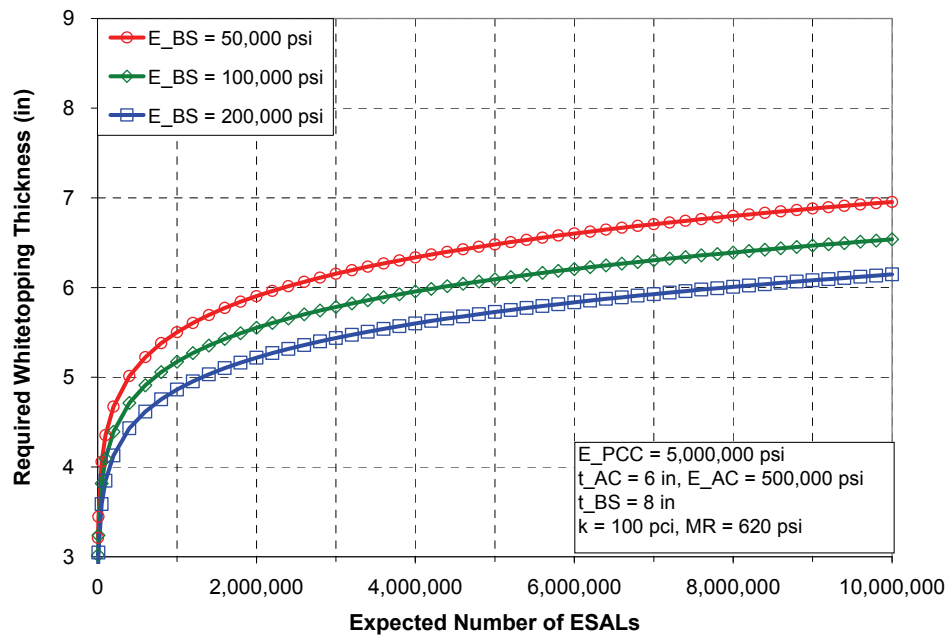


Figure 5.25: Whitetopping thickness sensitivity to base modulus

The minimum required asphalt thickness can be calculated under given conditions using the proposed design equation. Figure 5.26 presents the required minimum concrete thickness sensitivity to asphalt modulus and asphalt thickness. Even with a very high asphalt modulus (750,000 psi), the minimum asphalt layer thickness should not be lower than 4 in.

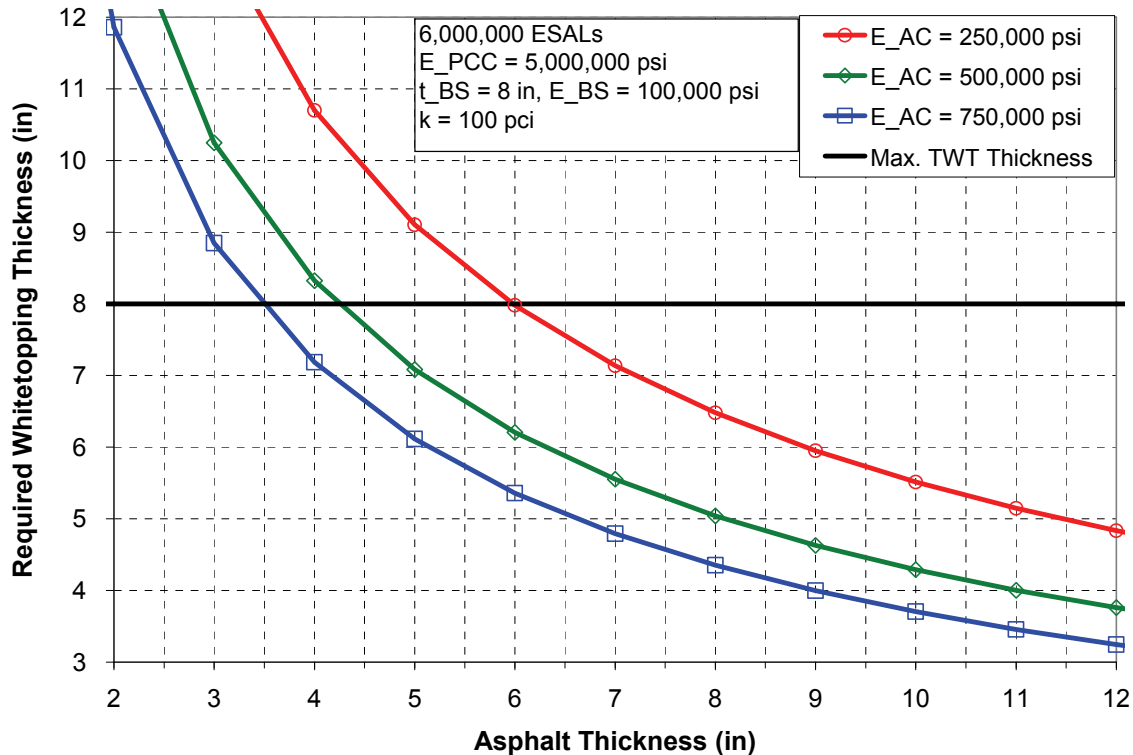


Figure 5.26: Minimum whitetopping thickness sensitivity to asphalt thickness

The subgrade reaction modulus (k-value) has the least effect on the calculation of the whitetopping thickness. The required concrete thickness is almost identical regardless of the k-values, as shown in Figure 5.27.

Concrete flexural strength has one of the greatest impacts on the whitetopping thickness, as shown in Figure 5.28.

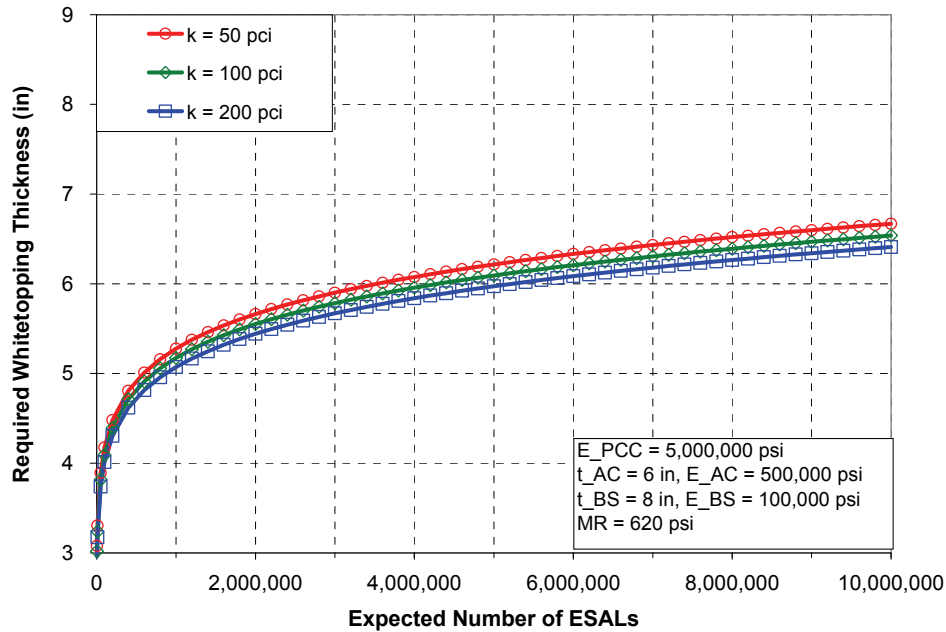


Figure 5.27: Whitetopping thickness sensitivity to subgrade reaction modulus

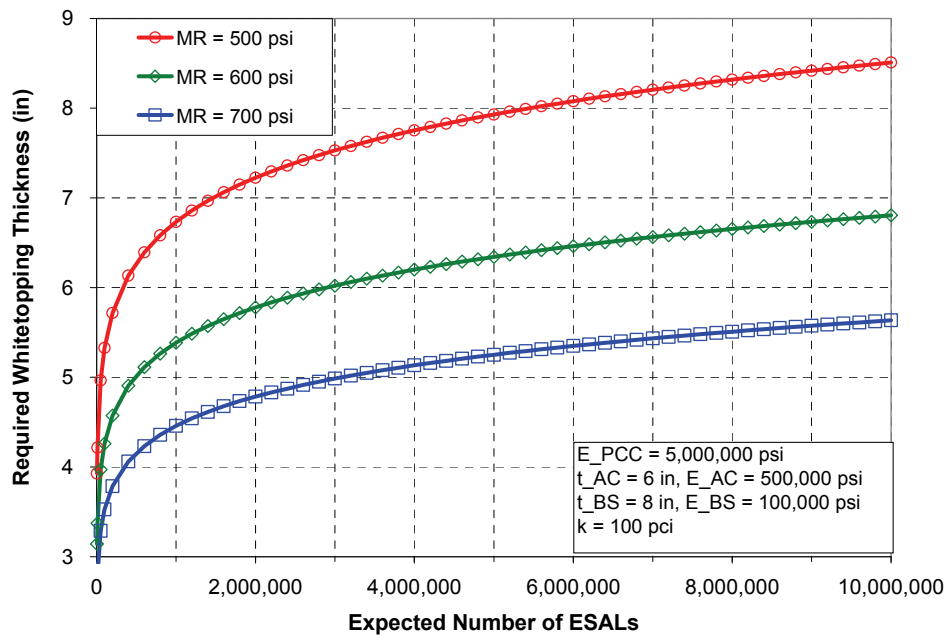


Figure 5.28: Whitetopping thickness sensitivity to modulus of rupture of concrete

## 5.6 Comparison with Current TxDOT Design Thickness

The current thin whitetopping thickness design from the TxDOT Pavement Design Manual (2006) is presented in Table 5.3.

**Table 5.3: Current TxDOT thin whitetopping thickness design**

<i>Trucks per Day</i>	<i>Design Life (yr)</i>					
	5	6	7	8	9	10
	thin whitetopping thickness (in.)					
200	4	4	4	4	4	4
250	4	4	4	4	5	5
300	4	4	4	5	5	5
350	4	4	5	5	5	5
400	4	5	5	5	5	5
450	5	5	5	5	5	6
500	5	5	5	5	6	6
600	5	5	5	6	6	6
700	5	5	6	6	7	7
800	5	6	6	7	7	7
900	6	6	6	7	7	n/a
<b>1,000</b>	6	6	7	7	n/a	n/a

To compare the current design values to the values from the proposed design equation, the “Trucks per day” in Table 5.3 should be converted to ESALs by using an equivalent axle load factor (EALF). Equation 5.6 was used for the conversion of trucks per day to ESALs.

$$ESALs = (trucks\ per\ day) \times EALF \times 365 \times (design\ life\ in\ years) \quad (5.6)$$

where,

$ESALs$  = number of 18-kip equivalent single axle load (ESAL), and

$EALF$  = equivalent axle load factor

An equivalent axle load factor (EALF) defines the damage per pass to pavement by the axle in question relative to the damage per pass of a standard axle load, usually an 18-kip single axle load (Huang, 2004). One of the most widely used EALFs is the AASHTO EALF, which was developed from the AASHTO Road Test (AASHTO, 1972). The AASHTO EALF equation is the empirical equation based on the serviceability concept, while the approach in this research project is purely mechanistic. Because of this, the use of AASHTO EALFs in Equation 5.6 to estimate the expected ESALs for the determination of the required thickness of a whitetopping system may lead to unreasonable ESAL values. Typical AASHTO EALFs for a concrete pavement system are presented in Table 5.4 for reference. The rigid pavement system in Table 5.4 assumed a terminal serviceability index of 2.5 ( $p_t = 2.5$ ) and 9- in thickness ( $D = 9$  in).

Tables 5.5 through 5.8 present the converted results of trucks per day to ESALs using Equation 5.6 with four different levels of EALF: 0.5, 1.0, 1.5, and 2.0.

**Table 5.4: AASHTO Equivalent axle load factors for rigid pavements ( $D = 9$  in,  $p_t = 2.5$ )**

Axle load (kips)	Equivalent axle load factor			Axle load (kips)	Equivalent axle load factor		
	Single axles	Tandem axles	Tridem axles		Single axles	Tandem axles	Tridem axles
2	0.0002	0.0001	0.0001	22	2.34	0.308	0.099
4	0.002	0.0005	0.0003	24	3.36	0.444	0.141
6	0.01	0.02	0.001	26	4.67	0.622	0.195
8	0.032	0.005	0.002	28	6.29	0.85	0.265
10	0.082	0.013	0.005	30	8.28	1.14	0.354
12	0.176	0.026	0.009	32	10.7	1.49	0.463
14	0.341	0.048	0.017	34	13.6	1.92	0.596
16	0.604	0.082	0.028	36	17.1	2.43	0.757
18	1.00	0.133	0.044	38	21.3	3.03	0.948
20	1.57	0.206	0.067	40	26.3	3.74	1.17

**Table 5.5: Converted ESALs for current TxDOT design: EALF = 0.5**

Trucks per Day	Design Life (yr)					
	5	6	7	8	9	10
	Converted 18-kip ESALs					
200	91,250	109,500	127,750	146,000	164,250	182,500
250	114,063	136,875	159,688	182,500	205,313	228,125
300	136,875	164,250	191,625	219,000	246,375	273,750
350	159,688	191,625	223,563	255,500	287,438	319,375
400	182,500	219,000	255,500	292,000	328,500	365,000
450	205,313	246,375	287,438	328,500	369,563	410,625
500	228,125	273,750	319,375	365,000	410,625	456,250
600	273,750	328,500	383,250	438,000	492,750	547,500
700	319,375	383,250	447,125	511,000	574,875	638,750
800	365,000	438,000	511,000	584,000	657,000	730,000
900	410,625	492,750	574,875	657,000	739,125	821,250
<b>1,000</b>	456,250	547,500	638,750	730,000	821,250	912,500

**Table 5.6: Converted ESALs for current TxDOT design: EALF = 1.0**

<i>Trucks per Day</i>	<i>Design Life (yr)</i>					
	5	6	7	8	9	10
	Converted 18-kip ESALs					
200	182,500	219,000	255,500	292,000	328,500	365,000
250	228,125	273,750	319,375	365,000	410,625	456,250
300	273,750	328,500	383,250	438,000	492,750	547,500
350	319,375	383,250	447,125	511,000	574,875	638,750
400	365,000	438,000	511,000	584,000	657,000	730,000
450	410,625	492,750	574,875	657,000	739,125	821,250
500	456,250	547,500	638,750	730,000	821,250	912,500
600	547,500	657,000	766,500	876,000	985,500	1,095,000
700	638,750	766,500	894,250	1,022,000	1,149,750	1,277,500
800	730,000	876,000	1,022,000	1,168,000	1,314,000	1,460,000
900	821,250	985,500	1,149,750	1,314,000	1,478,250	1,642,500
<b>1,000</b>	912,500	1,095,000	1,277,500	1,460,000	1,642,500	1,825,000

**Table 5.7: Converted ESALs for current TxDOT design: EALF = 1.5**

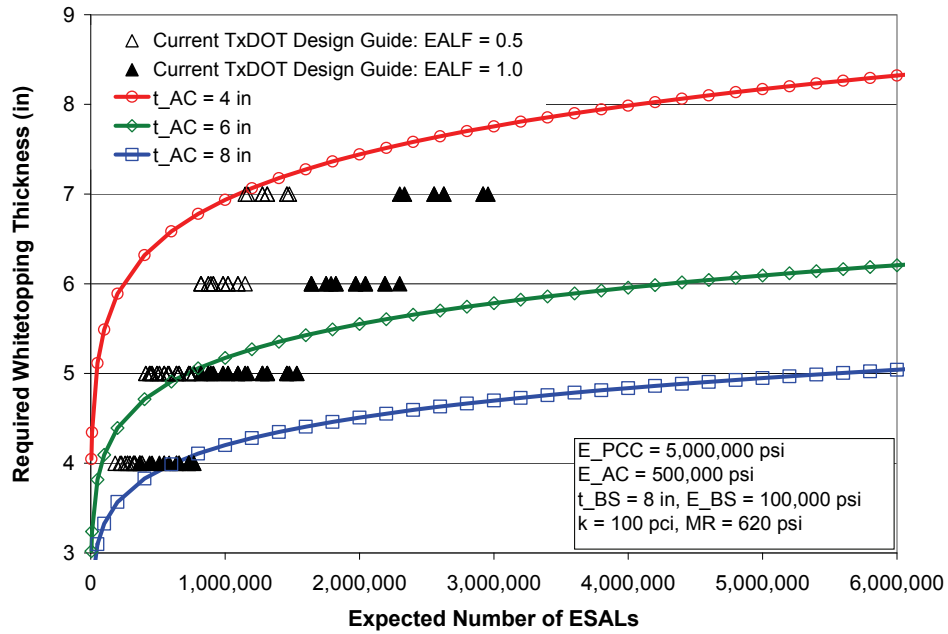
<i>Trucks per Day</i>	<i>Design Life (yr)</i>					
	5	6	7	8	9	10
	Converted 18-kip ESALs					
200	273,750	328,500	383,250	438,000	492,750	547,500
250	342,188	410,625	479,063	547,500	615,938	684,375
300	410,625	492,750	574,875	657,000	739,125	821,250
350	479,063	574,875	670,688	766,500	862,313	958,125
400	547,500	657,000	766,500	876,000	985,500	1,095,000
450	615,938	739,125	862,313	985,500	1,108,688	1,231,875
500	684,375	821,250	958,125	1,095,000	1,231,875	1,368,750
600	821,250	985,500	1,149,750	1,314,000	1,478,250	1,642,500
700	958,125	1,149,750	1,341,375	1,533,000	1,724,625	1,916,250
800	1,095,000	1,314,000	1,533,000	1,752,000	1,971,000	2,190,000
900	1,231,875	1,478,250	1,724,625	1,971,000	2,217,375	2,463,750
<b>1,000</b>	1,368,750	1,642,500	1,916,250	2,190,000	2,463,750	2,737,500

**Table 5.8: Converted ESALs for current TxDOT design: EALF = 2.0**

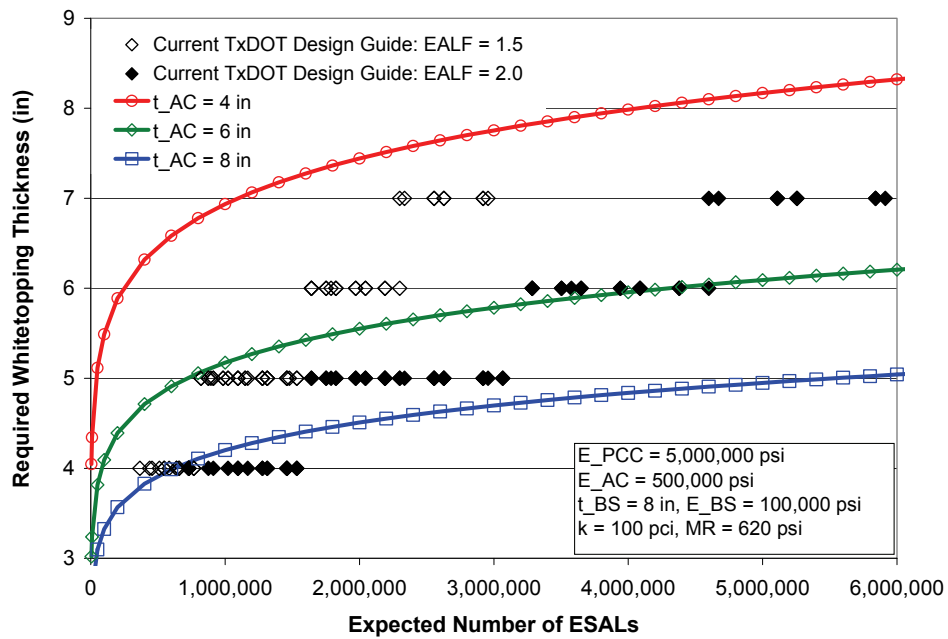
<i>Trucks per Day</i>	<i>Design Life (yr)</i>					
	5	6	7	8	9	10
	Converted 18-kip ESALs					
200	365,000	438,000	511,000	584,000	657,000	730,000
250	456,250	547,500	638,750	730,000	821,250	912,500
300	547,500	657,000	766,500	876,000	985,500	1,095,000
350	638,750	766,500	894,250	1,022,000	1,149,750	1,277,500
400	730,000	876,000	1,022,000	1,168,000	1,314,000	1,460,000
450	821,250	985,500	1,149,750	1,314,000	1,478,250	1,642,500
500	912,500	1,095,000	1,277,500	1,460,000	1,642,500	1,825,000
600	1,095,000	1,314,000	1,533,000	1,752,000	1,971,000	2,190,000
700	1,277,500	1,533,000	1,788,500	2,044,000	2,299,500	2,555,000
800	1,460,000	1,752,000	2,044,000	2,336,000	2,628,000	2,920,000
900	1,642,500	1,971,000	2,299,500	2,628,000	2,956,500	3,285,000
<b>1,000</b>	1,825,000	2,190,000	2,555,000	2,920,000	3,285,000	3,650,000

Two design examples are presented to compare whitetopping thicknesses from proposed design equation and current TxDOT design. As discussed earlier, the two most significant design variables for the thickness of whitetopping is the thickness and elastic modulus of the asphalt layer, in addition to design traffic. Figures 5.29 and 5.30 illustrate the thicknesses of whitetopping pavement using the proposed design equation and TxDOT design table.

The primary difference between the two design methods is that the current TxDOT method does not consider the condition of existing deteriorated asphalt pavement. Rather, it solely depends on design traffic in terms of number of trucks. On the other hand, the proposed design equation is more realistic in that it accounts for all the design variables including layer characteristics. It also utilizes ESALs as a traffic loading input, as the current practice at TxDOT is that TP&P provides design traffic information in terms of ESALs, not number of trucks. Therefore, the proposed design equation will provide TxDOT engineers with a more accurate and convenient design tool for TWT.



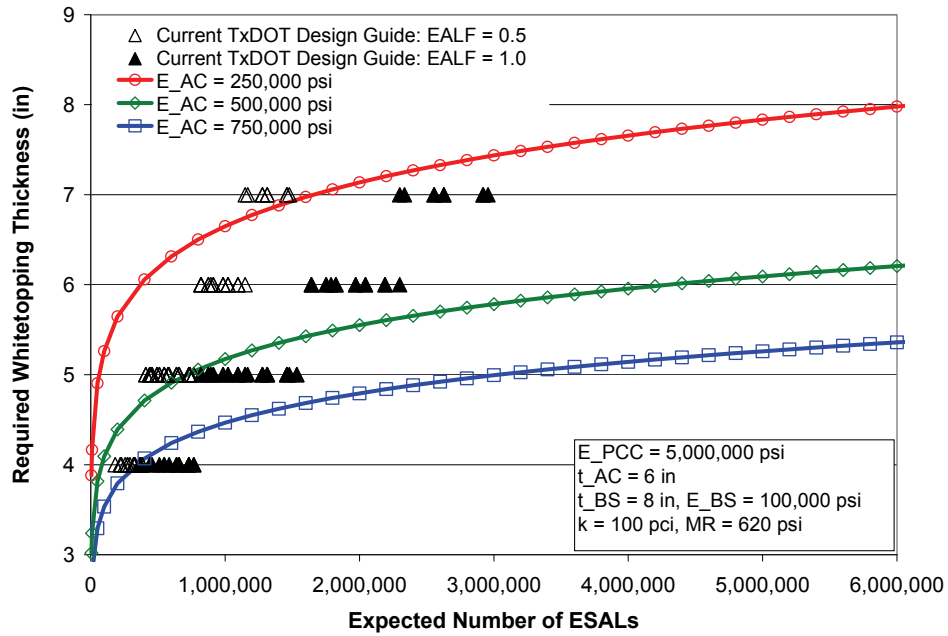
(a)  $EALF = 0.5$  and  $1.0$



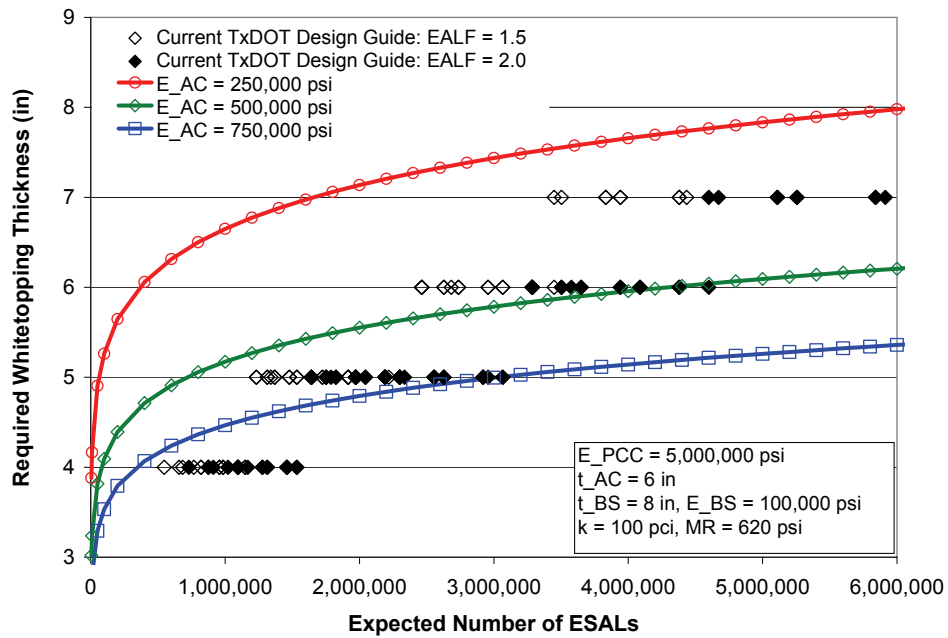
(b)  $EALF = 1.5$  and  $2.0$

Figure 5.29: Whitetopping thickness with various AC thickness using design equation





(a)  $EALF = 0.5$  and  $1.0$



(b)  $EALF = 1.5$  and  $2.0$

Figure 5.30: Whitetopping thickness with various AC modulus using design equation

## 5.7 TWT Design Procedures for TxDOT

It has been shown that the structural condition as well as material characteristics of existing asphalt pavement could have substantial effects on the required TWT slab thickness. Current TxDOT design procedures do not take the effects of existing pavement condition into account. This limitation could lead to under-designs or over-designs of TWT depending on the existing asphalt pavement condition. Almost all overlay design procedures available for other types of pavement rehabilitation require in-depth evaluation of structural condition and material characteristics of the existing pavement. TWT should not be an exception.

TWT design procedures developed in this study are summarized here:

### Step 1

Evaluate the structural condition and material properties using FWD and DCP. If accurate information is available on the thickness and material properties of each layer, go to Step 4. If not, complete steps 2 and 3.

### Step 2

Estimate subgrade resilient modulus using DCP from the following equation:

$$M_R = \frac{438,000}{DCP^{1.12}} \quad (5.7)$$

where,

$M_R$  = resilient modulus = elastic modulus (psi), and

$DCP$  = DCP index (mm/blow).

Use this modulus value to estimate the modulus of the subgrade reaction using a layered program such as ELSYM5. Divide this value by 2 to get the static modulus of subgrade reaction (k).

### Step 3

Use the resilient modulus obtained in Step 2 as a seed value for a back-calculation program to estimate the resilient modulus of the subbase layer. If the asphalt thickness is more than 3 in., use the asphalt layer as a separate layer in the back-calculation program and estimate the modulus values for base and asphalt layers. Otherwise, combine the asphalt layer and base layer as one layer and estimate the modulus for base. In this case, estimate the modulus of the asphalt layer using appropriate laboratory testing.

### Step 4

Using design traffic and modulus values obtained either in Step 1 or in Steps 2–3, estimate the required slab thickness in accordance with Equation 5.8.

$$\begin{aligned}\log(t_{PCC}) = & 3.5615 + 0.1017 \cdot \log(ESALs) + 0.4982 \cdot \log(E_{PCC}) \\ & - 0.7232 \cdot \log(t_{AC}) - 0.3624 \cdot \log(E_{AC}) - 0.2695 \cdot \log(t_{BS}) - 0.0891 \cdot \log(E_{BS}) \\ & - 0.0287 \cdot \log(k) - 1.2250 \cdot \log(MR)\end{aligned}\tag{5.8}$$

where,

- $t_{PCC}$  = required thickness of the whitetopping concrete, in.,
- $ESALs$  = expected number of 18-kips ESALs,
- $E_{PCC}$  = concrete modulus of elasticity, psi,
- $t_{AC}$  = thickness of the asphalt layer, in.,
- $E_{AC}$  = asphalt modulus of elasticity, psi,
- $t_{BS}$  = thickness of the base layer, in.,
- $E_{BS}$  = base modulus of elasticity, psi,
- $k$  = modulus of subgrade reaction, pci, and
- $MR$  = modulus of rupture of whitetopping concrete, psi.



## **Chapter 6. Conclusions and Recommendations**

This chapter provides a summary of the work undertaken over the course of this study. Also presented in this chapter are recommendations for TxDOT in the design of thin whitetopping.

The following conclusions are made on the basis of the results of this study.

### **A) Performance of Whitetopping Projects**

- 1) The performance of several thin whitetopping (TWT) projects, nationwide and in Texas as well, shows that even though overall performance has been excellent in Texas, some variations in distress types and levels were observed in other states. In some projects, severe corner cracking developed under the wheel paths on the driving lane when the joints were close to or in the wheel paths. In other projects, cracking in the panels on the driving lane near the shoulder was more pronounced. Reflective and load-related cracking was common on all projects.
- 2) The findings in the literature review also show that joint spacing has a significant effect on performance because improperly selected joint spacing puts joints directly in the wheel path, causing corner cracking. Corner cracking appears to be the primary failure mode, and fatigue cracking is believed to be the primary cracking mechanism.
- 3) Ultrathin whitetopping (UTW) provides small joint spacing intended to minimize stresses from wheel load applications as well as temperature and moisture variations. However, as stated, the short joint spacing forces joint elements directly in the wheel paths, resulting in corner cracking and severe distresses. Cost for concrete materials is relatively low in whitetopping projects compared with other items, such as saw cutting. Short joint spacing increases the saw cutting cost, while compromising potential performance. It is more economical to use TWT, instead of UTW, with 6-ft joint spacing, especially when considering performance.

### **B) Development of TWT Design Procedures for TxDOT**

- 1) In order to develop mechanistic design procedures for whitetopping pavement for TxDOT, the mechanistic analysis program, ISLAB2000, a 2.5-dimensional program, was selected for analysis of the pavement system. A factorial experiment was set up with a number of input variables at different levels that form a large inference space encompassing the Texas conditions, which resulted in nearly 7,800 cells.
- 2) A series of numerical simulations using ISLAB2000 were performed in accordance with the factorial experiment developed. Pavement structures consisted of concrete topping, asphalt, base, and subgrade, along with varying levels of material properties.
- 3) Using log-log regression, the calculation results of ISLAB2000 were statistically analyzed to develop reasonable design equations for slab thickness.
- 4) A full-scale whitetopping pavement, which consisted of nine 6-ft by 6-ft panels, was constructed and tested under static and constant cyclic loading for fatigue. The super-

accelerated pavement (SAP) testing technique that was developed at The University of Texas was used in the field. The stationary dynamic deflectometer (SDD) was used to load the full-scale concrete slabs. To monitor the response of the whitetopping pavement, several instruments were installed, and dynamic and static loading behavior of slabs was analyzed during entire testing period.

- 5) All test panels reached fatigue failure under the edge loading configuration using the SDD. This field loading system was found to be a practical and effective tool for testing the full-scale rigid pavement system. During fatigue loading, cracks formed at the bottom of loading points first, and propagated to the top surface. The field slabs showed a stress redistribution phenomenon during the crack propagation period. The dynamic displacement generally increased at a higher rate after the occurrences of the first visible crack.
- 6) The concept of equivalent fatigue life was applied to correct the effect of the different stress ratios. The S-N curve from this study is very close to Thompson and Barenburg's S-N curve after the application of the equivalent fatigue life concept.
- 7) The current TxDOT design method for TWT does not account for the condition of the existing hot mix asphalt pavement. Rather, the slab thickness is determined solely by the future truck traffic. In addition, the current TxDOT design method for TWT requires truck traffic volume as input while TP&P provides traffic loading information in terms of ESALs. The proposed design equation is more realistic in that it accounts for all the design variables, including layer characteristics. It also utilizes ESALs as traffic input. Therefore, the proposed design equation will provide TxDOT engineers with a more accurate and convenient design tool for TWT.

Based on the research efforts in this study, the following recommendations are proposed.

- 1) Since several factors of existing asphalt pavements have substantial effects on the required TWT thickness, it is recommended that the condition of the existing asphalt pavement be evaluated with FWD and/or DCP.
- 2) The design procedures developed in this study for thin whitetopping design can be implemented in TxDOT.

## References

- AASHTO, "AASHTO Interim Guide for Design of Pavement Structures," American Association of State Highway Transportation Officials, 1972.
- Bay, J. A., K. H. Stokoe, II., and J. D. Jackson. Development and Preliminary Investigation of a Rolling Dynamic Deflectometer. In Transportation Research Record 1473, TRB, National Research Council, Washington, D.C., 1995, pp. 43–54.
- Bay, J. A., K. H. Stokoe, II., B. F. McCullough, and D. R. Alexander. Profiling Flexible Highway Pavement Continuously with Rolling Dynamic Deflectometer and at Discrete Points with Falling Weight Deflectometer. In Transportation Research Record 1655, TRB, National Research Council, Washington, D.C., 1999, pp. 74–85.
- Burnham, T. R., "Forensic Investigation Report for Mn/Road Ultra-thin Whitetopping Test Cells 93, 94, and 95," Report No. MN/RC-2005-45, September 2005.
- Huang, Y. H., "Pavement Analysis and Design," 2<sup>nd</sup> Edition, Prentice Hall, 2004, pp. 244 – 278.
- Kesler, C. E., Effect of Speed of Testing on Flexural Fatigue Strength of Plain Concrete. Proceedings, Thirty-Second Annual Meeting, Highway Research Board, Washington, D.C., V. 32, 1953, pp. 251-258.
- Matthew J.S, S.M. Tarr, and S. Tayabji, "Instrumentation and Field Testing of Thin Whitetopping Pavement in Colorado and Revision of the Existing Colorado Thin Whitetopping Procedure," Report No. CDOT-DTD-R-2004-12 Final Report, Colorado Department of Transportation Research, August 2004.
- Nenad G., "Development of a Design Guide for Ultra-thin Whitetopping (UTW)," Report No. FHWA 2001-018, New Jersey Department of Transportation, November 1998.
- Nishizawa, T., Y. Murata, and K. Kokubo, "Mechanical Behavior of Ultra-Thin Whitetopping Structure Under Stationary and Moving Loads," Transportation Research Record 1823, Transportation Research Board, National Research Council, Washington, D.C., pp.102-109, 2003.
- Nishizawa, T., Y. Murata, and T. Nakagawa, "Curling Stress in Concrete Slab of Ultra-Thin Whitetopping Structure," Presented at the 81st Annual Meeting of the Transportation Research Board, Washington, D.C., Jan. 2002.
- Packard, R. G., and S. D. Tayabji. New PCA Thickness Design Procedure for Concrete Highway and Street Pavements. Proceedings, Third International Conference on Concrete Pavement Design, 1985, pp. 225-236.

- Roesler, J. R., and E. J. Barenberg. Effect of Static and Fatigue Cracking on Concrete Strain Measurements. In Transportation Research Record, No. 1684, TRB, National Research Council, Washington, D.C., 1999, pp. 51-60.
- Roesler, J. R., and E. J. Barenberg. Fatigue and Static Testing of Concrete Slabs. Transportation Research Record, No. 1684, TRB, National Research Council, Washington, D.C., 1999, pp. 71-80.
- Scott M. T., M. J. Sheehan, and P. A. Okamoto, "Guidelines for the Thickness Design of Bonded Whitetopping Pavement in the State of Colorado," Report No. CDOT-DTD-R-98-10, Colorado Department of Transportation Research, December 1998.
- Shi, X. P., T. W. Fwa, and S. A. Tan. Flexural Fatigue Strength of Plain Concrete, ACI Materials Journal, V. 90, No. 5, 1993, pp. 435-440.
- Stokoe, K. H., II, and J. A. Bay, Rosenblad, B. L., M. R. Murphy, Fults, K. W., and D. C. Chen. Super-Accelerated Testing of a Flexible Pavement with the Stationary Dynamic Deflectometer (SDD). Presented in the 79th Annual Meeting of the Transportation Research Board, Washington, D.C., January 2000.
- Thompson, M. R., and E. J. Barenberg. NCHRP Report 1-26: Calibrated Mechanistic Structural Analysis Procedure for Pavements-Phase 2, TRB, National Research Council, Washington, D.C., 1992.
- Vesic, A. S., and S. K. Saxena. Analysis of Structural Behavior of Road Test Rigid Pavements. Highway Research Record 291, HRB, National Research Council, Washington, D.C., 1969, pp. 156-158.
- Winkelman, T. J., "Whitetopping Construction and Early Performance in Illinois," Construction Report, Physical Research Report No. 144, Illinois Department of Transportation, June 2002.
- Wu, C. L., S. M. Tarr, T. M. Refai, M. A. Nagai, and M. J. Sheehan, Development of Ultra-Thin Whitetopping Design Procedure, Portland Cement Association, 1998.



## **Appendix: Modified Standards and Specifications for Thin Whitetopping and Full Depth PCC Pavement**

Research findings from this study did not identify any reasons to modify current Special Specifications for thin whitetopping (SS3002) or current design standards for thin whitetopping, “Thin Whitetopping Details, TWT-04.”